Remote Sensing - Multispectral Applications

Lectures in Ostuni
June 2006

Paul Menzel
NOAA/NESDIS/ORA

Application Opportunities with Multispectral Remote Sensing Data

Satellite Remote Sensing
Energy Balance
VIS, IR, and MW Radiative Transfer
EOS Terra & Aqua MODIS
Multispectral Applications
(Ocean Color, Snow/Ice, Vegetation, Aerosols, Fires, Volcanic Ash, Clouds, Moisture)
Detecting Climate Trends

Satellite remote sensing of the Earth-atmosphere

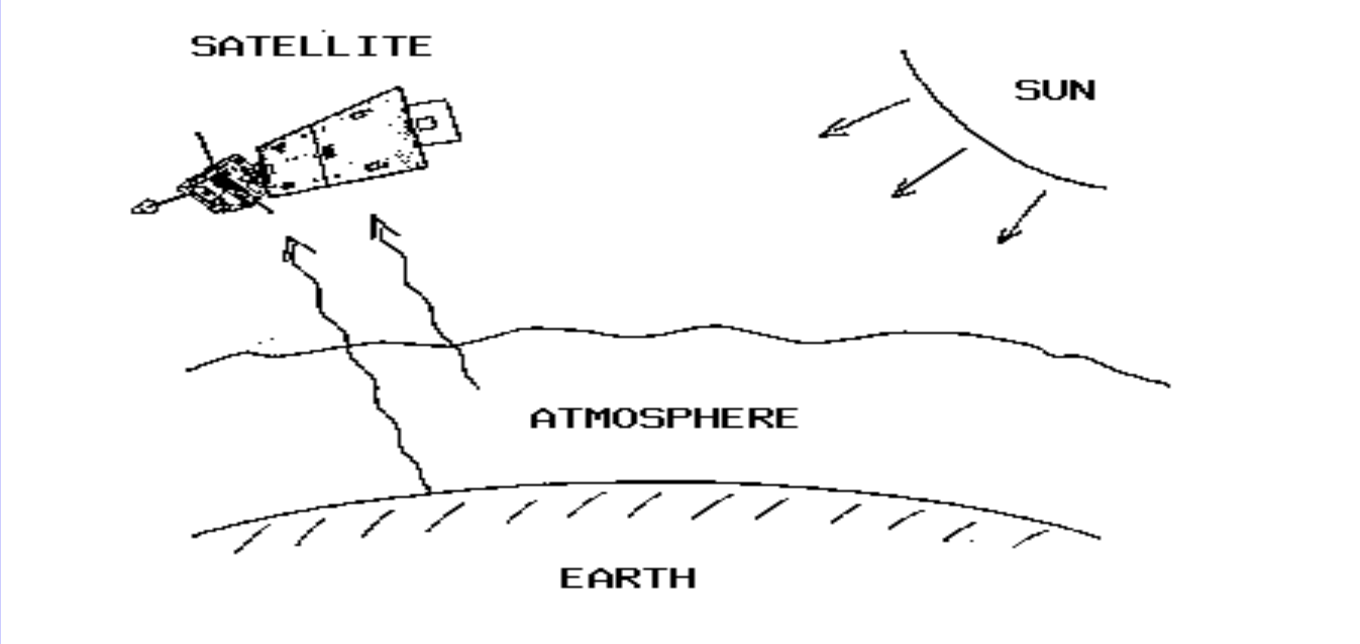

Observations depend on

telescope characteristics (resolving power, diffraction)
detector characteristics (signal to noise)
communications bandwidth (bit depth)
spectral intervals (window, absorption band)
time of day (daylight visible)
atmospheric state (T, Q, clouds)
earth surface (Ts, vegetation cover)

Solar (visible) and Earth emitted (infrared) energy

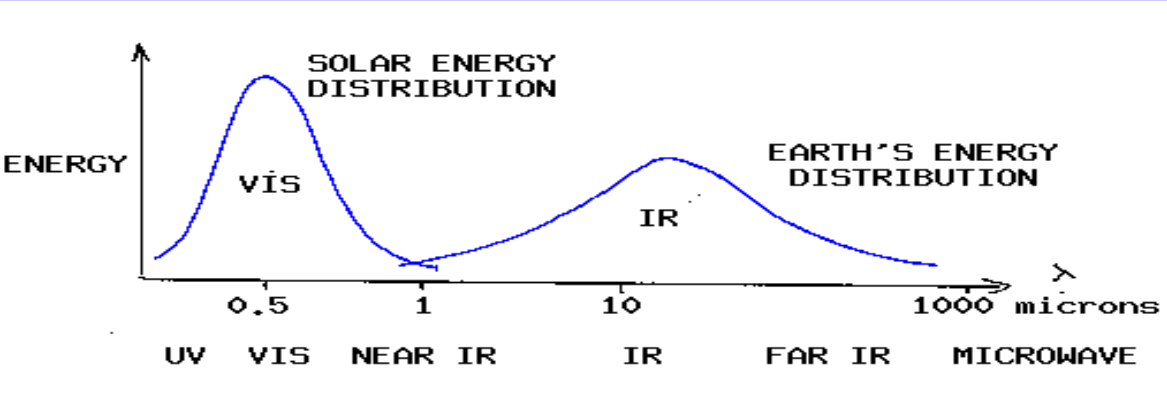

Incoming solar radiation (mostly visible) drives the earth-atmosphere (which emits infrared).

Over the annual cycle, the incoming solar energy that makes it to the earth surface (about 50 %) is balanced by the outgoing thermal infrared energy emitted through the atmosphere.

The atmosphere transmits, absorbs (by H2O, O2, O3, dust) reflects (by clouds), and scatters (by aerosols) incoming visible; the earth surface absorbs and reflects the transmitted visible. Atmospheric H2O, CO2, and O3 selectively transmit or absorb the outgoing infrared radiation. The outgoing microwave is primarily affected by H2O and O2.

Radiative Energy Balance

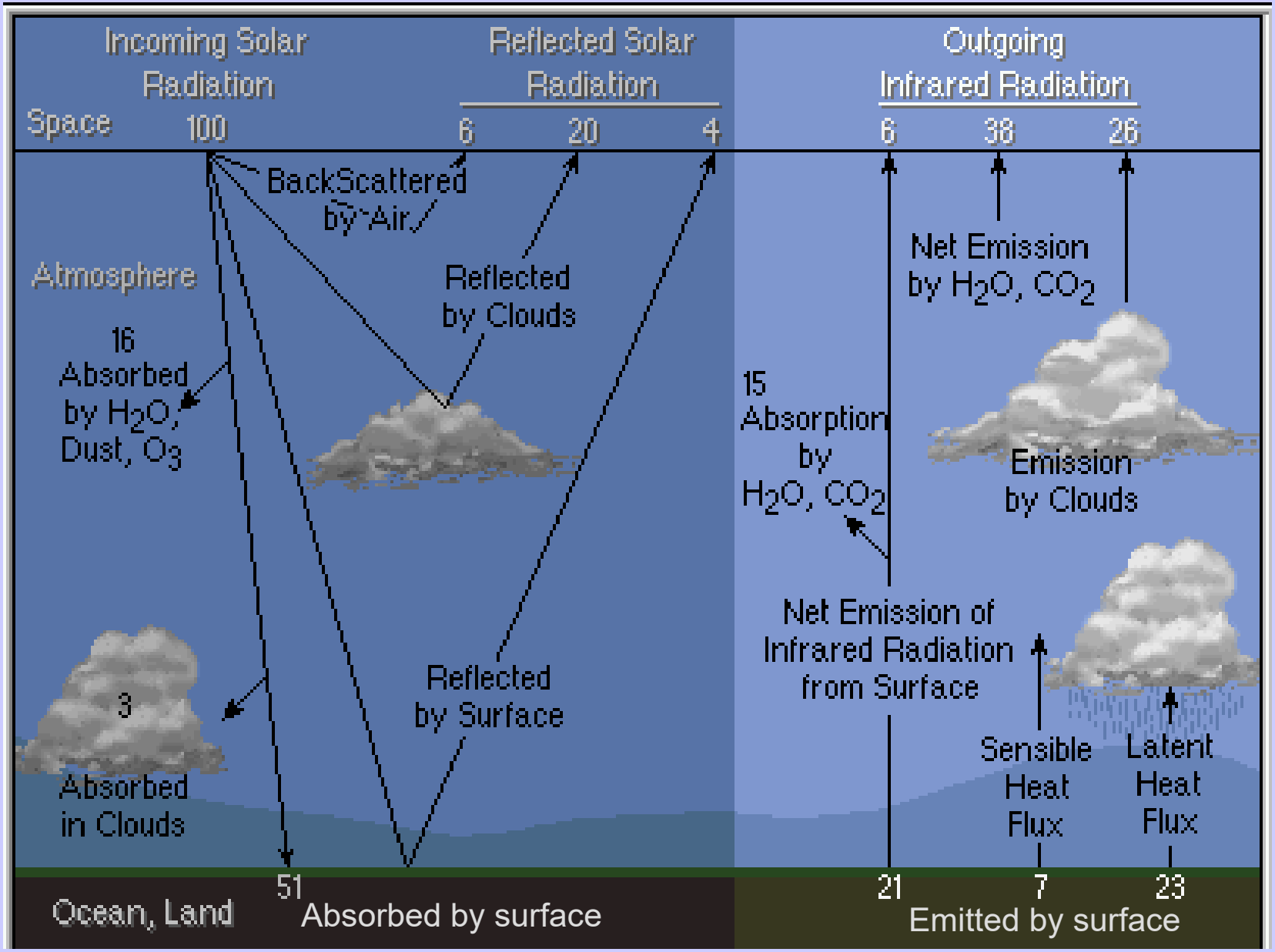

Solar Spectrum

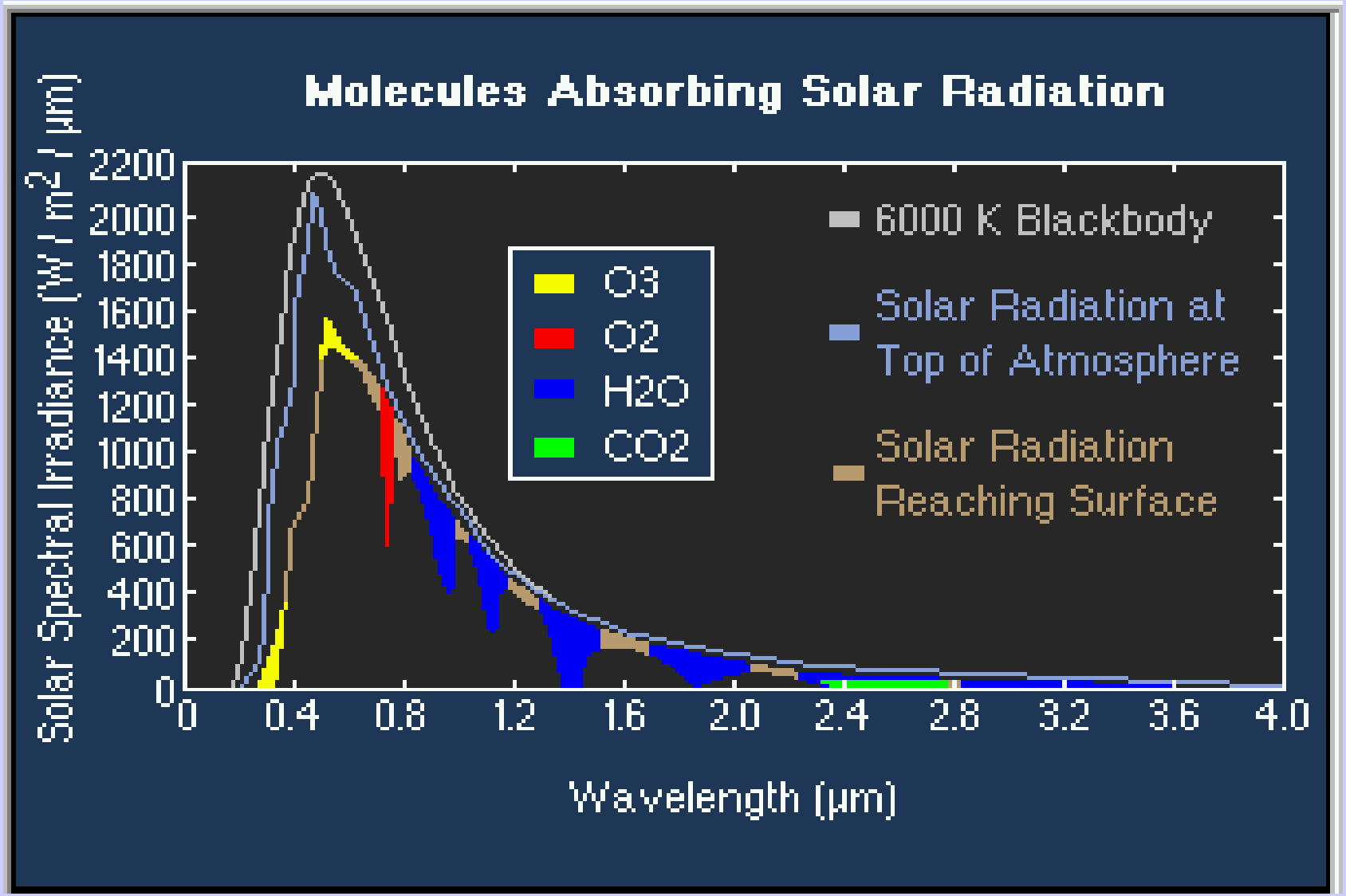

Earth emitted spectra overlaid on Planck function envelopes

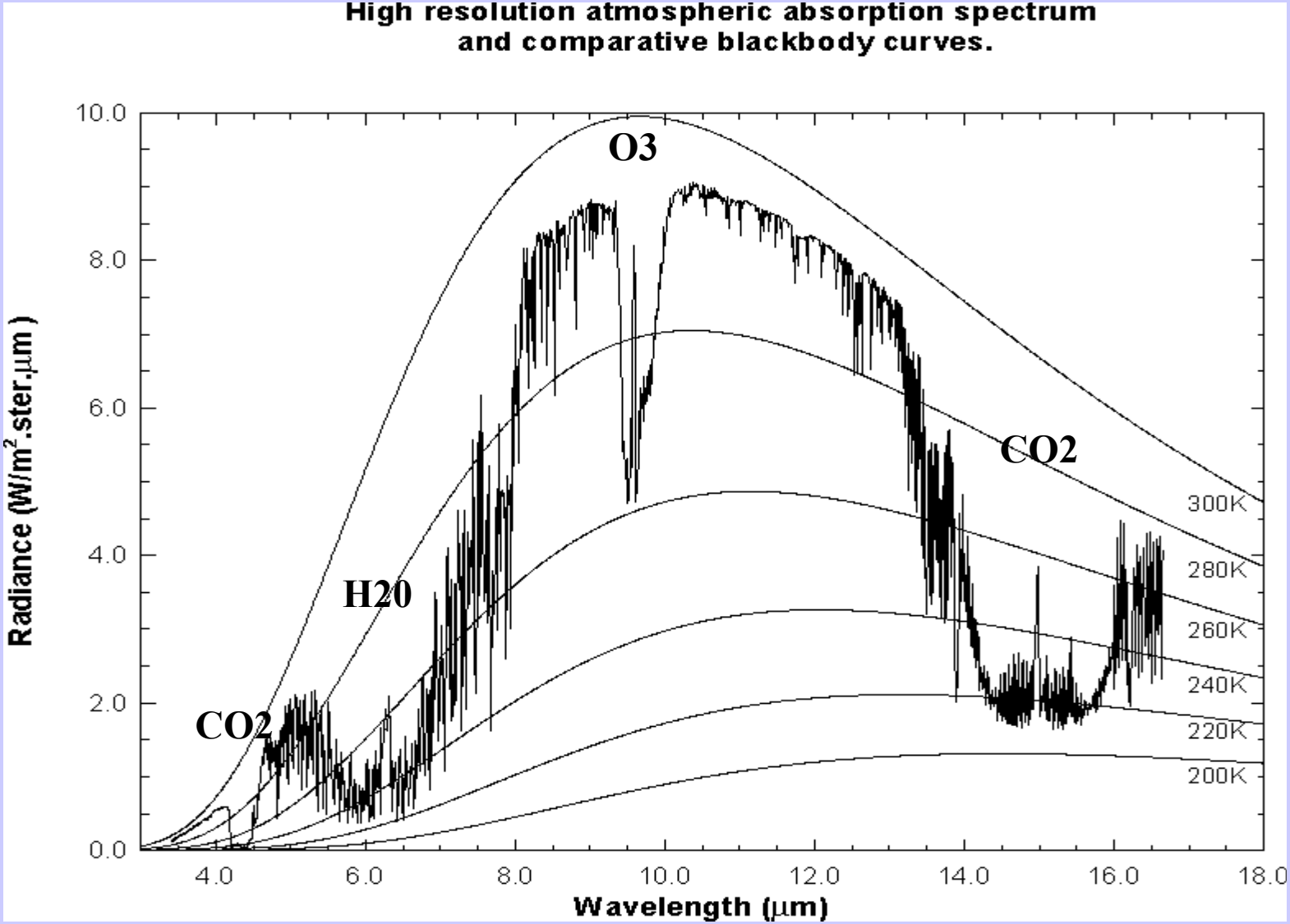

Clouds viewed from polar orbiting TIROS launched 1 Apr 1960

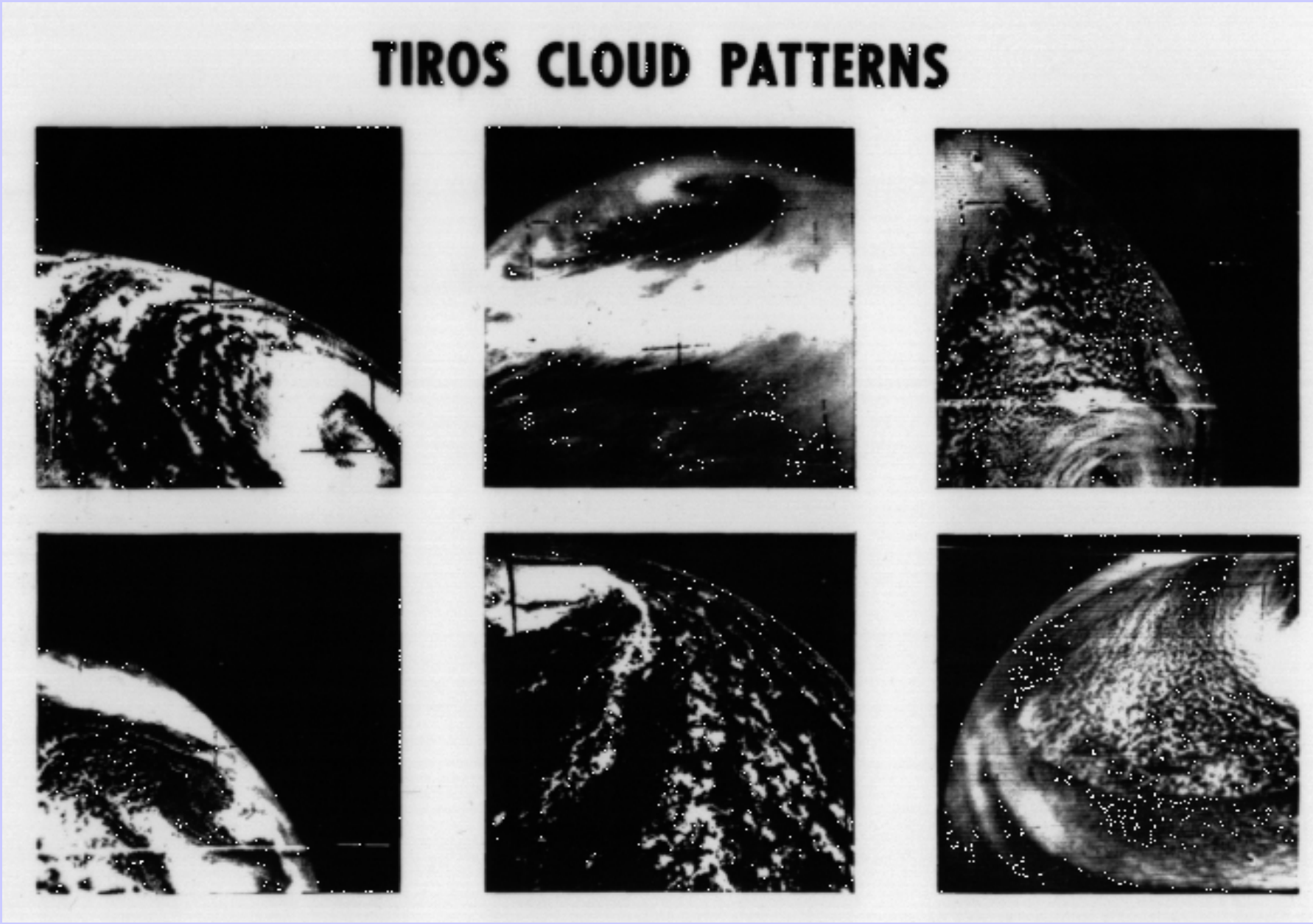

Evolution of Leo Obs

Terra was launched in 1999 and the EOS Era began

MODIS, CERES, MOPITT, ASTER, and MISR reach polar orbit

Aqua and ENVISAT followed in 2002

MODIS and MERIS leading to VIIRS
AIRS leading to IASI and CrIS
AMSU leading to ATMS

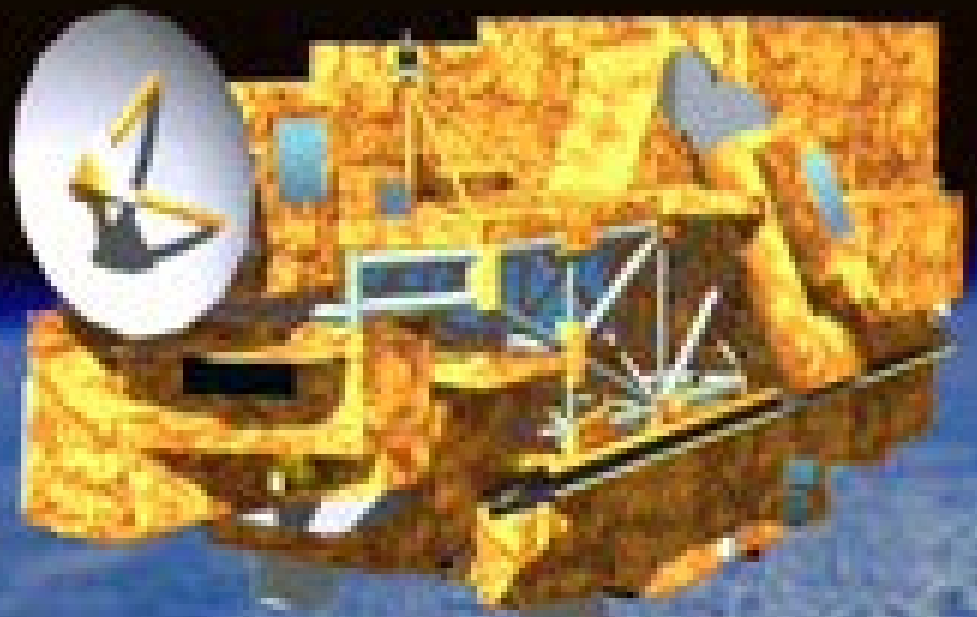

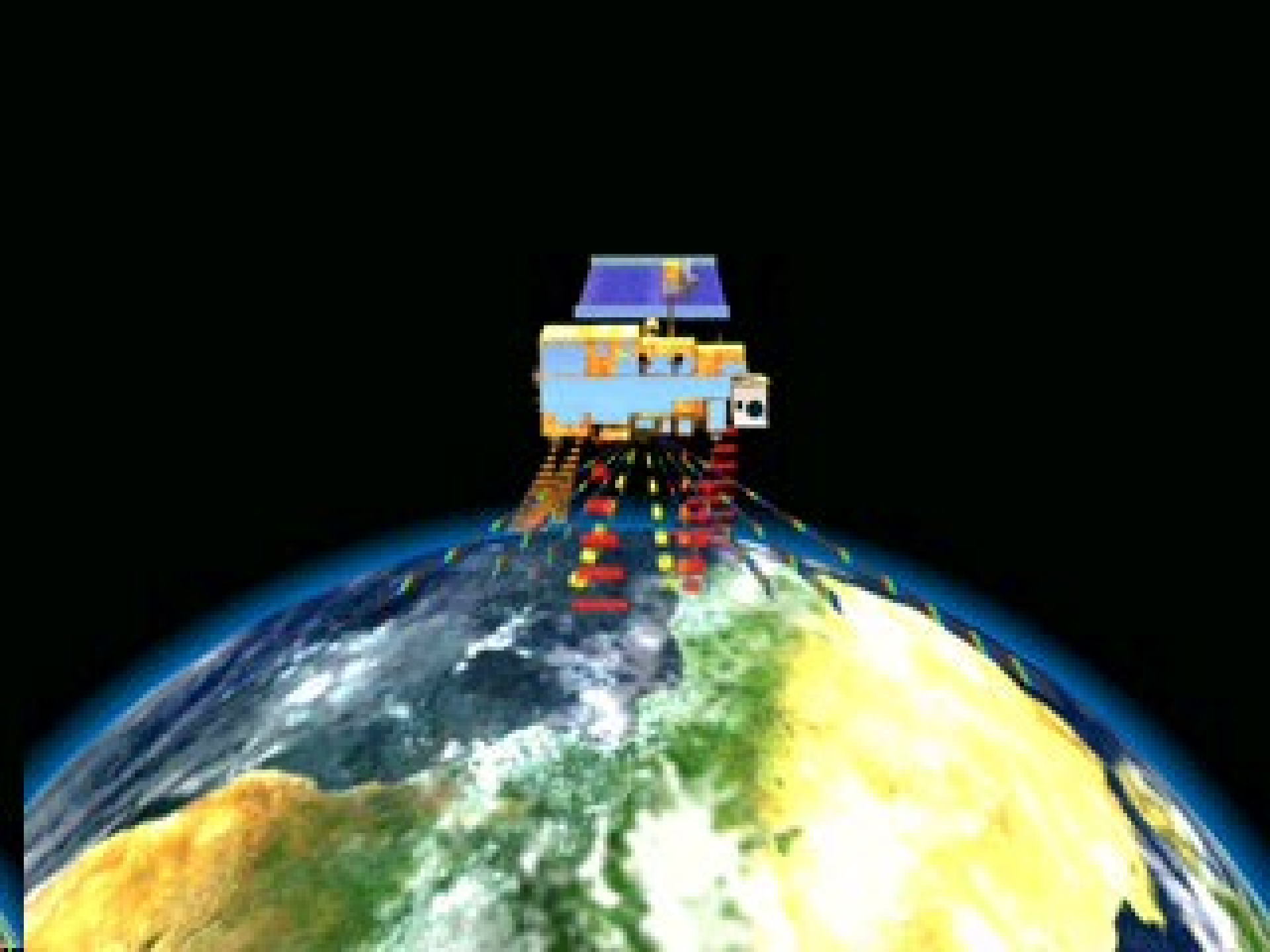

Launch of EOS-Terra (EOS-AM) Satellite - A New Era Begins

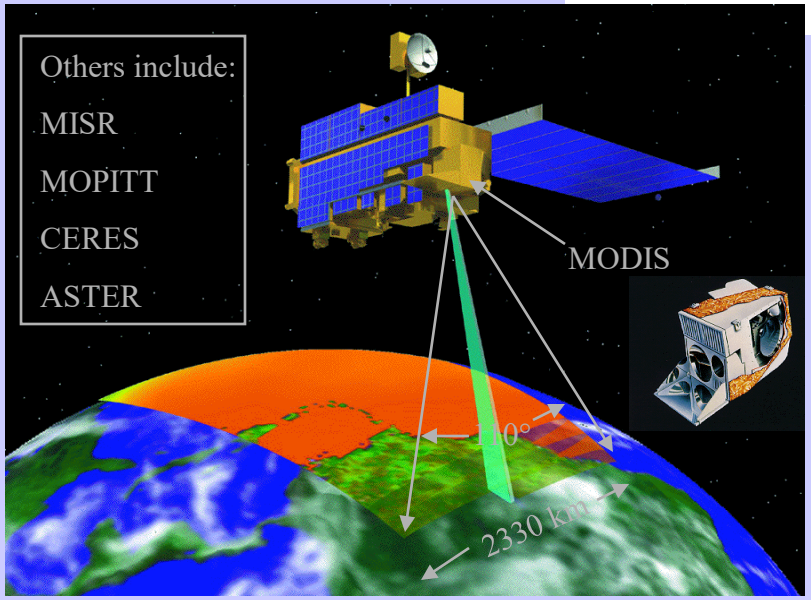

MODIS instrument Specifications:

Bands 1-2 (0.66,0.86 μm): 250 m

Bands 3-7 (0.47, 0.55, 1.24, 1.64, 2.13 μm): 500 m

Bands 8-36: 1 km

Launch date: December 18, 1999, 1:57 PT
Earth viewdoor open date: February 24, 2001

Allen Chu/NASA GSFC

Followed by the launch of EOS-Aqua (EOS-PM) Satellite

“ ”

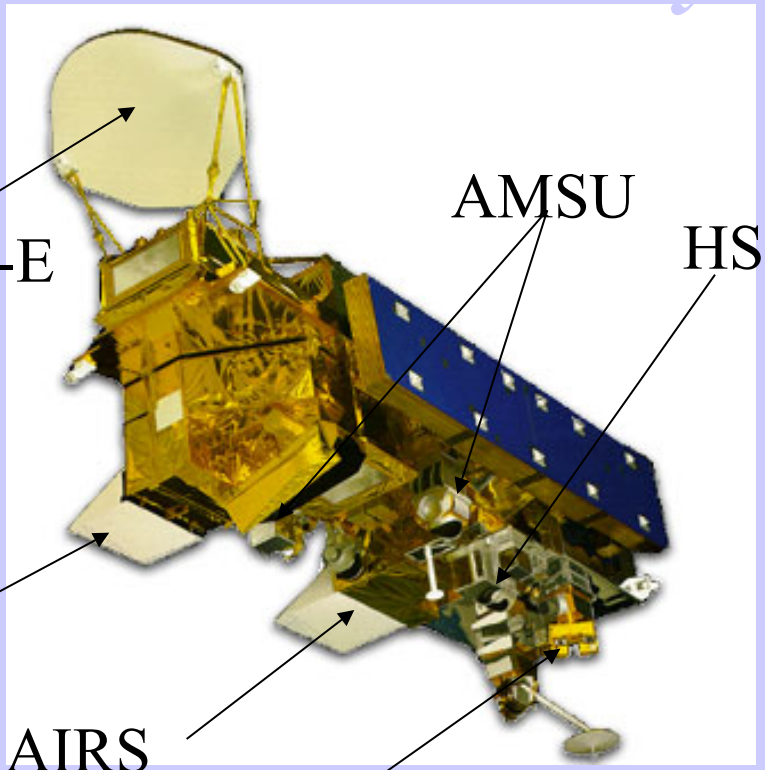

Launch date: May 4, 2002, 2:55 PDT
Earth view door open date: June 25, 2002

VIIRS, MODIS, FY-1C, AVHRR

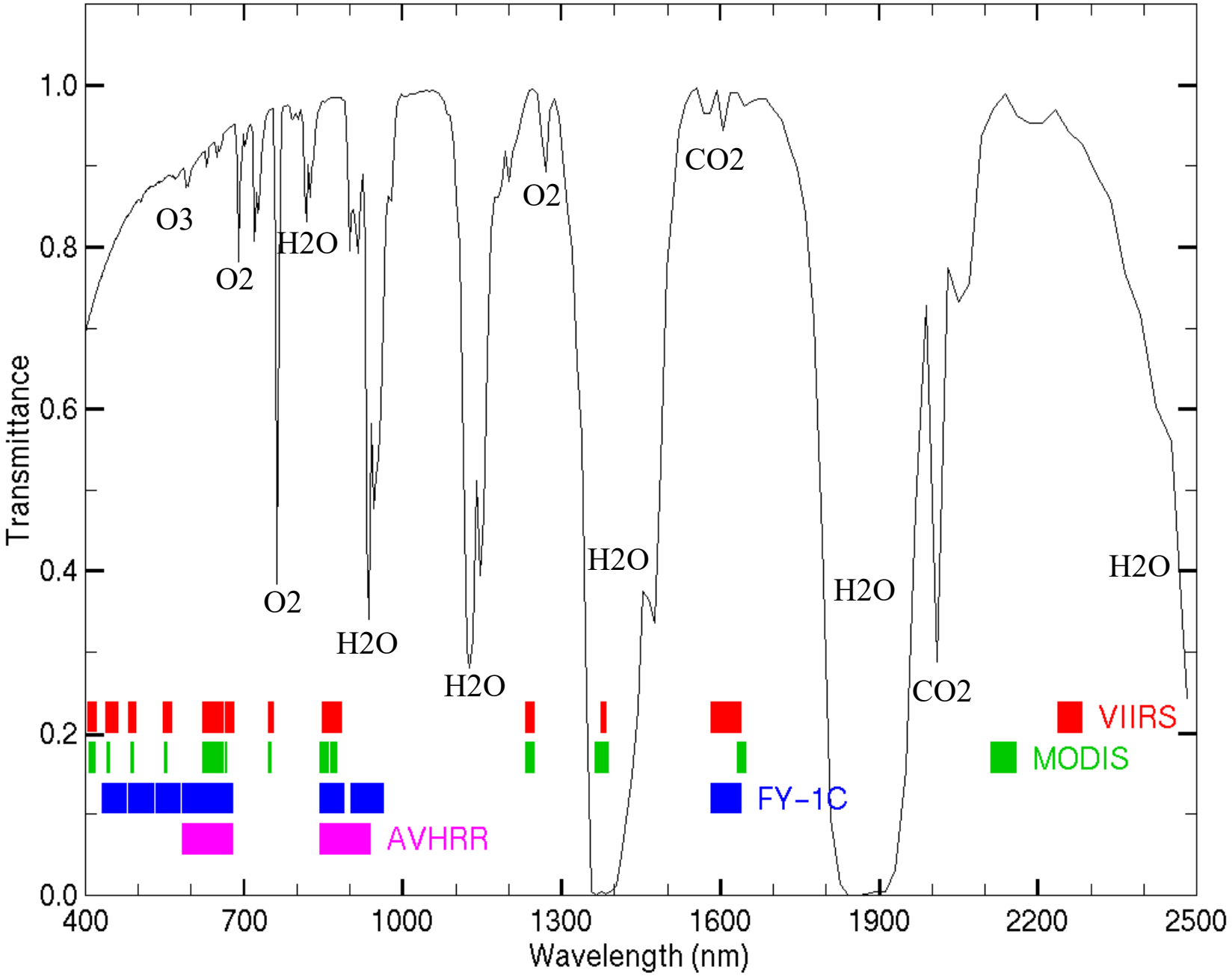

MODIS IR Spectral Bands

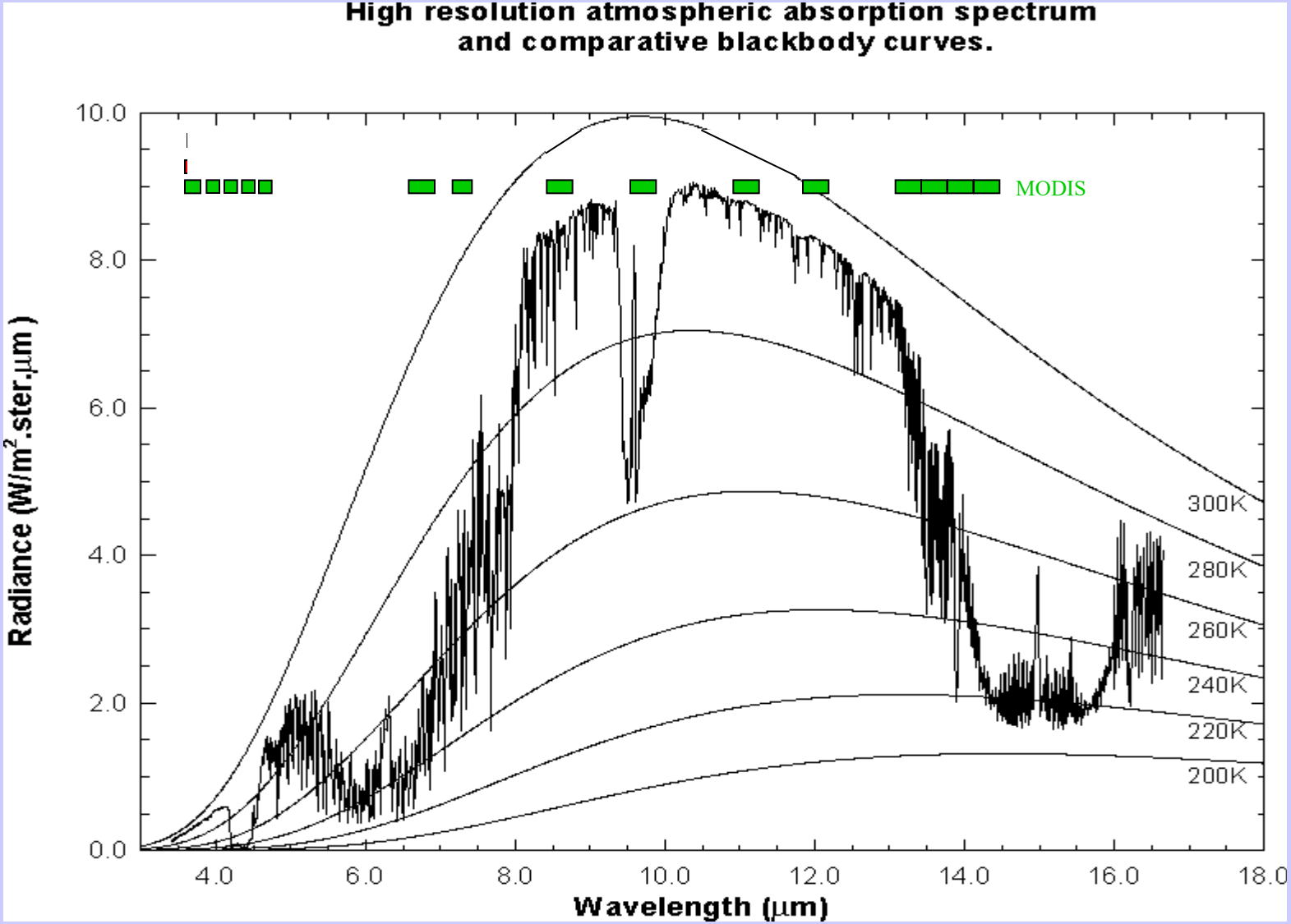

Application Opportunities with Multispectral Remote Sensing Data

Satellite Remote Sensing

Energy Balance

VIS, IR, and MW Radiative Transfer

EOS Terra & Aqua MODIS

Multispectral Applications

(Ocean Color, Snow/Ice, Vegetation, Aerosols, Fires, Volcanic Ash, Clouds)

Detecting Climate Trends

OCEAN-SOLAR RADIATION

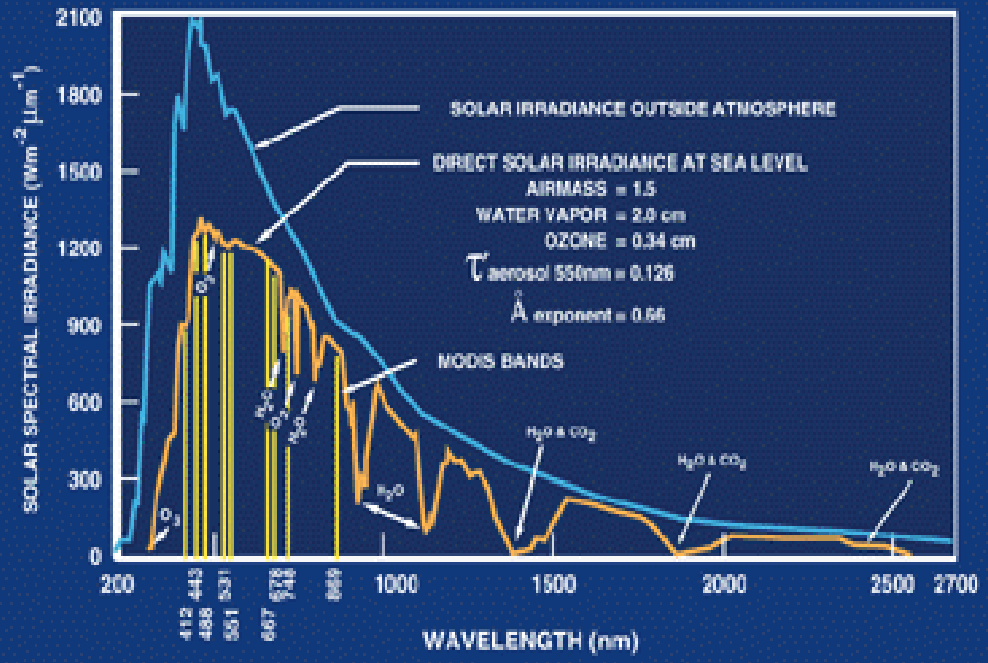

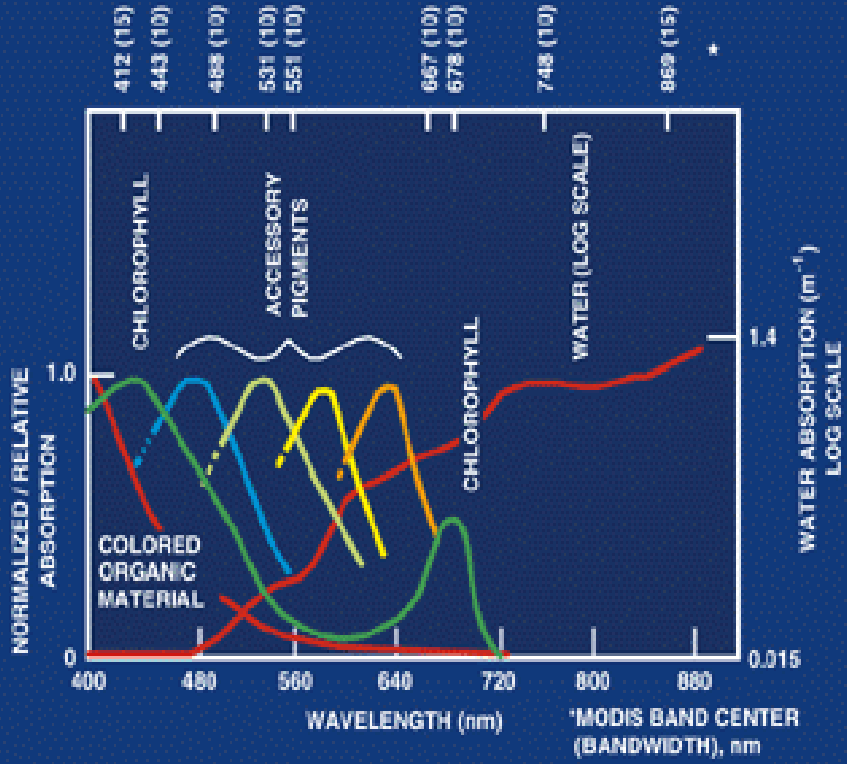


MODIS views the Mississippi

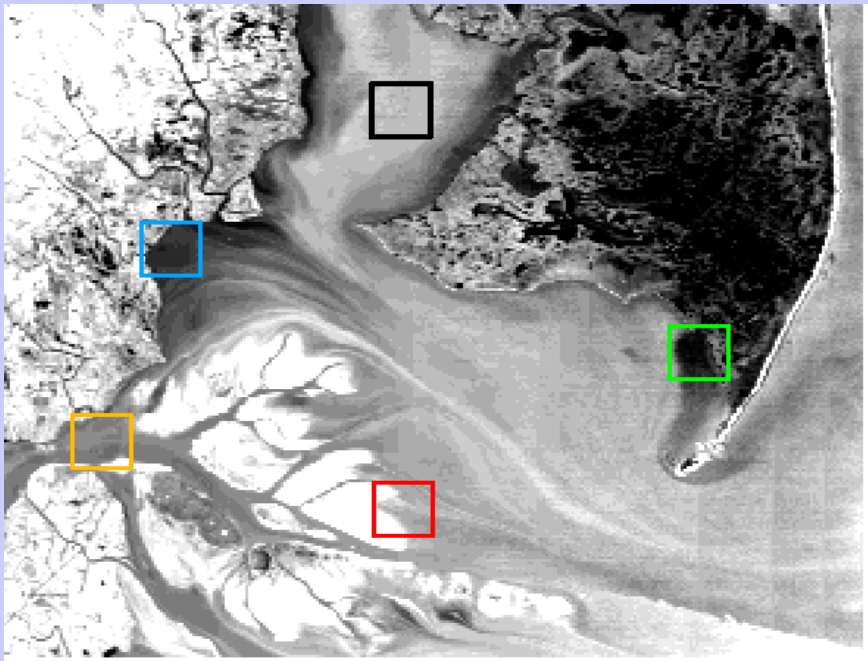

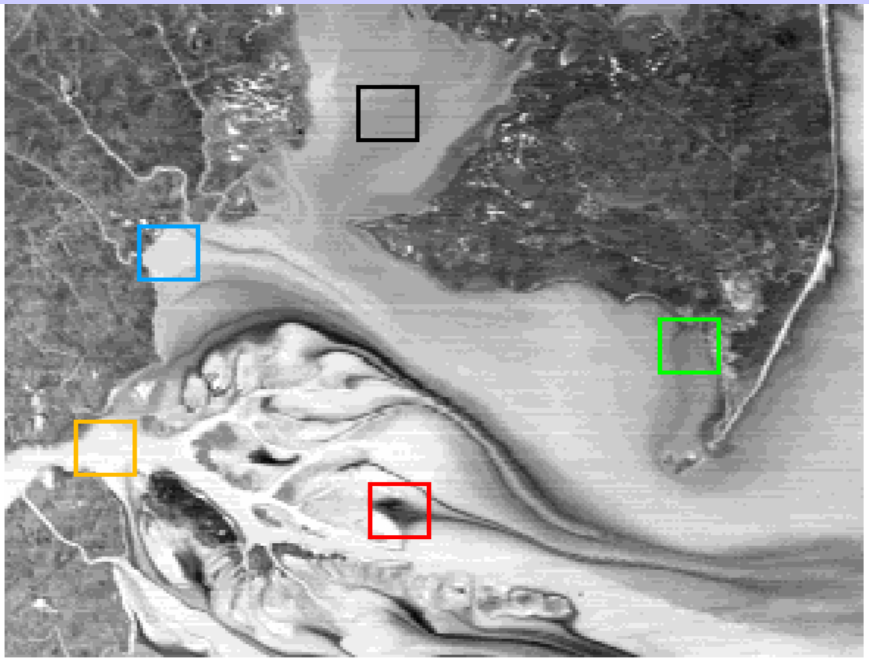

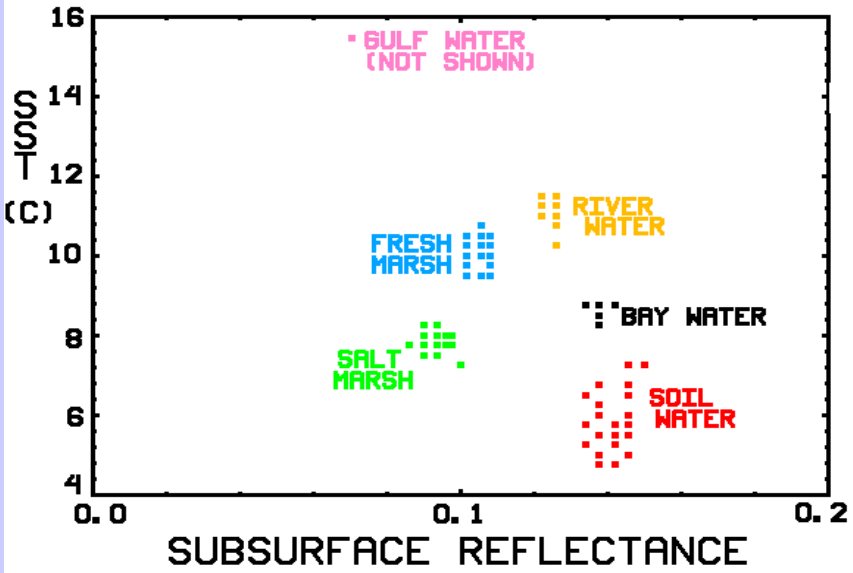

MAMS WATER TYPE ANALYSIS
DEC 4 1990

SHOWN:

* .66um REFLECTANCE (LEFT)
* SPLIT WINDOW SST (RIGHT)

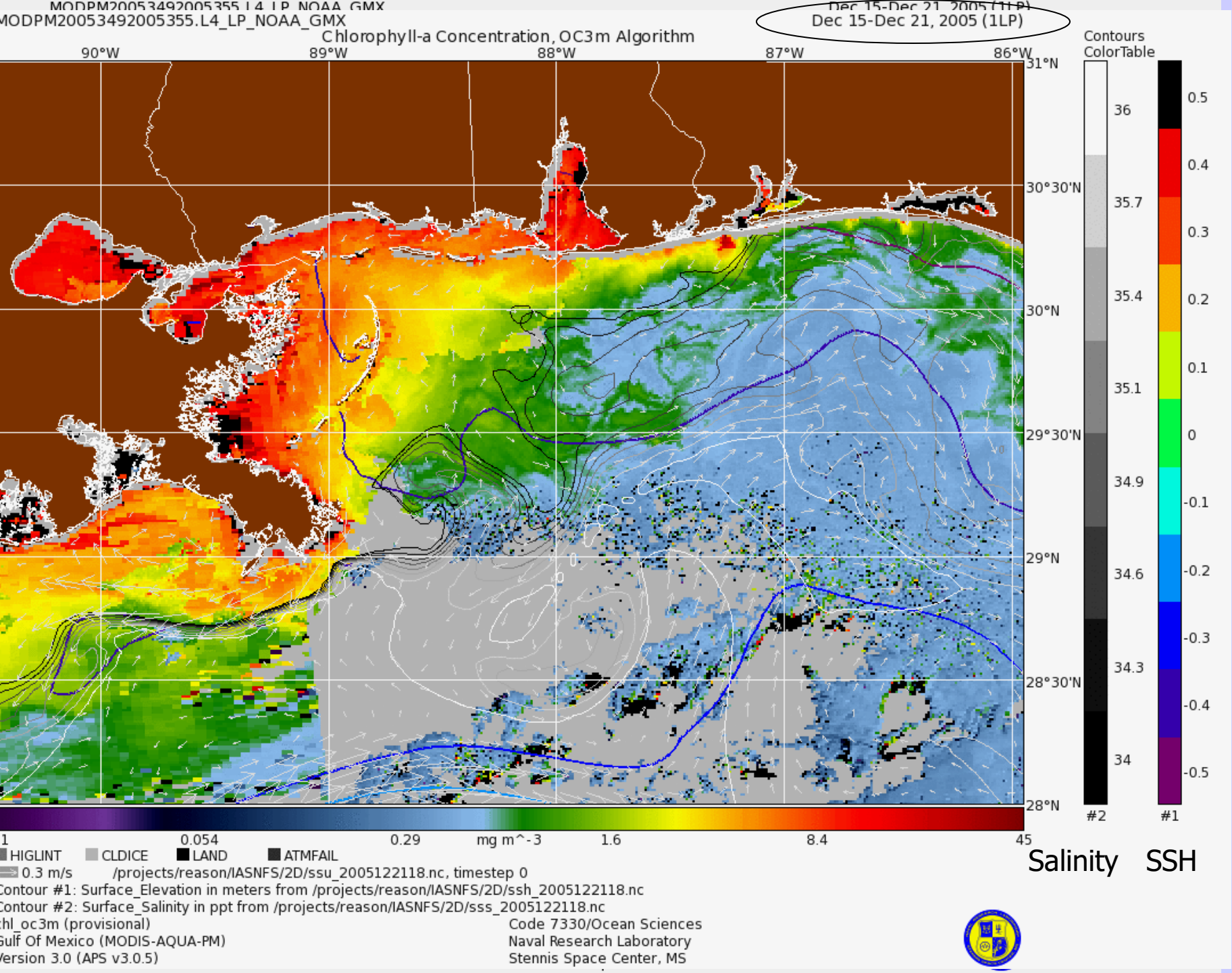
MODPM20053492005355.L4_LP_NOAA_GMX
Chlorophyll-a Concentration, OC3m Algorithm
Dec 15-Dec 21, 2005 (1LP)
90°W
89°W
88°W
87°W
86°W
31°N
30°30'N
30°N
29°30'N
29°N
28°30'N
28°N
Contours
ColorTable
36
35.7
35.4
35.1
34.9
34.6
34.3
34
#2
0.5
0.4
0.3
0.2
0.1
0
-0.1
-0.2
-0.3
-0.4
-0.5
#1
1
0.054
0.29
mg m^-3
1.6
8.4
45
HIGLINT
CLDICE
LAND
ATMFAIL
0.3 m/s
/projects/reason/IASNFS/2D/ssu_2005122118.nc, timestep 0
Contour #1: Surface_Elevation in meters from /projects/reason/IASNFS/2D/ssh_2005122118.nc
Contour #2: Surface_Salinity in ppt from /projects/reason/IASNFS/2D/sss_2005122118.nc
chl_oc3m (provisional)
Gulf Of Mexico (MODIS-AQUA-PM)
Version 3.0 (APS v3.0.5)
Code 7330/Ocean Sciences
Naval Research Laboratory
Stennis Space Center, MS
Salinity
SSH

Comparison of Spatial resolutions Chesapeake Bay March 13, 2004 Monitoring the Estuarine and Riverine Environment

New Capabilities for Managing Coastal Resources

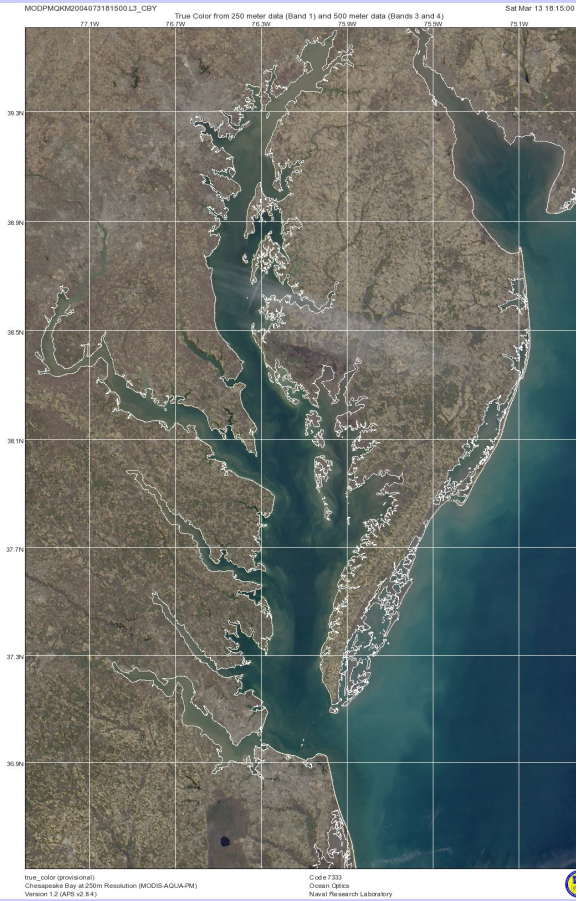

(Franz, McClain, Martinolich, Casey)

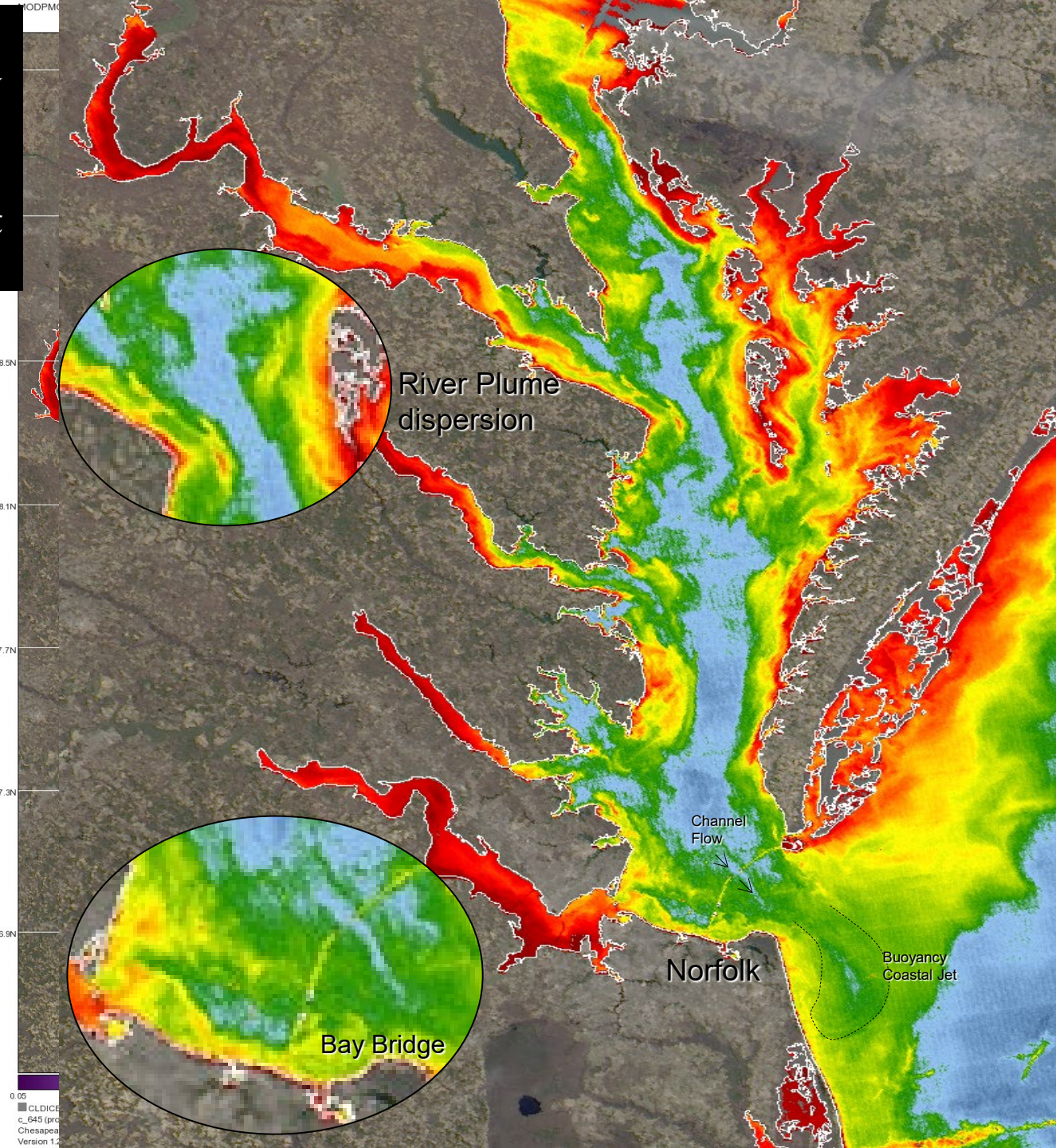

MODIS SEA SURFACE TEMPERATURE

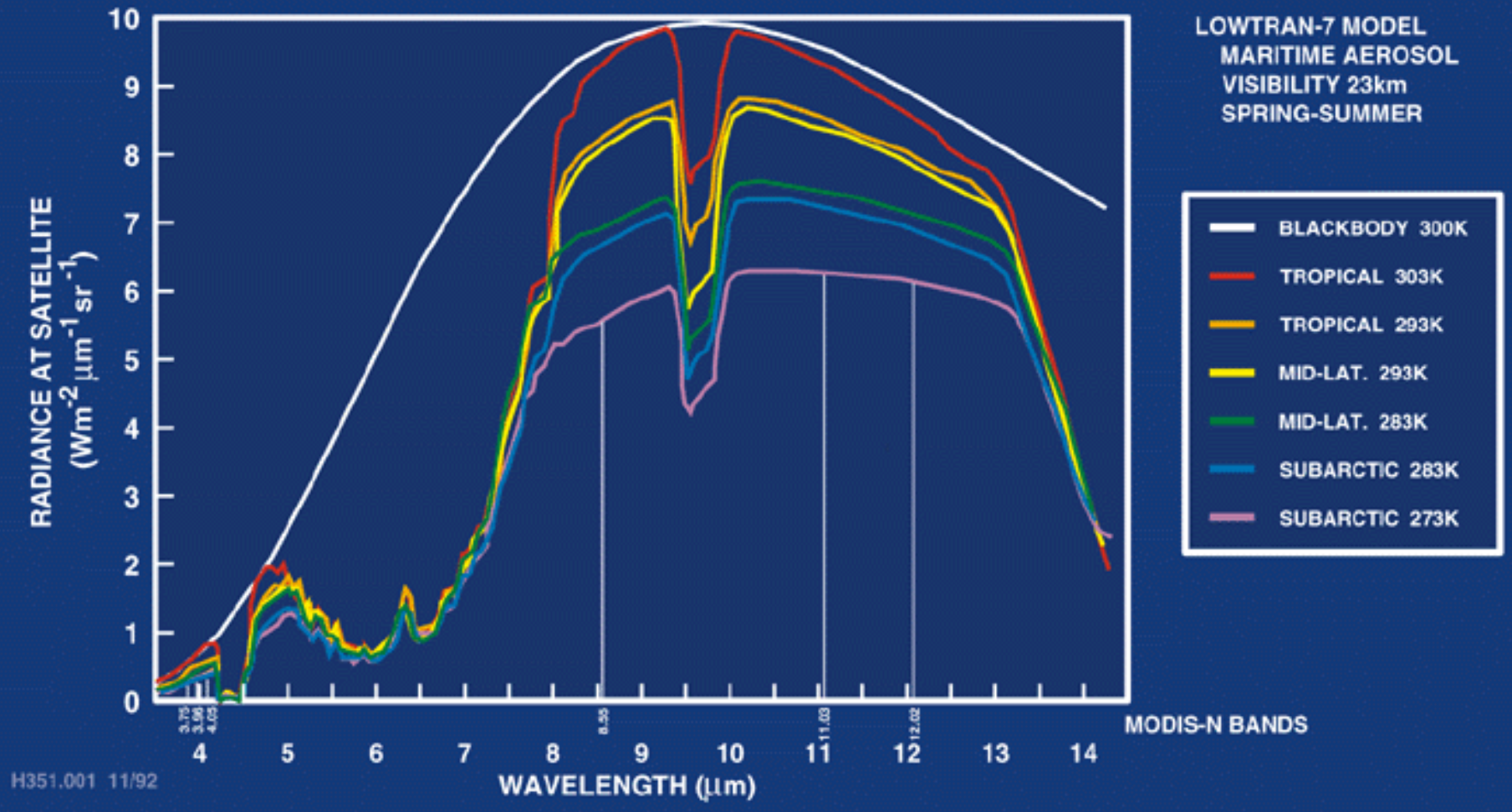

SST - MODIS and AVHRR

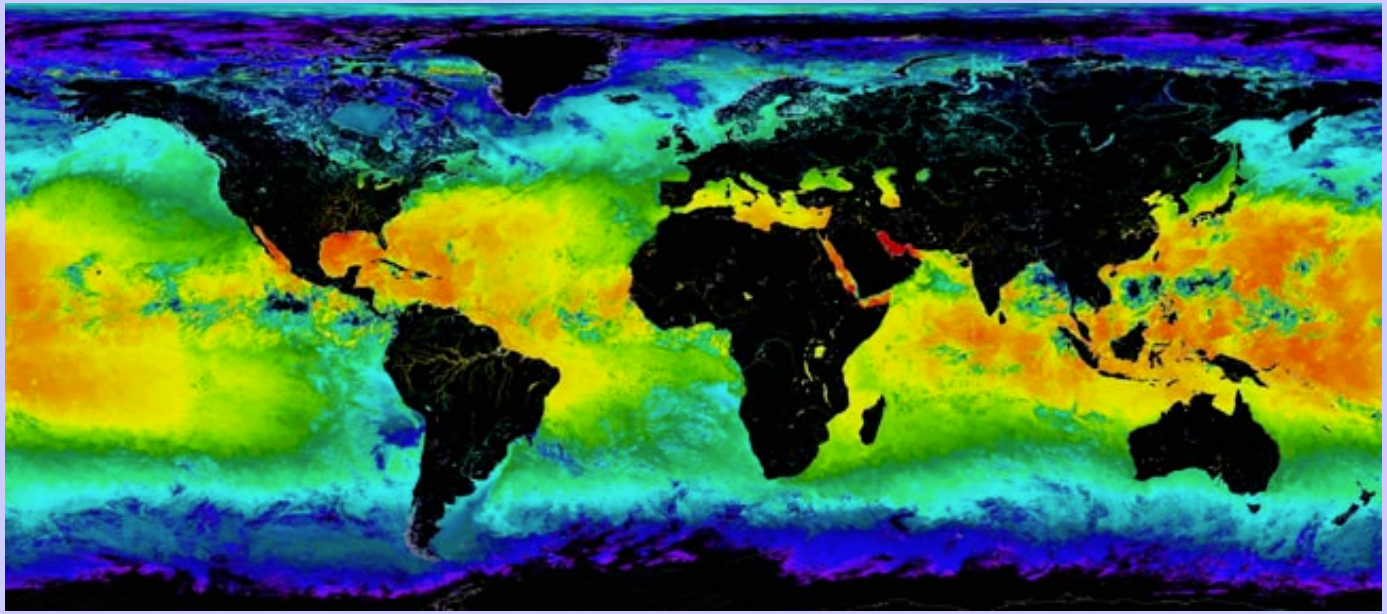

MODIS 4 µm Night SST

Improved coverage in tropical regions. Color scales are not identical, cloud mask is not applied.

AVHRR Night SST

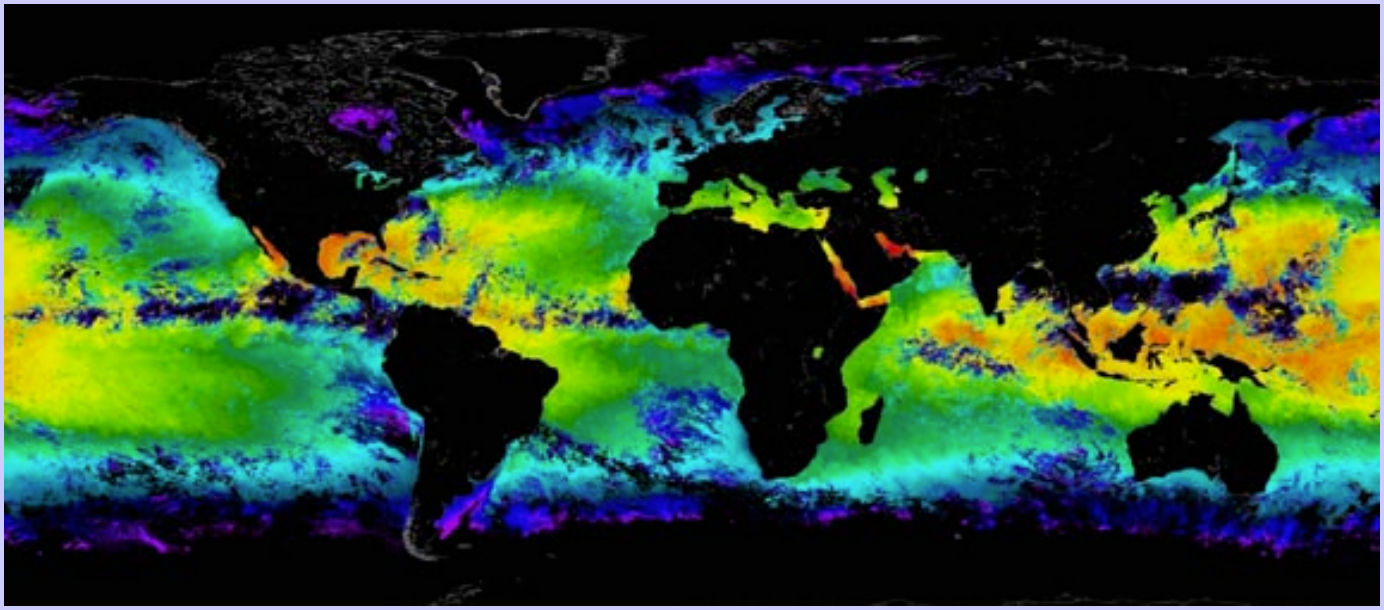

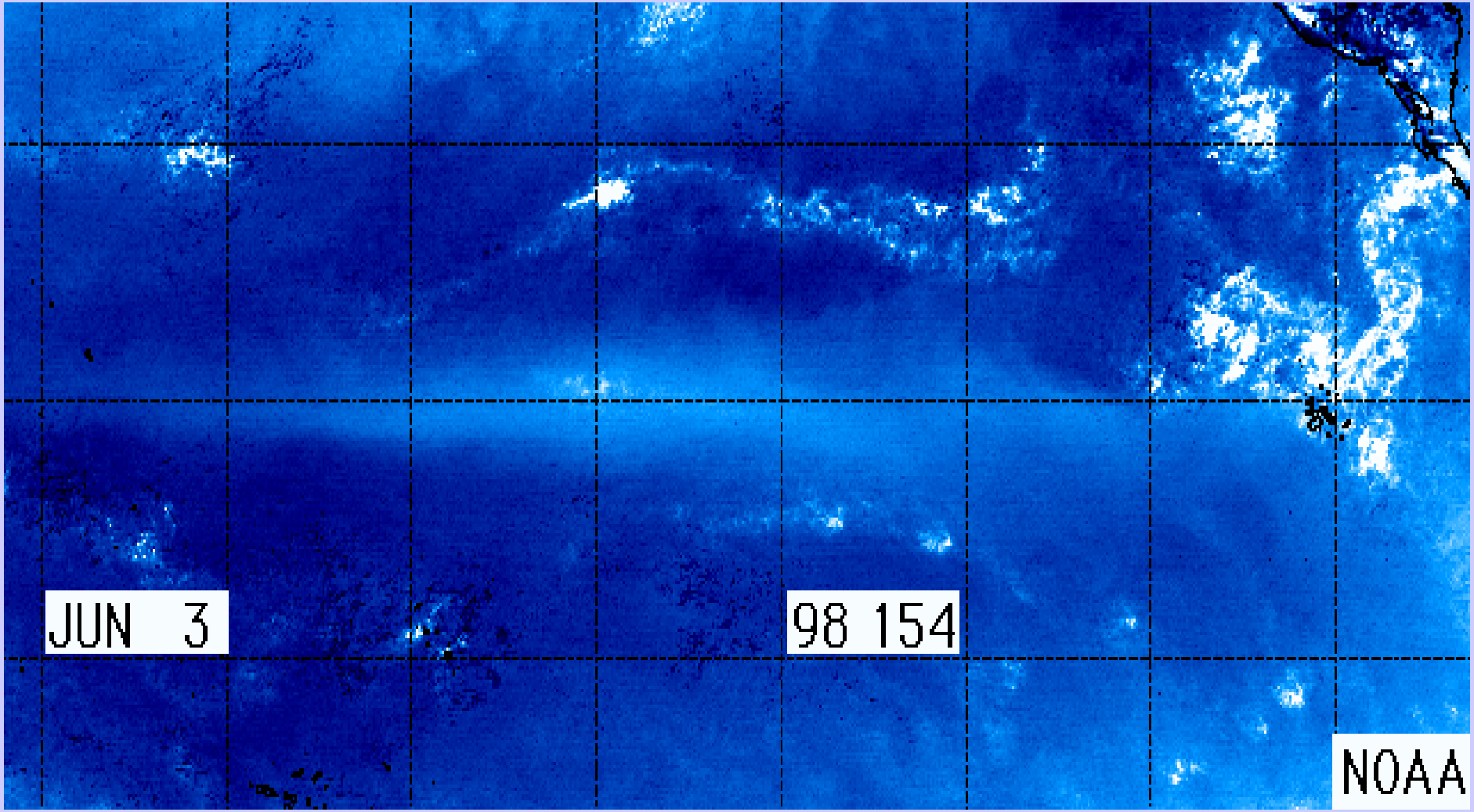

SST Waves from Legeckis

LAND - THERMAL RADIATION

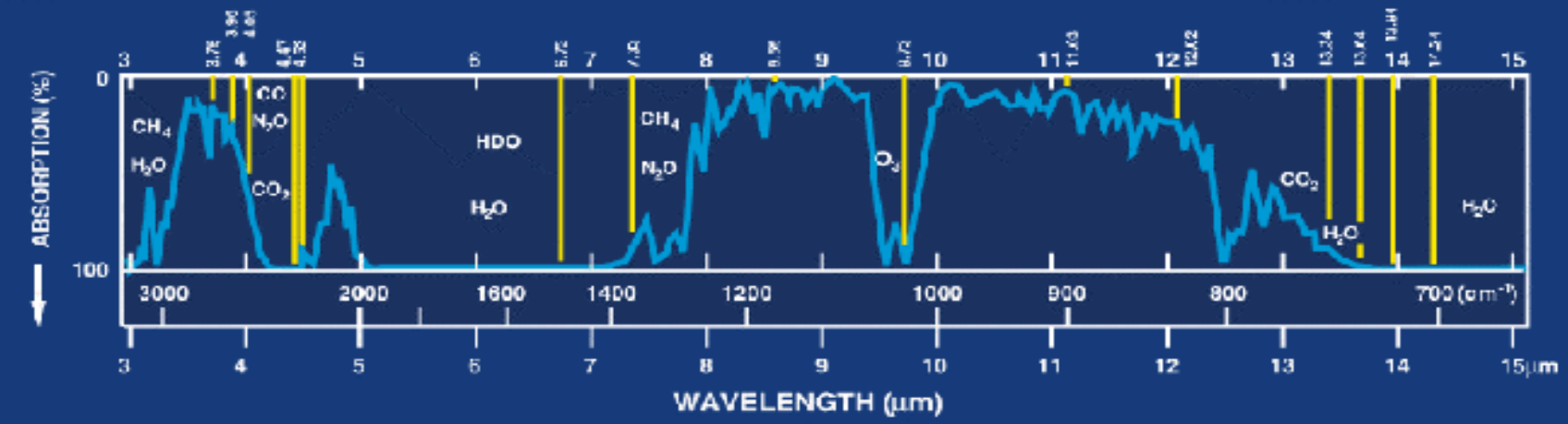

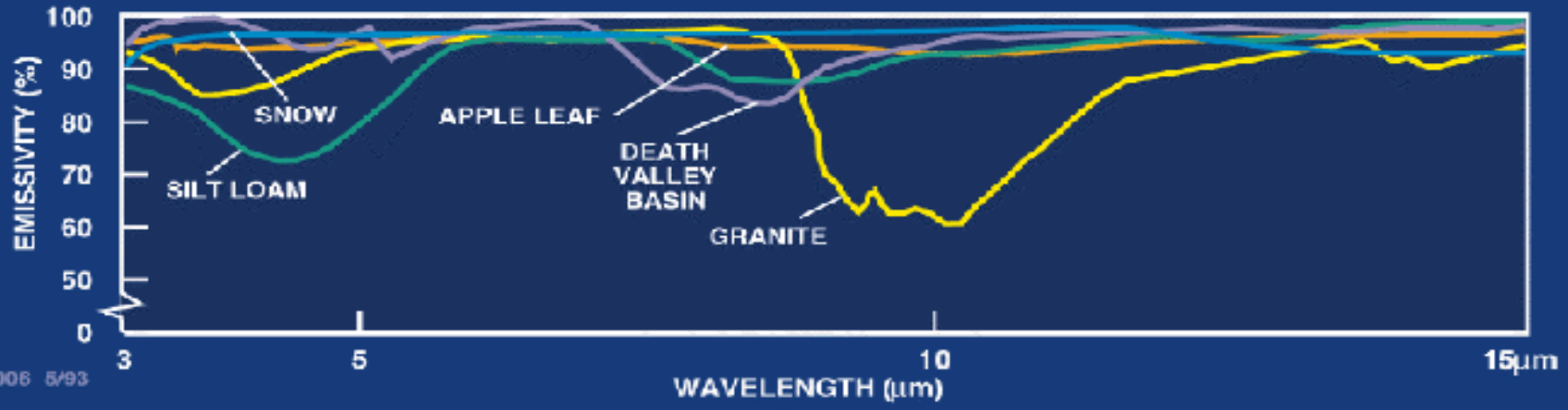

C351.006 5/93

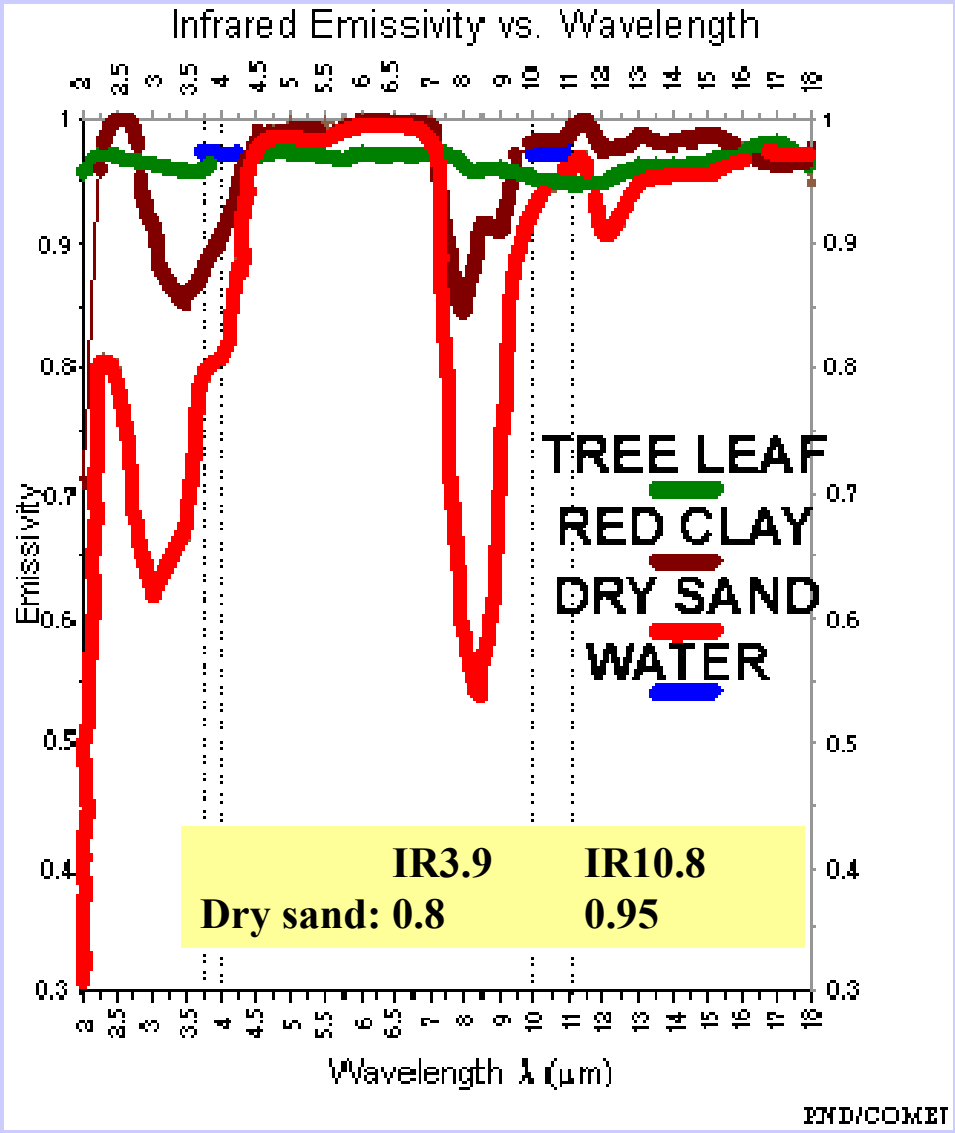

Emissivity as a function of wavelength and surface type

- Emissivity more variable near 3.9 μm
- Sandy areas appear 5-10 K cooler at IR3.9 than at IR10.8 (at night, dry atmosphere)
- Different appearance of land surfaces during daytime, depending on surface type

LAND-SOLAR RADIATION

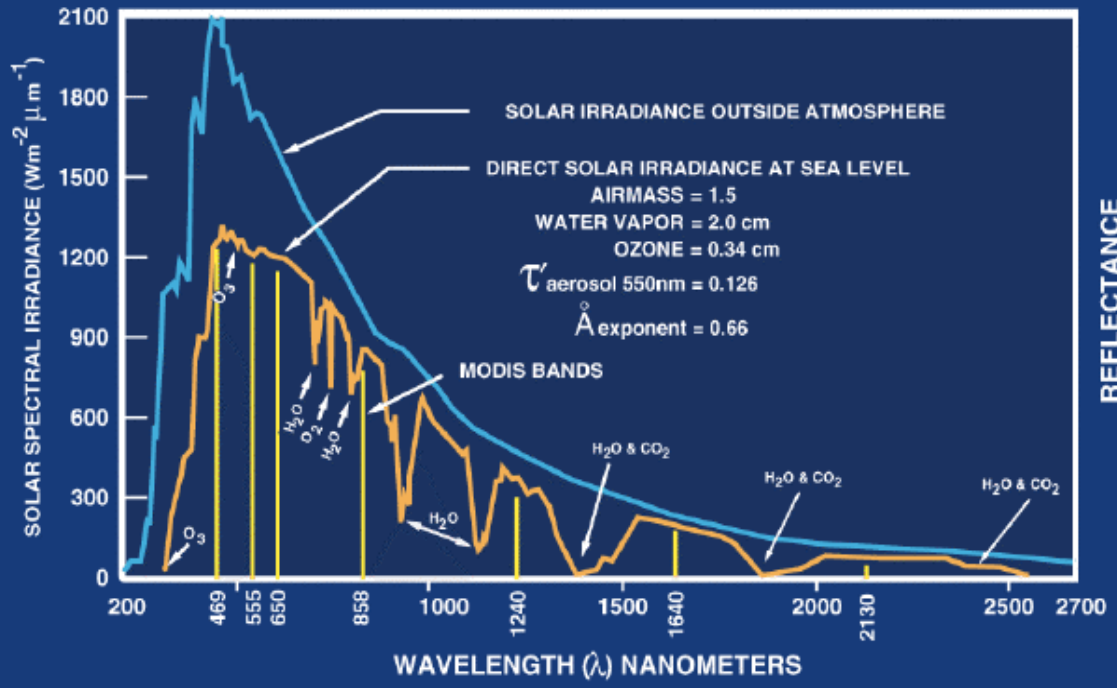

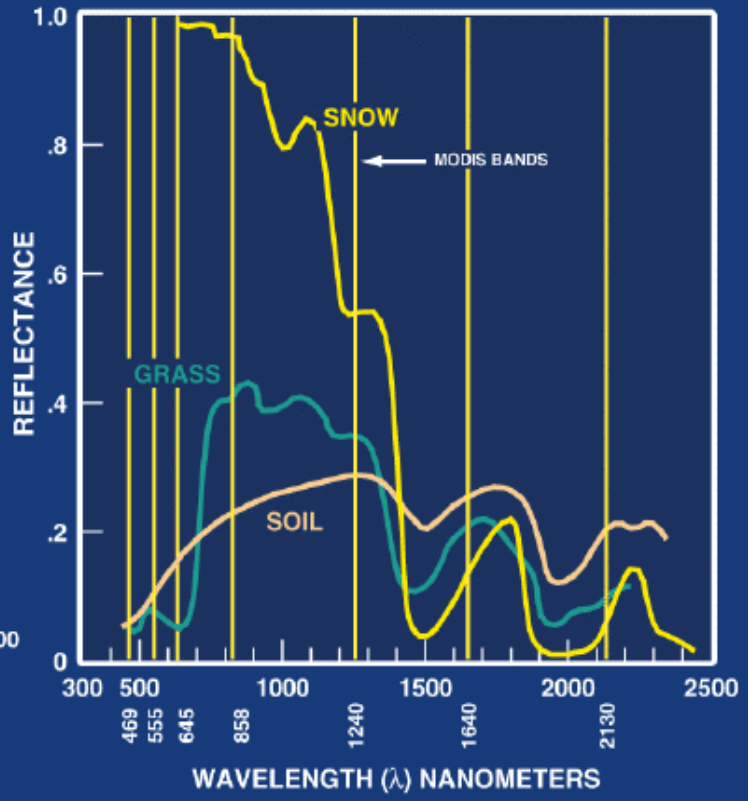

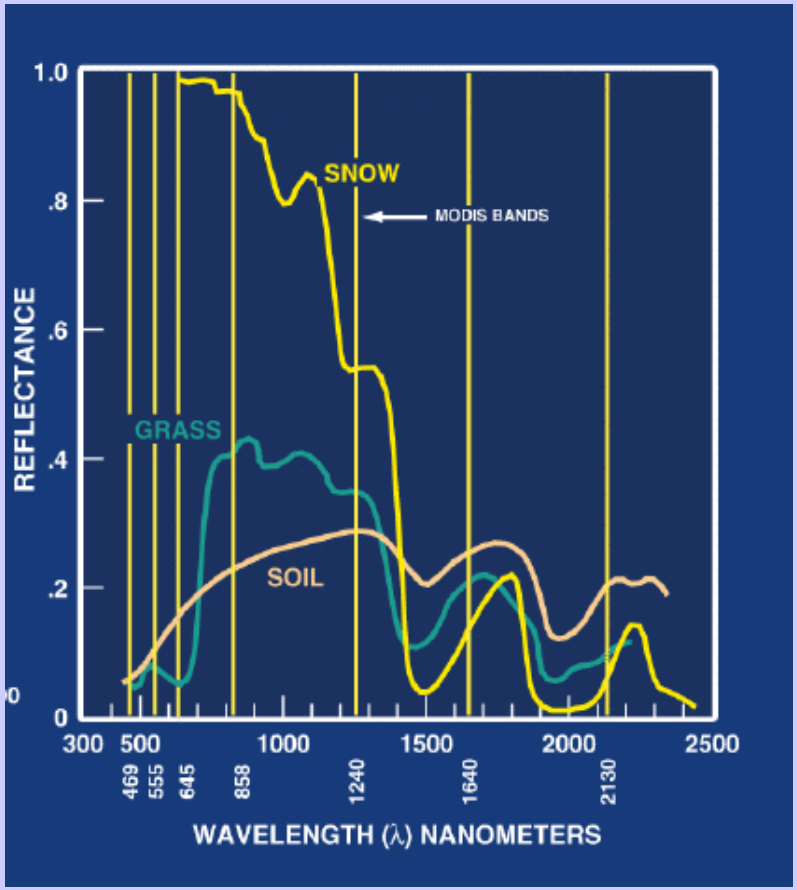

Investigating with Multi-spectral Combinations

Given the spectral response of a surface or atmospheric feature

Select a part of the spectrum where the reflectance or absorption changes with wavelength

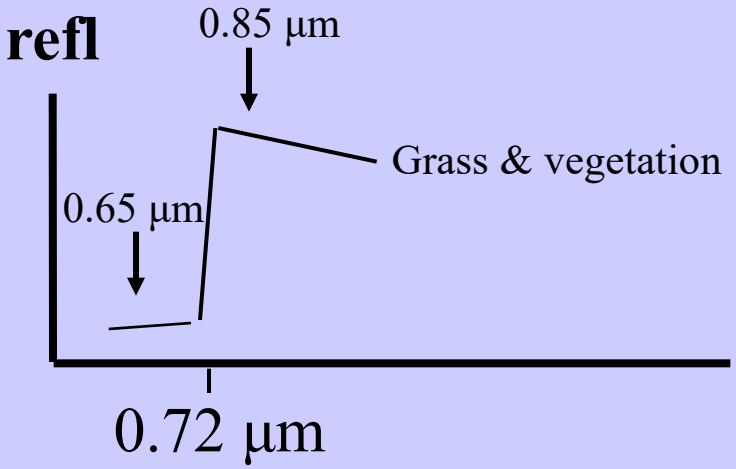

e.g. reflection from grass

If 0.65 μm and 0.85 μm channels see the same reflectance than surface viewed is not grass;
if 0.85 μm sees considerably higher reflectance than 0.65 μm then surface might be grass

AVIRIS Movie #2

AVIRIS Image - Porto Nacional, Brazil
20-Aug-1995
224 Spectral Bands: 0.4 - 2.5 μm
Pixel: 20m x 20m Scene: 10km x 10km

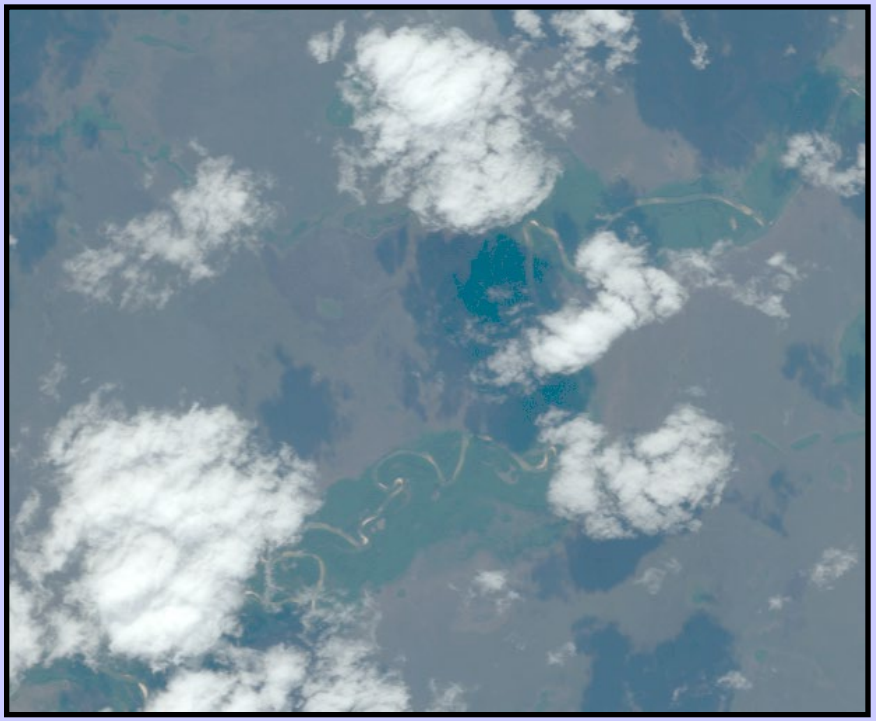

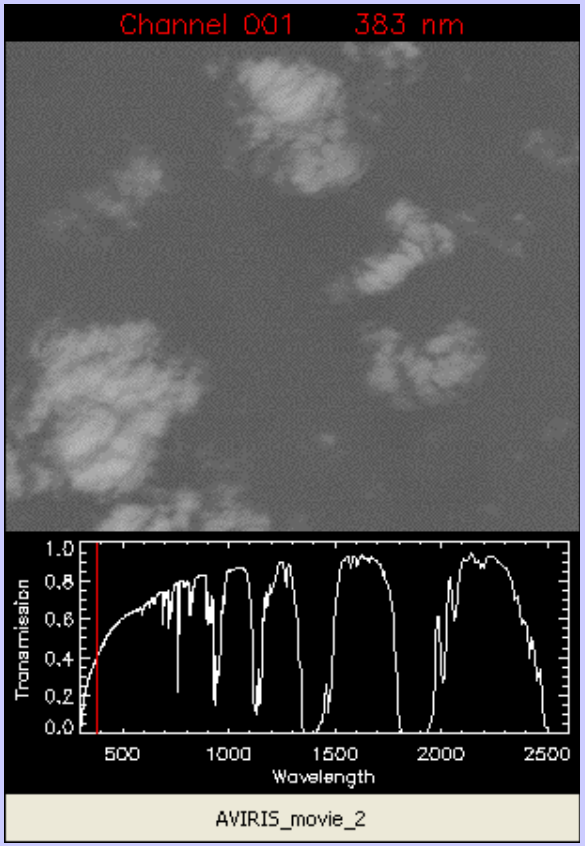

NDVI versus EVI

EVI is a useful proxy for 'greenness' or photosynthetically active vegetation in optically dense canopies, as found throughout the Amazon (LAI= 4 -7), by relying on the more sensitive NIR canopy reflectance which is less prone to saturate

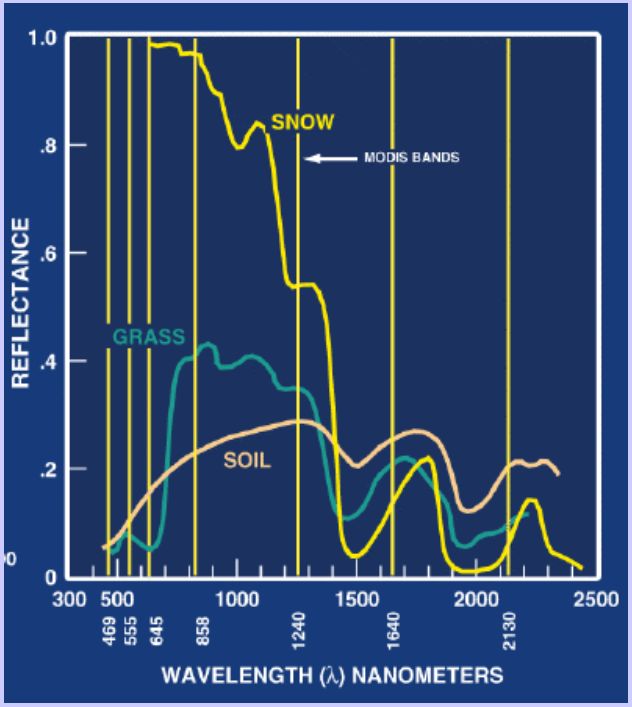

$$NDVI = (\rho 0.8 - \rho 0.6) / (\rho 0.8 + \rho 0.6)$$

$$EVI = 2.5 \times \frac{\rho_{NIR} - \rho_{red}}{1 + \rho_{NIR} + (6 \times \rho_{red} - 7.5 \times \rho_{blue})}$$

Basin-wide greening in dry season

October EVI (dry) minus June EVI (wet season) CMG

from Huete et al

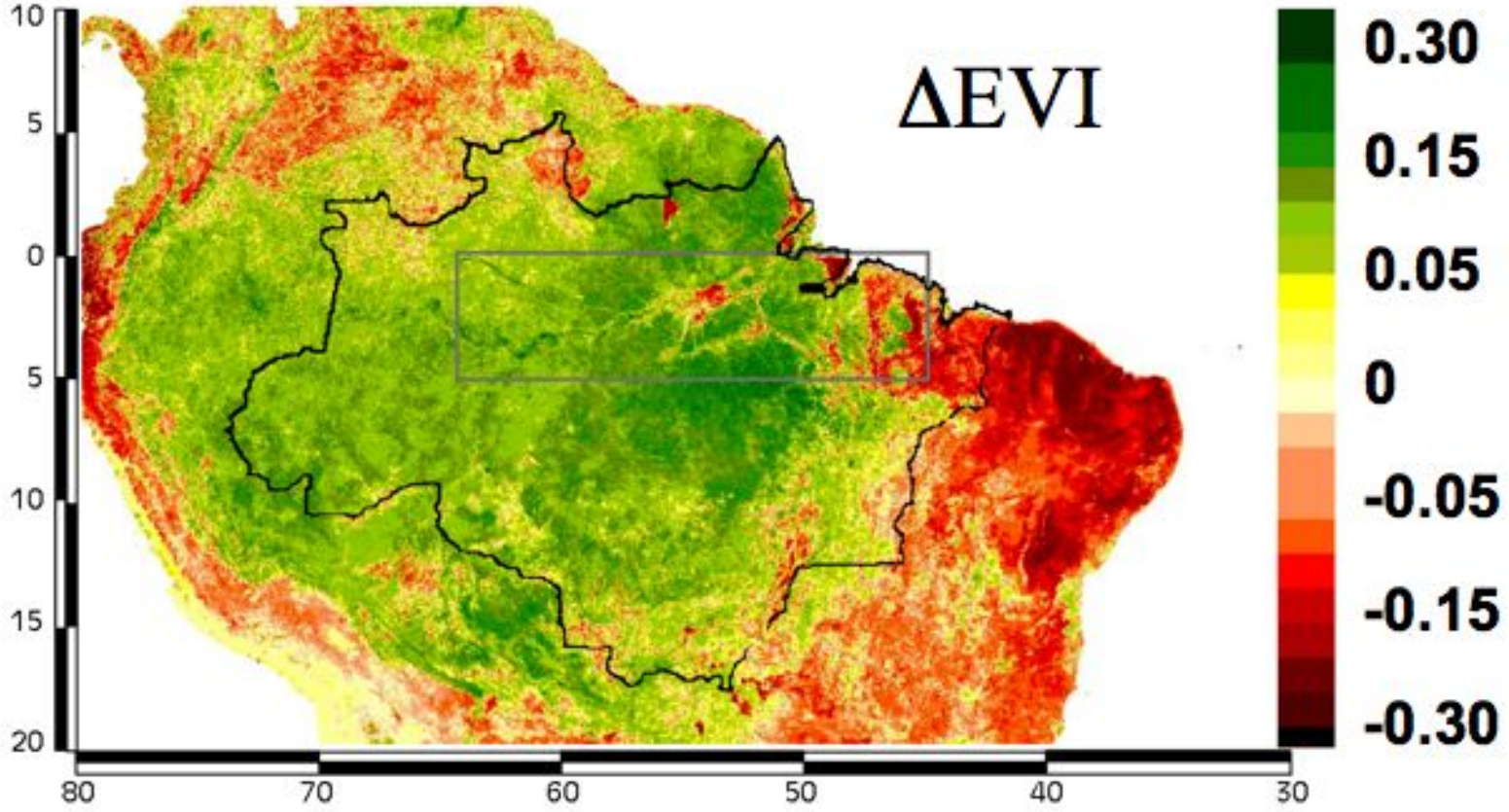

- green colors depict 'greening' and red colors depict 'browning' in the dry season

Spatially Explicit Behavior: Pattern

a

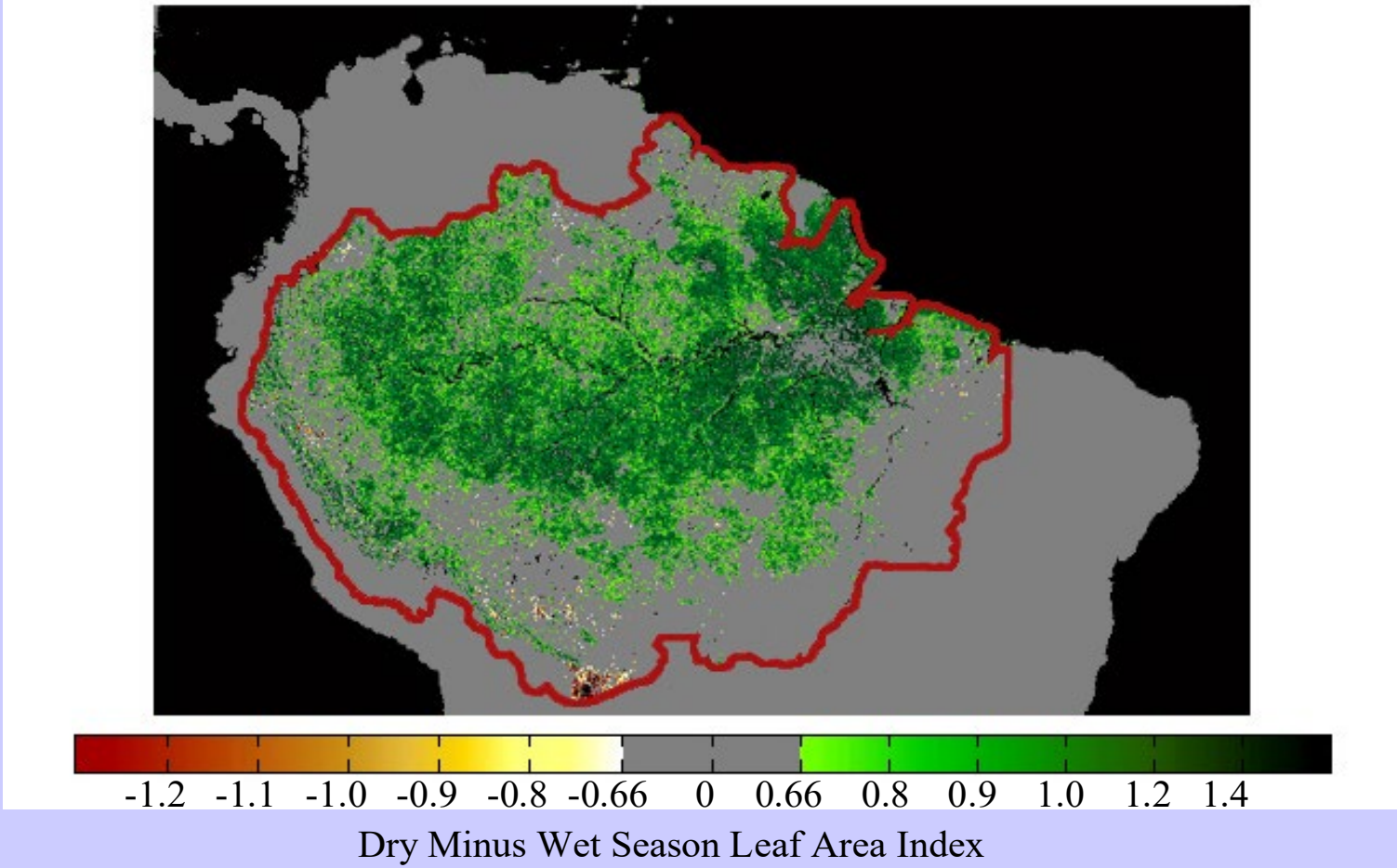

The derived spatial pattern of seasonal LAI amplitude reveals a heretofore unknown picture of phenology over a broad contiguous swath of land, anchored to the Amazon river, from its mouth in the east to its western-most reaches in Peru, in the heart of the basin.

Spatially Averaged Behavior: LAI Amplitude

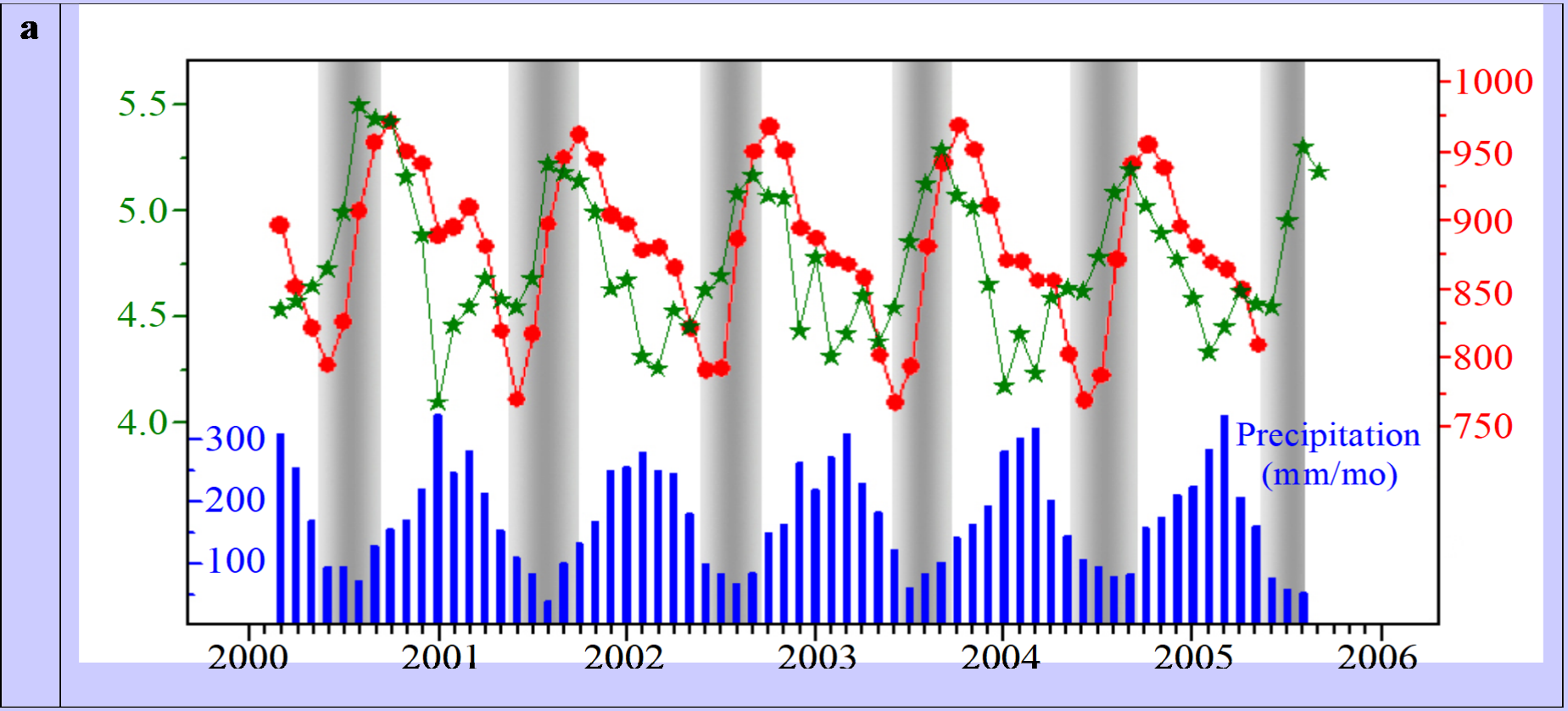

- **Leaf area data of the Amazon rainforests exhibit *notable seasonality*, with an amplitude (peak to trough difference) that is about 25% of the average annual LAI of 4.7, over the entire course of the data record. (from Myneni et al.)**

Example with MODIS

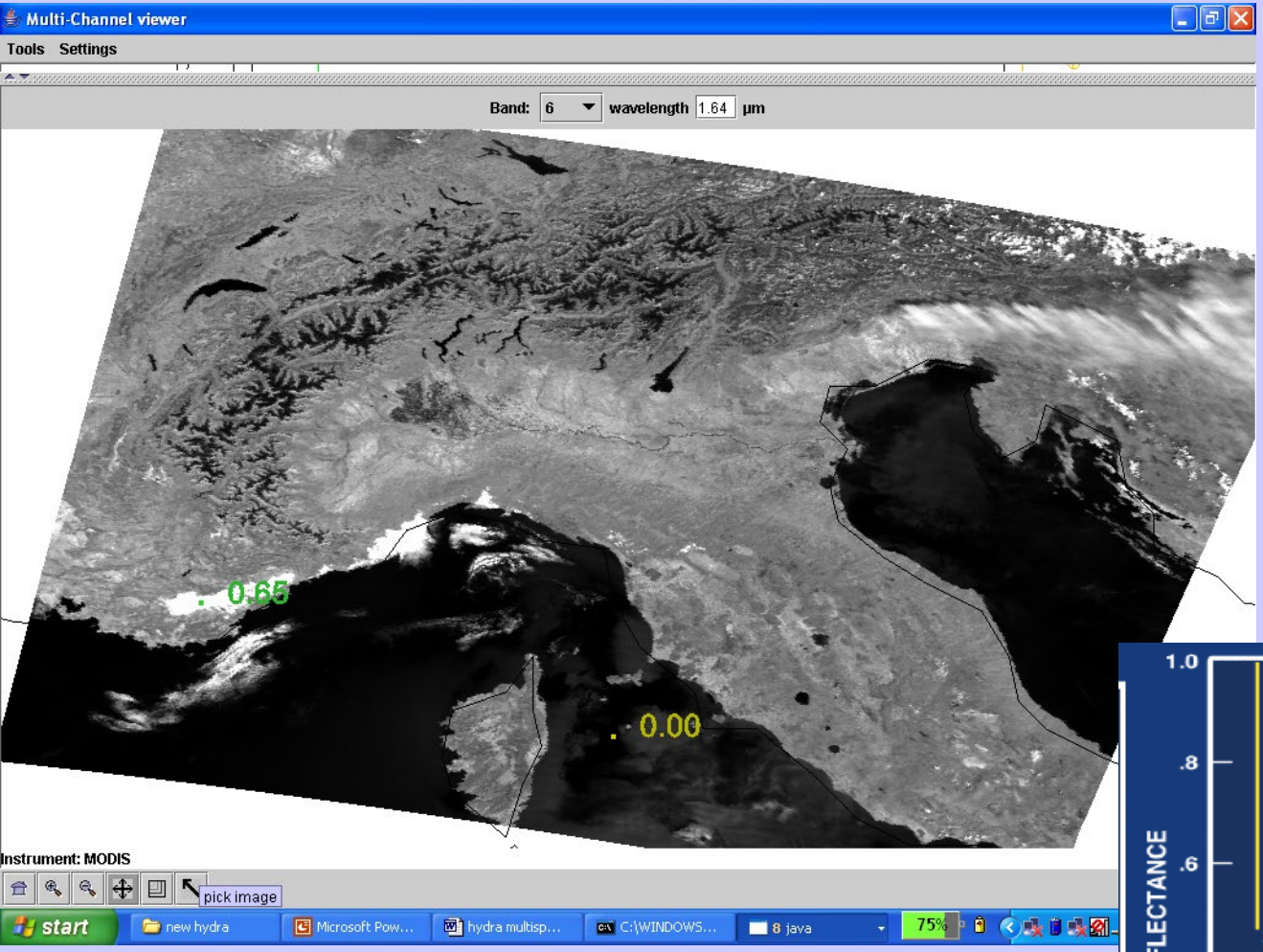

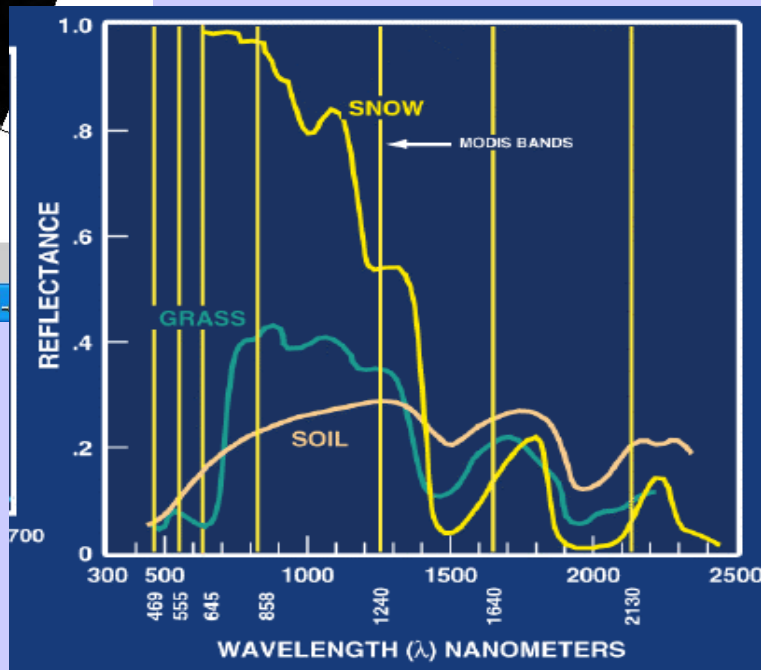

low refl at 1.6 um from snow in mountains

MODIS scatterplot of r1.6 (y-axis) and BT11 (x-axis)

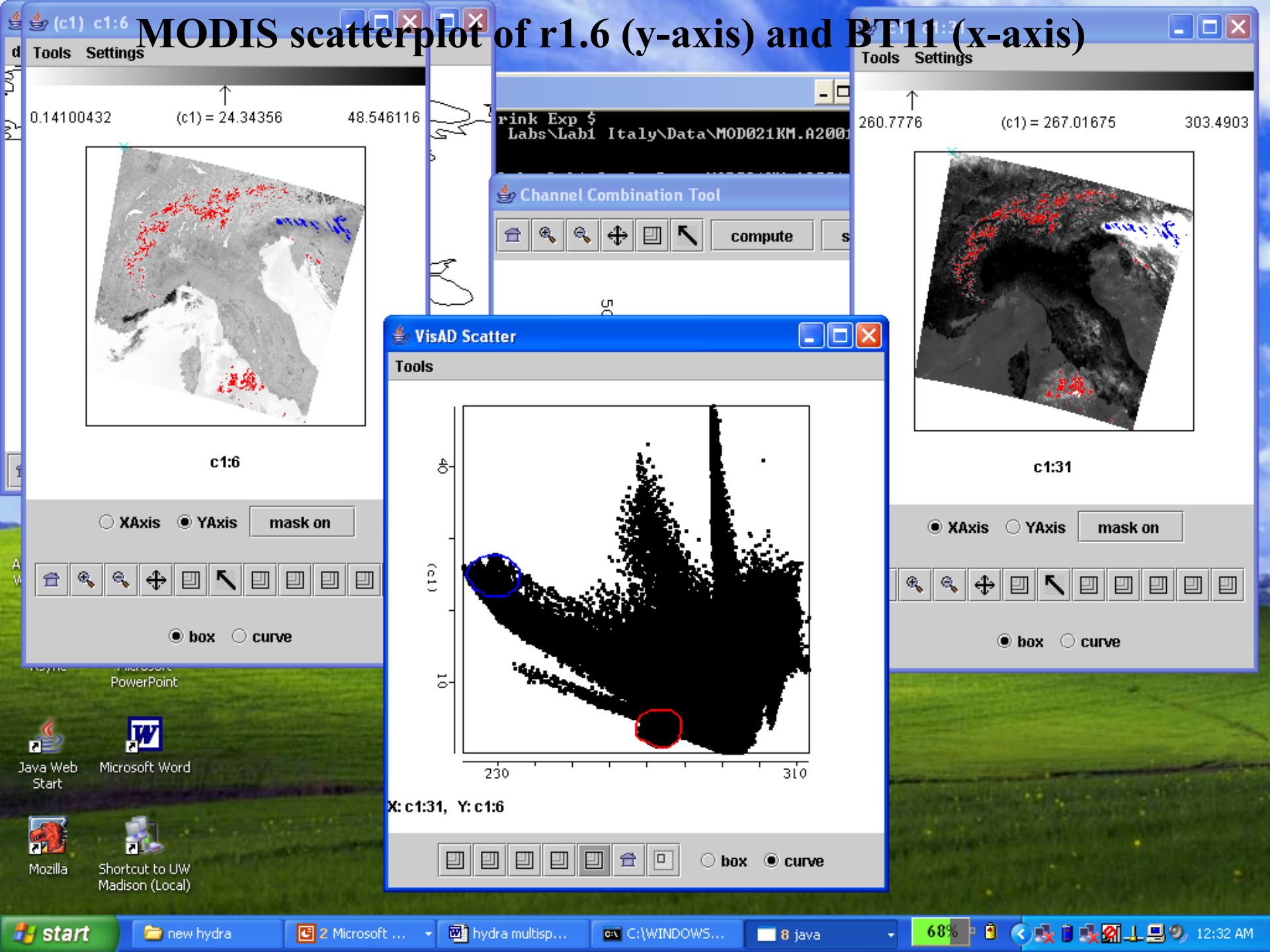

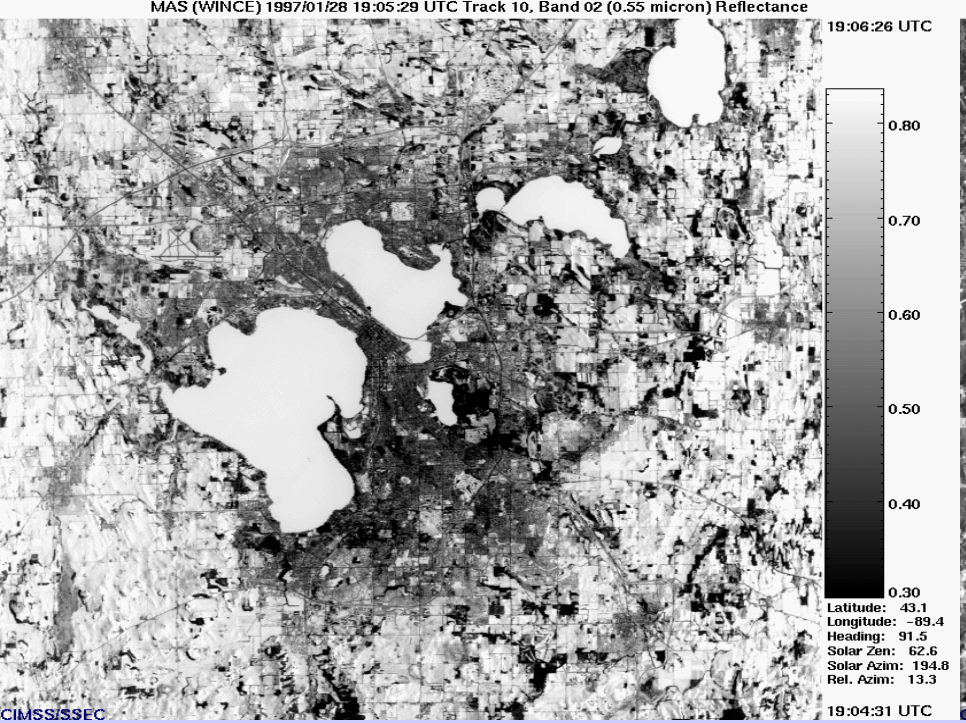

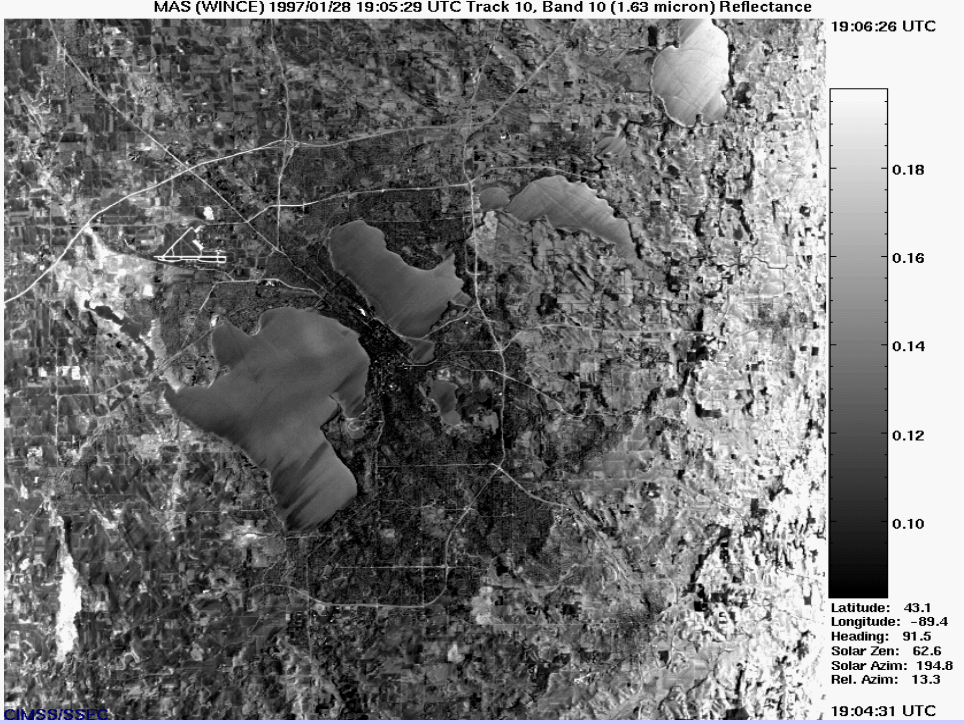

MODIS Airborne Simulator (MAS)
0.6, 1.6, & 11.0 um data over Madison in Jan 97

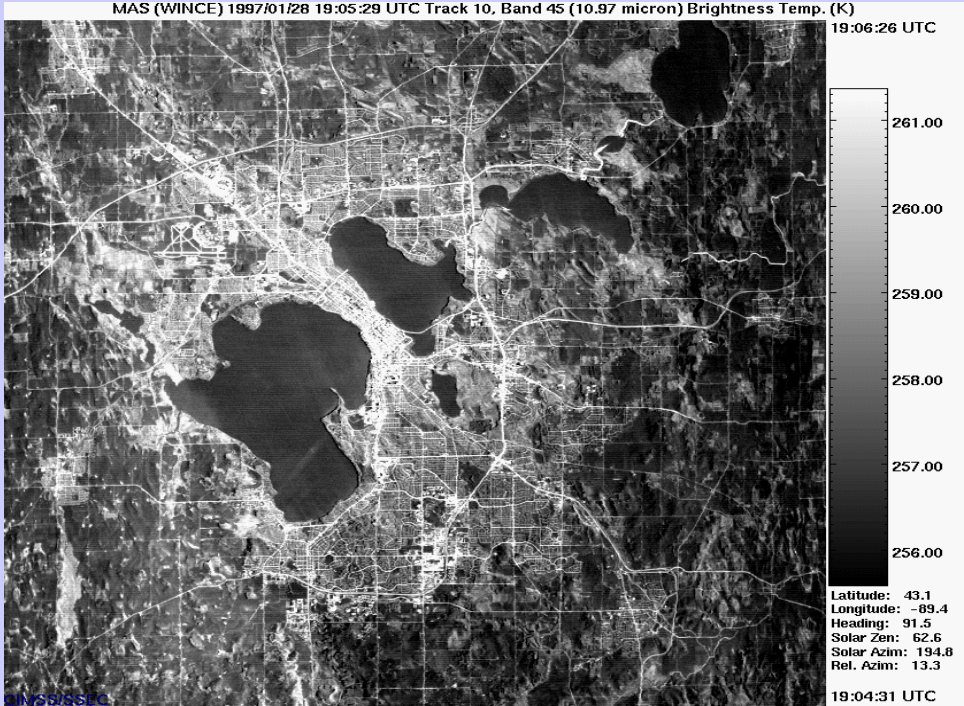

MODIS Image and snow map - November 3, 2000

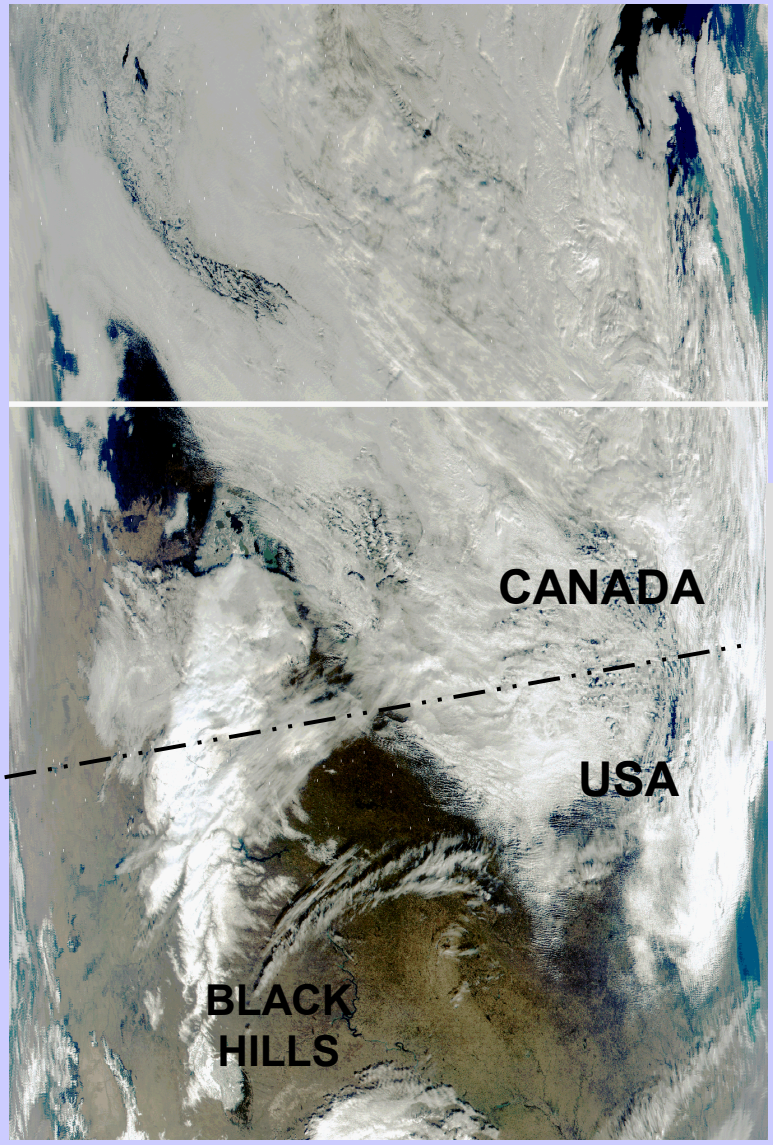

MODIS bands 1, 4, 3

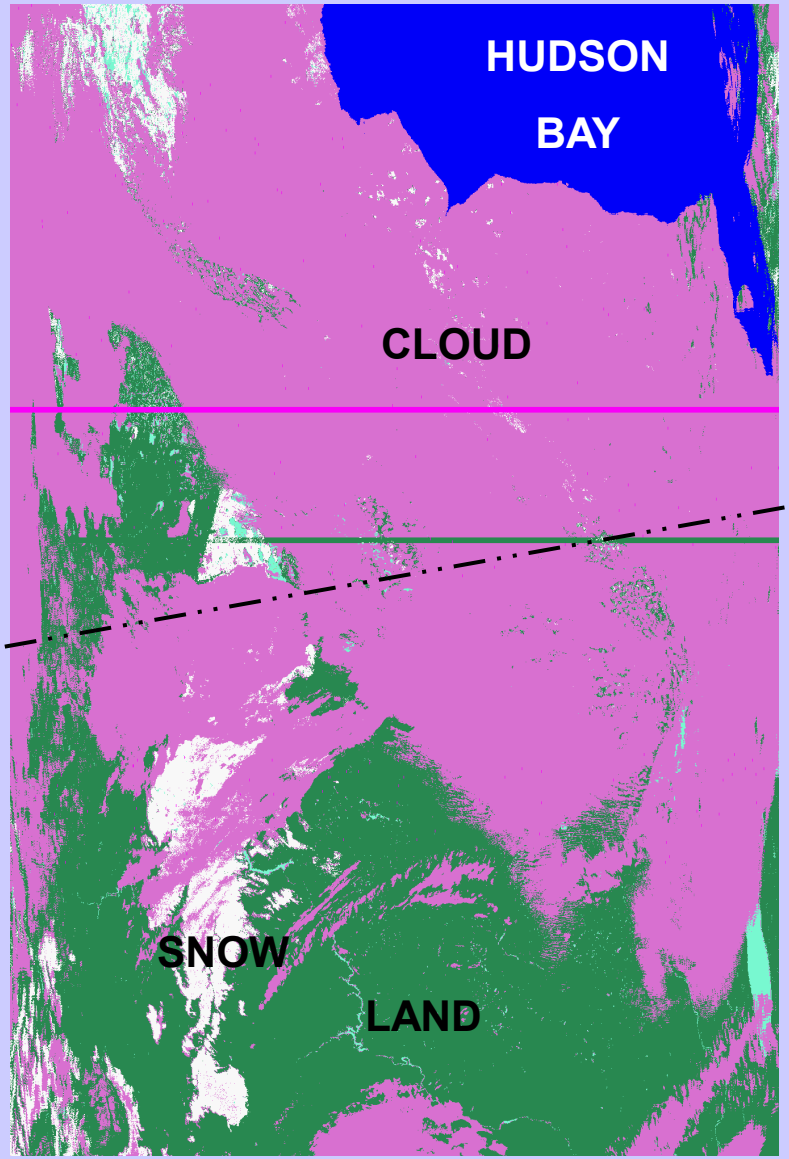

9.0 million sq. km of snow cover

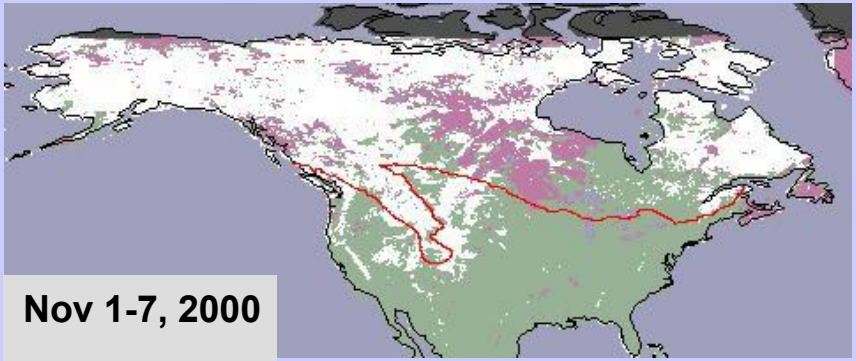

10.8 million sq. km of snow cover

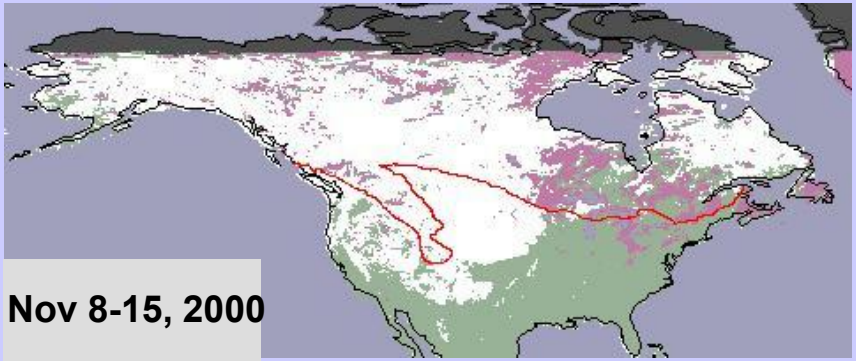

Change in maximum snow extent between two composite periods seen above (1.8 million sq. km)

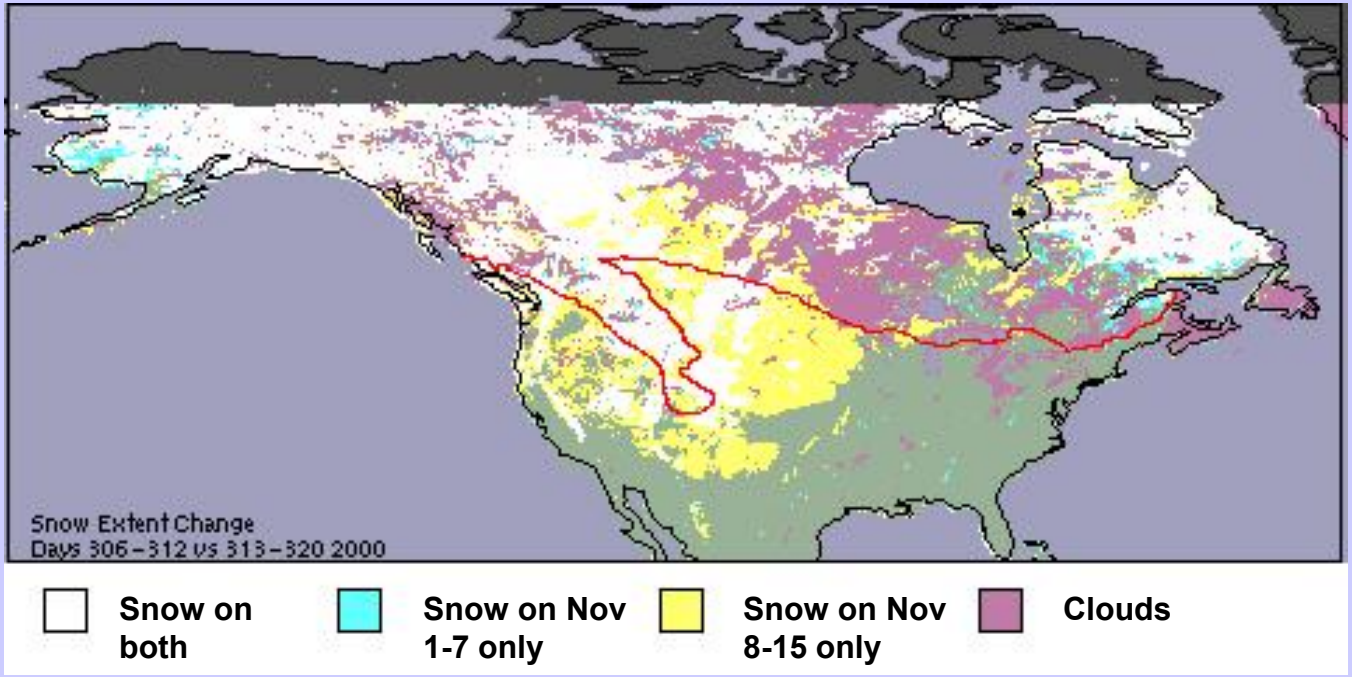

Observing Sea Ice Leads With MODIS

MODIS Band 1 Image of Western Arctic, 1 km (subsampled)

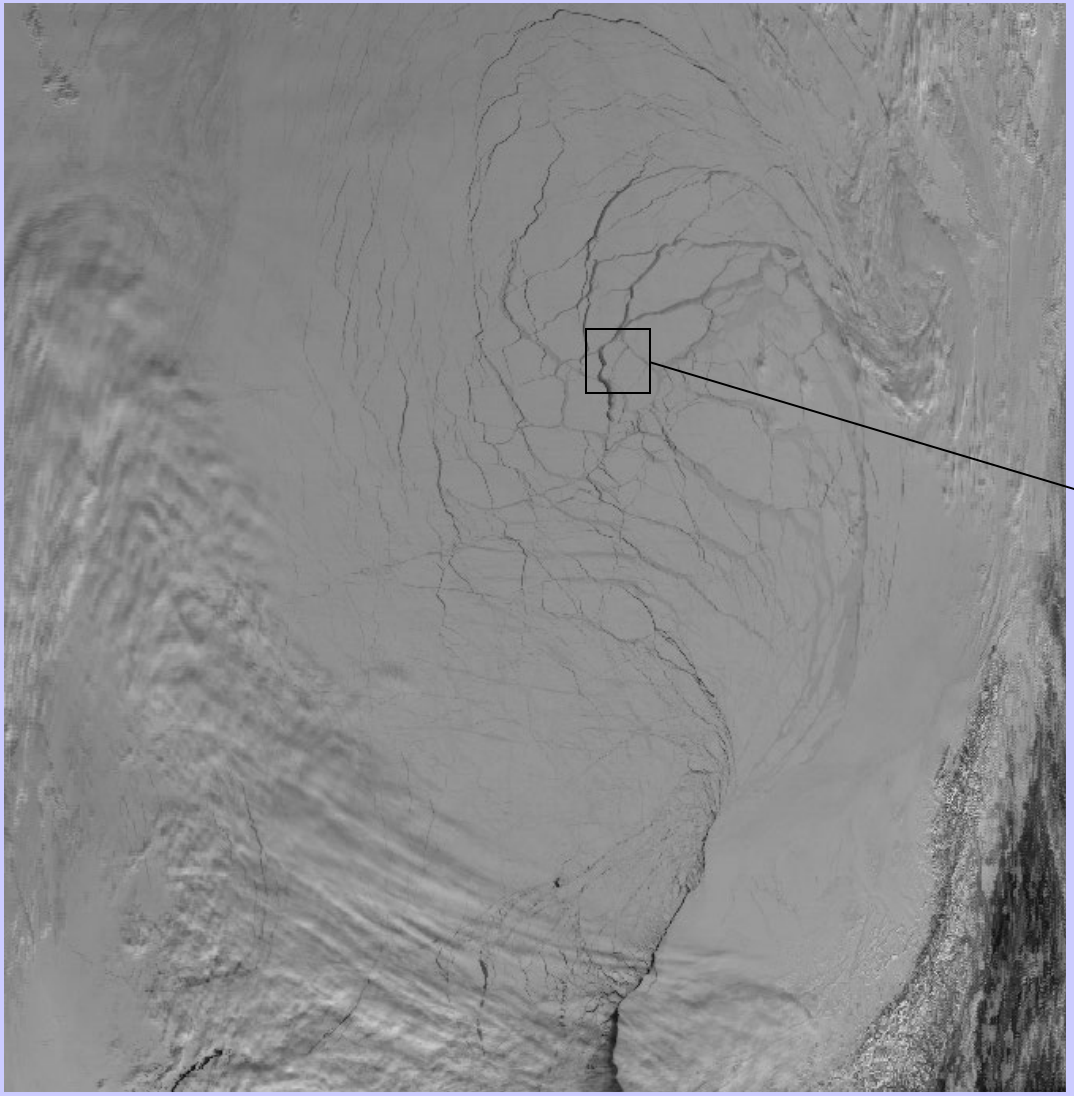

MODIS Full Resolution, 250 m Pixels

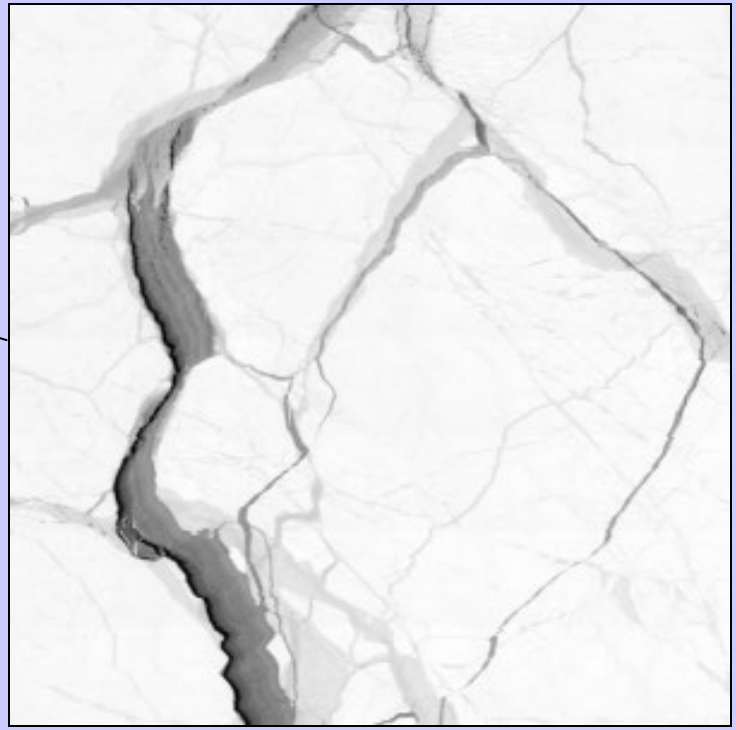

Aerosol Types and Origin

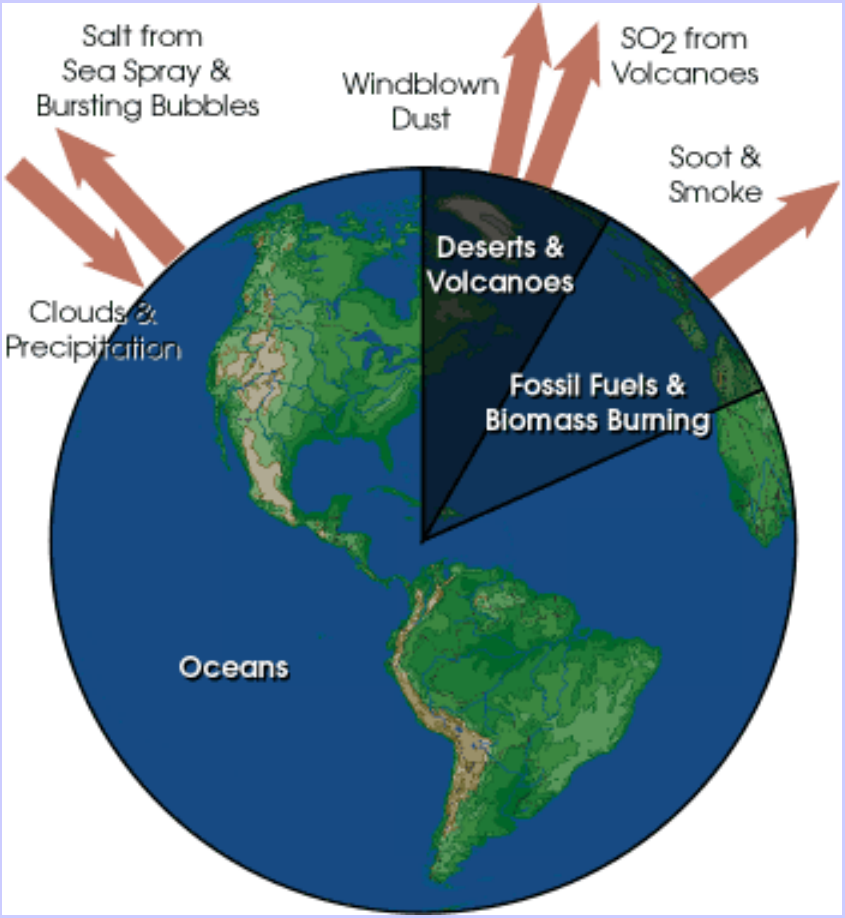

- Aerosol particles larger than about 1 μm in size are produced by windblown dust and sea salt from sea spray and bursting bubbles
- Aerosols smaller than 1 μm are mostly formed by condensation processes such as conversion of sulfur dioxide (SO2) gas (released from volcanic eruptions) to sulfate particles and by formation of soot and smoke during burning processes.
- After formation, aerosols are mixed and transported by atmospheric motions and are primarily removed by clouds and precipitation.

Aerosol Size Distribution

There are 3 modes :

- « **nucleation** »: radius is between 0.002 and 0.05 µm. They result from combustion processes, photo-chemical reactions, etc.

- « **accumulation** »: radius is between 0.05 µm and 0.5 µm. Coagulation processes.

- « **coarse** »: larger than 1 µm. From mechanical processes like aeolian erosion.

« fine » particles (nucleation and accumulation) result from anthropogenic activities, coarse particles come from natural processes.

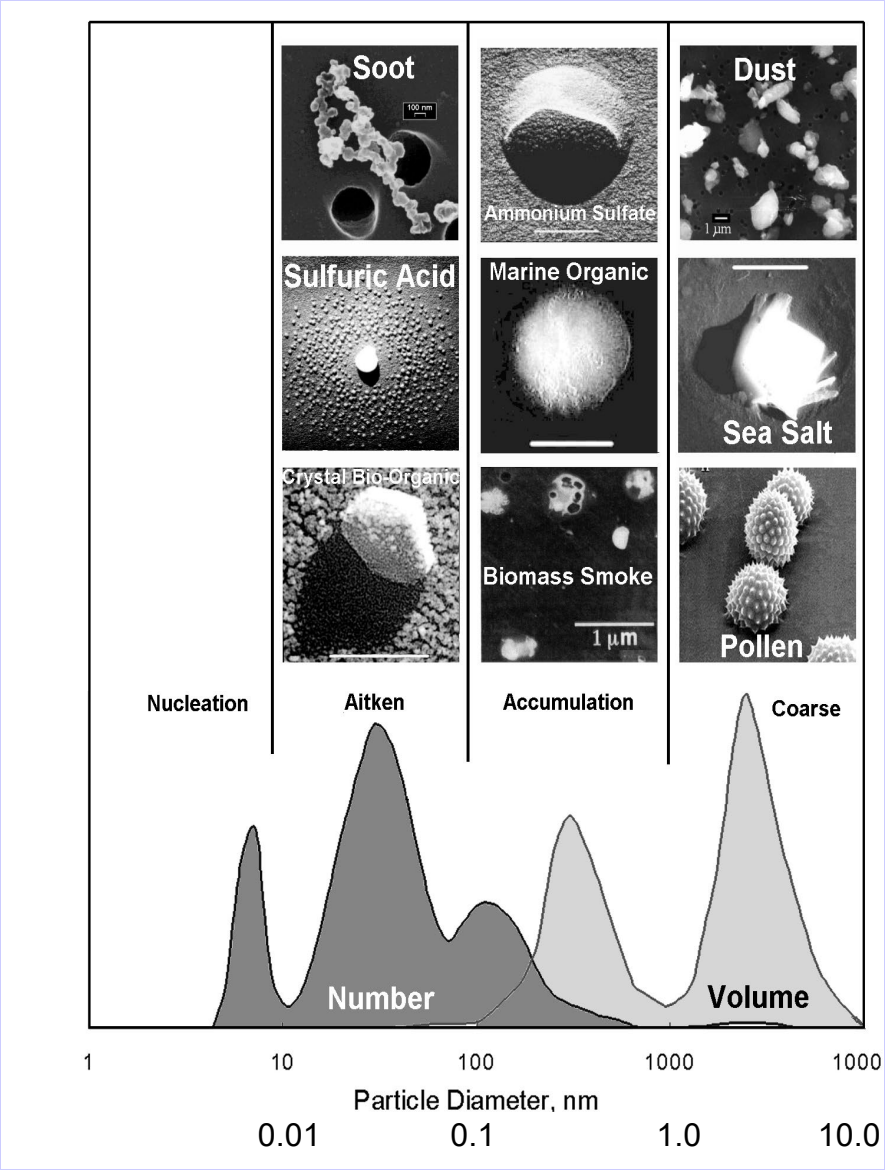

Pollution off Northeast United States (08/14/02)

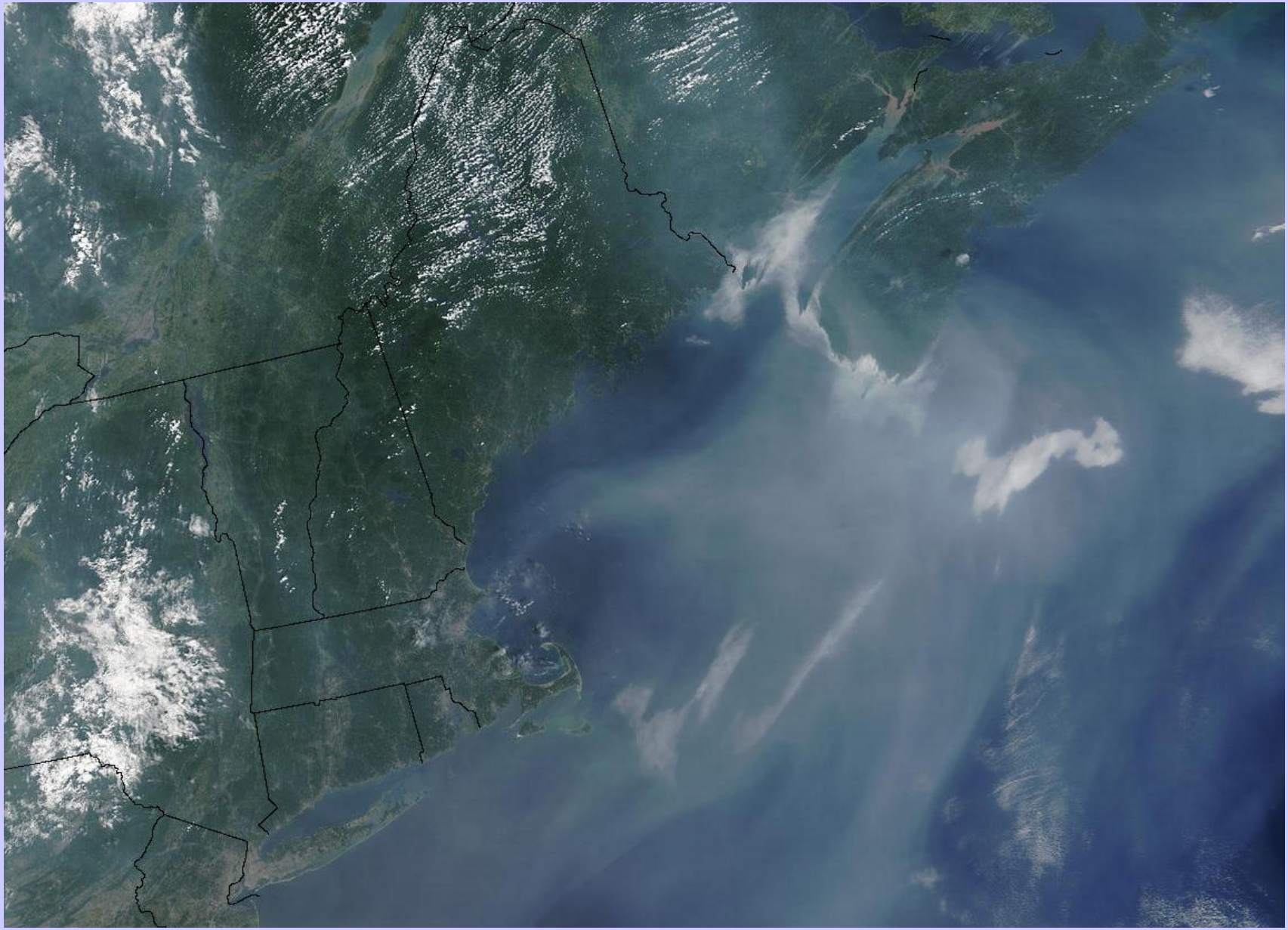

True color composite

AOT (0.55 um)

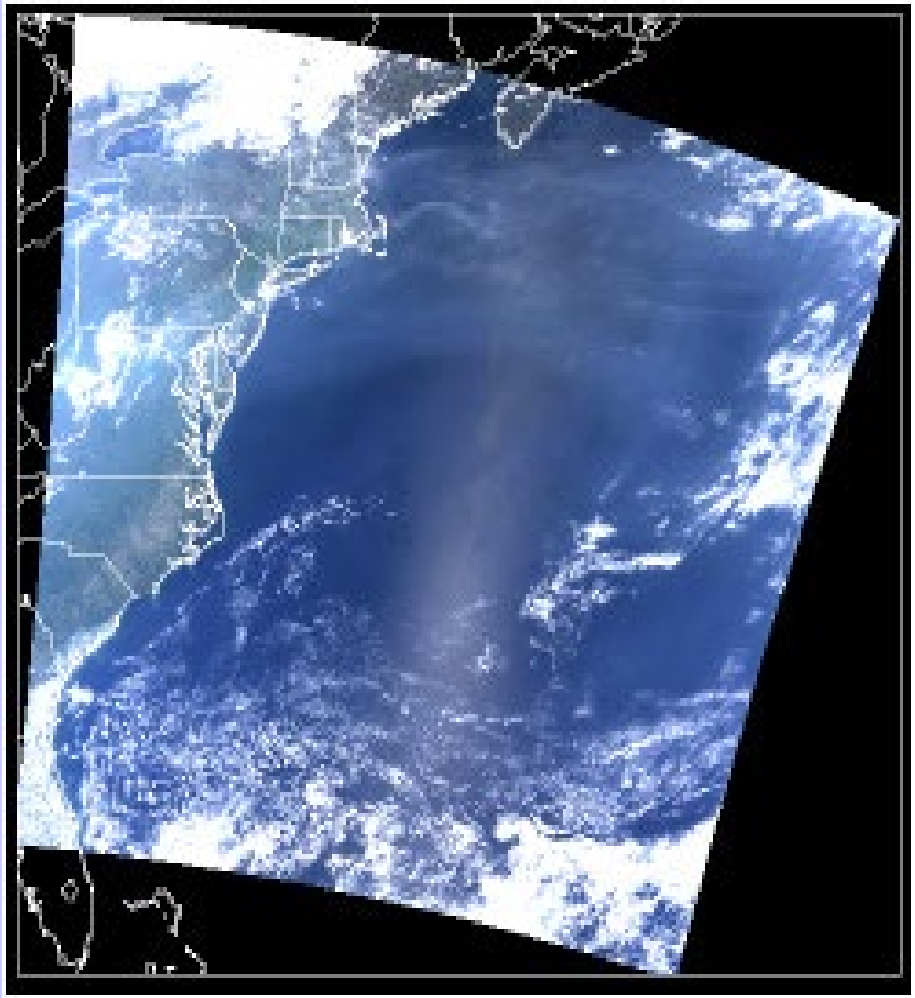

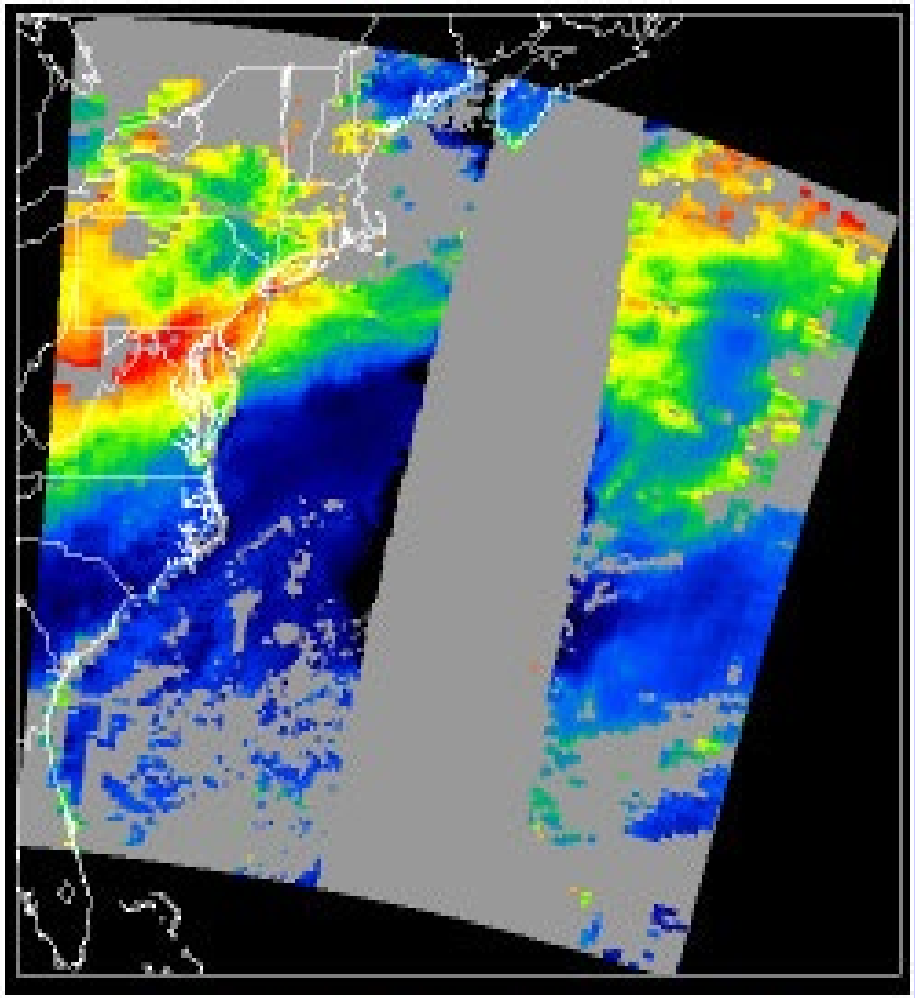

Ohio Valley pollution heading over N. Atlantic

τ_a (0.56 µm)

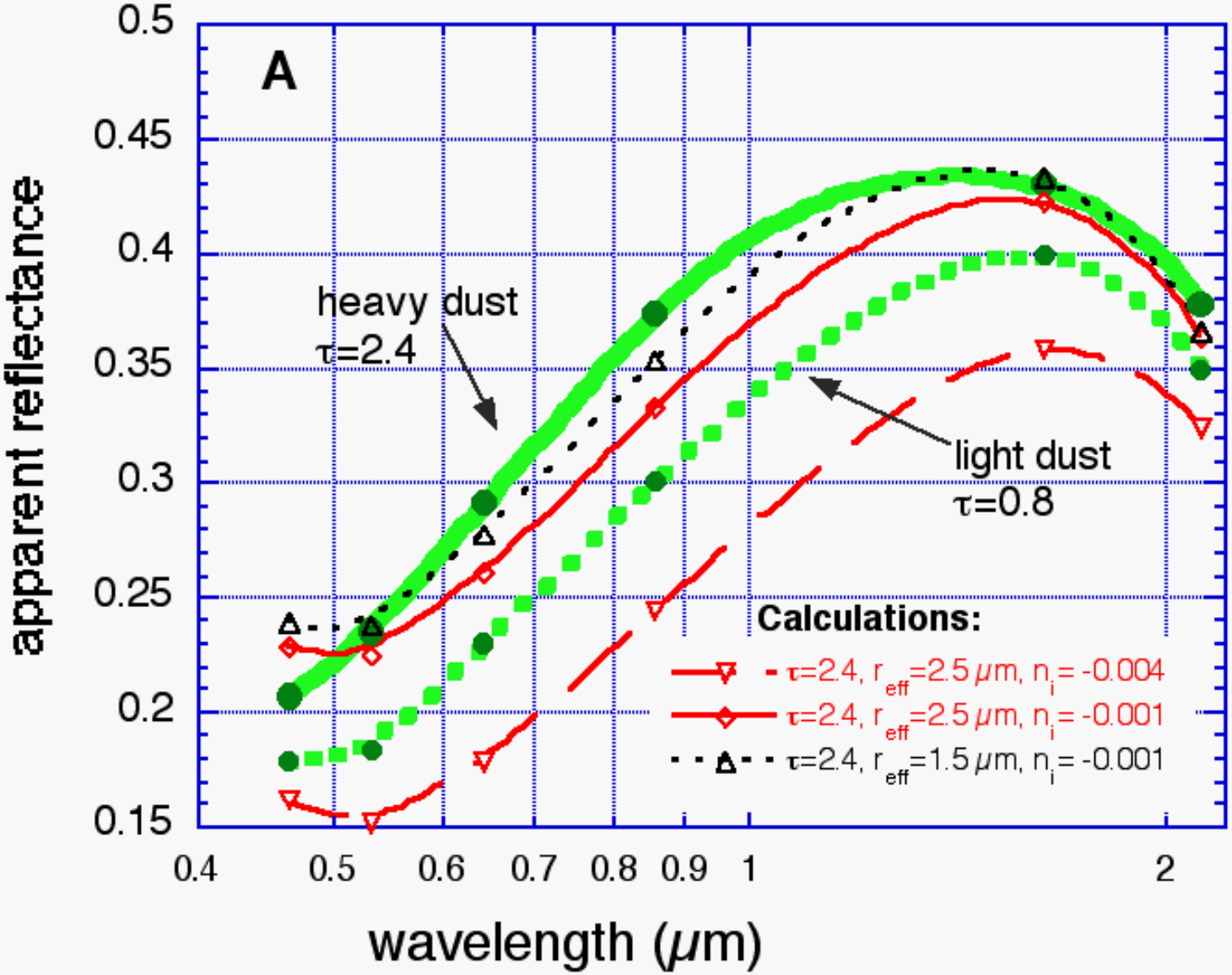

Dust brightens the already bright desert. There is no way to explain it with large absorption in the red to near-IR

Effect of aerosol on climate:

Cooling past climates, possibly warming future climates

Effect of aerosol on hydrologic cycle:

Less evaporation from cooler land and ocean, more stable atmosphere, less clouds and precipitation.

Effect of aerosol on health:

May be more important then ozone in causing cancer and heart problems.

Effect on agriculture, vegetation:

Shift of precipitation away from polluted land, less sunlight to vegetation

Does Population cause Pollution ?

POLDER aerosol index Feb. 1997 & population density

(Kaufman, Tanré & Boucher, Nature 2002)

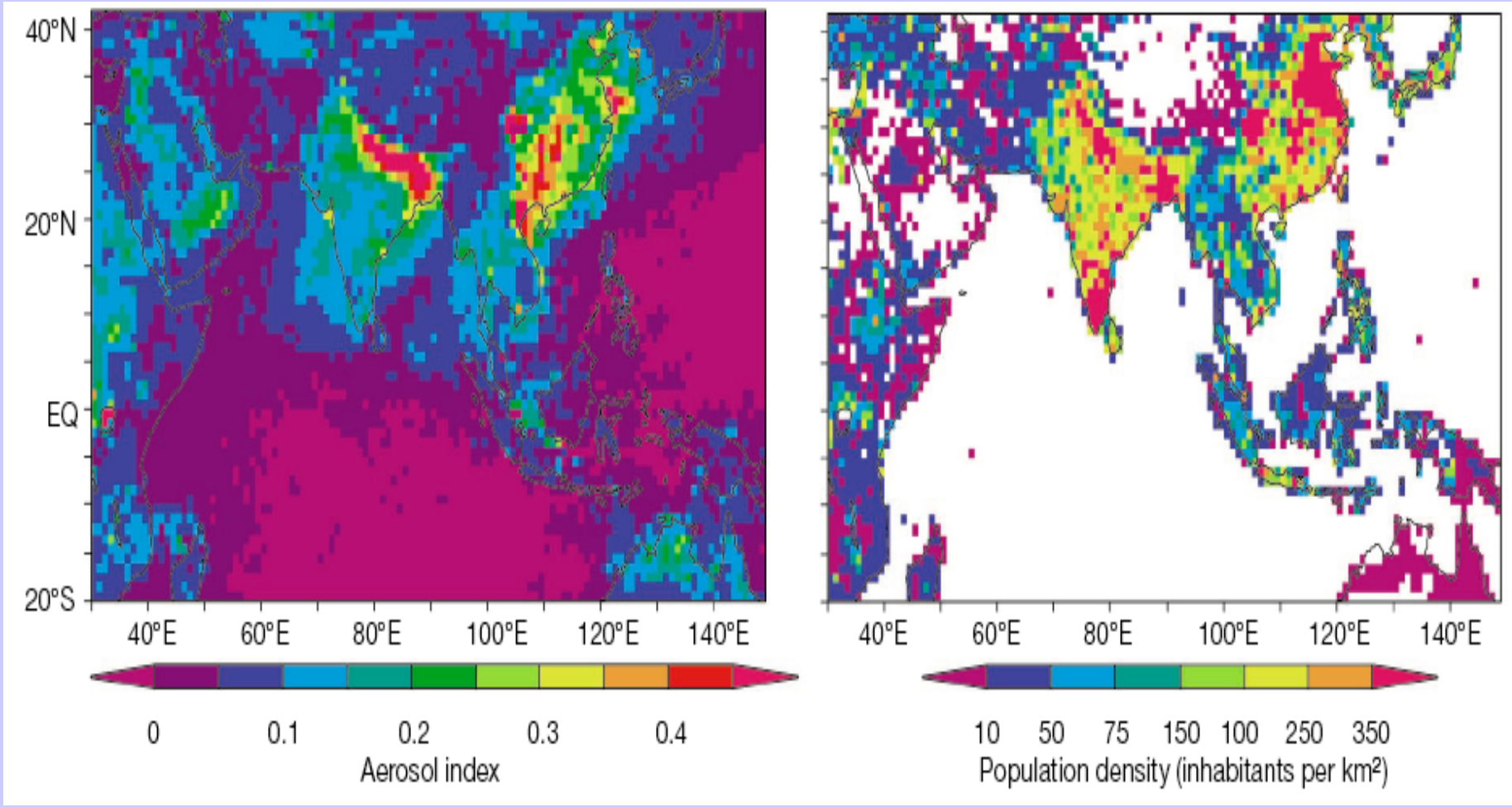

Aerosol Optical Thickness
(Coarse Particle Mode)

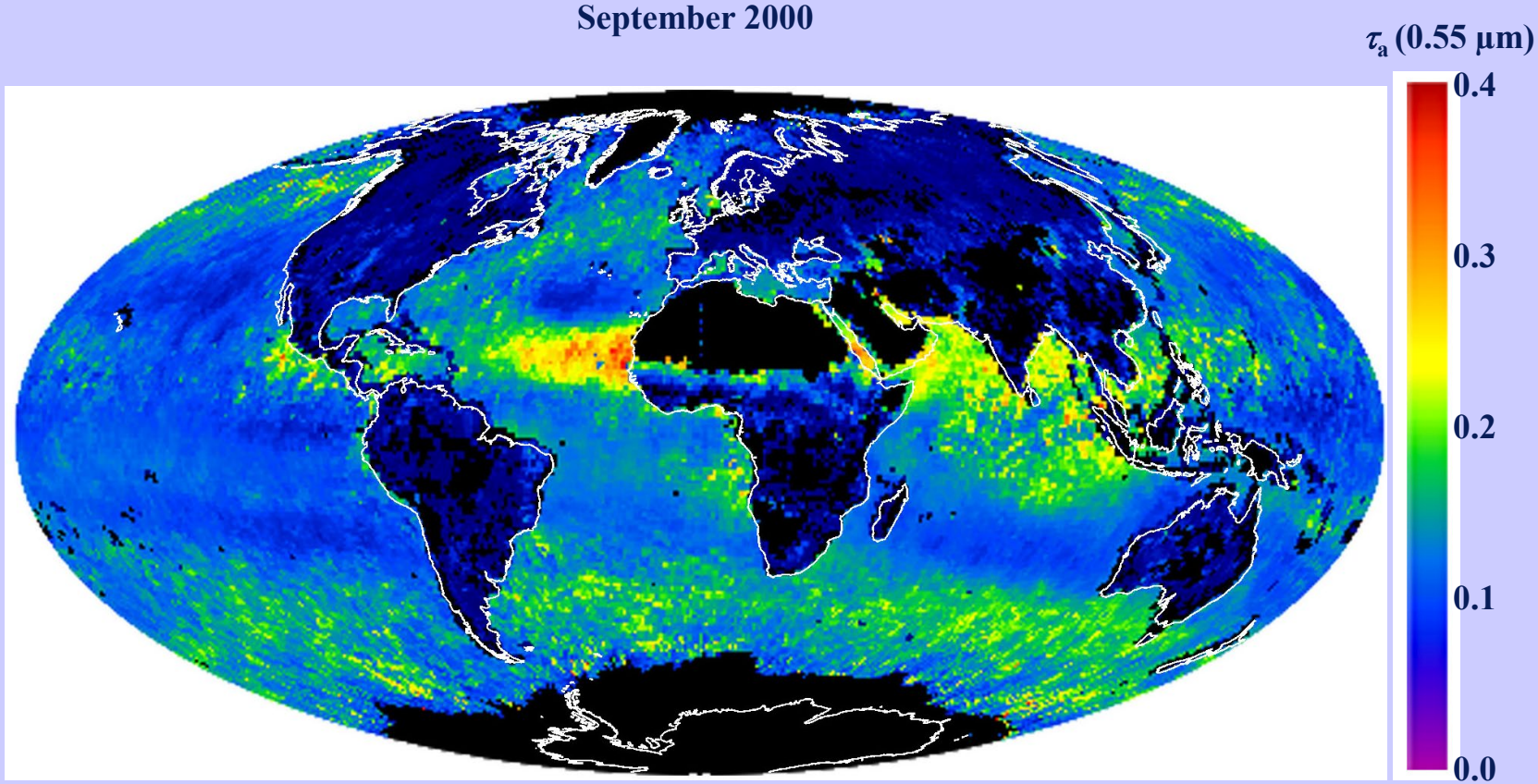

bands for aerosol retrieval over ocean (550, 660, 865, 1230, 1640, 2130 nm)

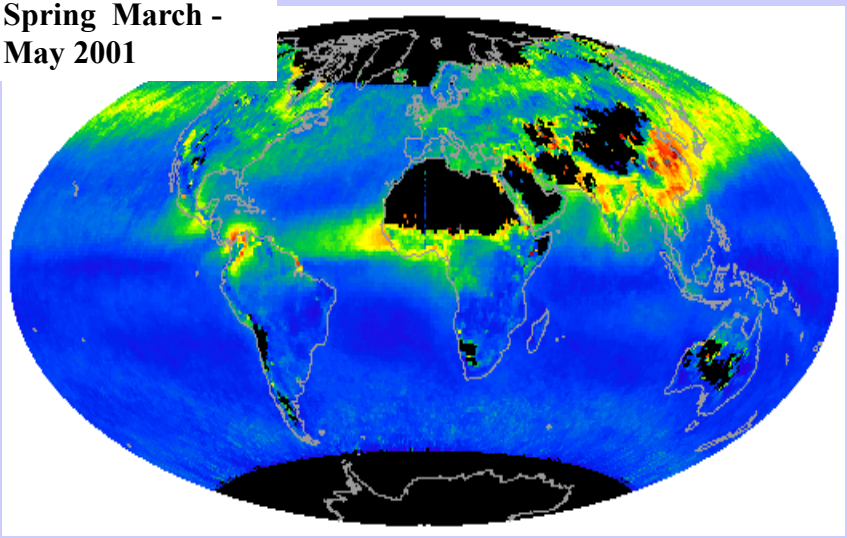

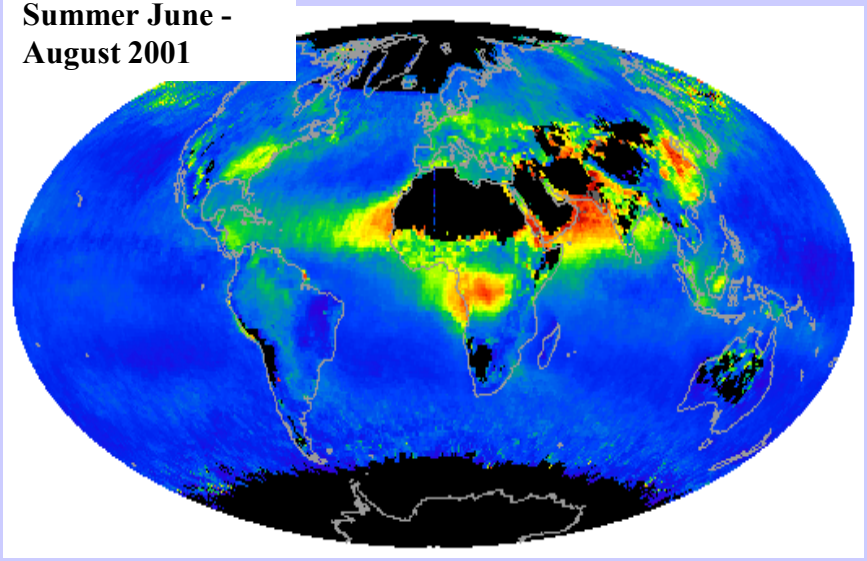

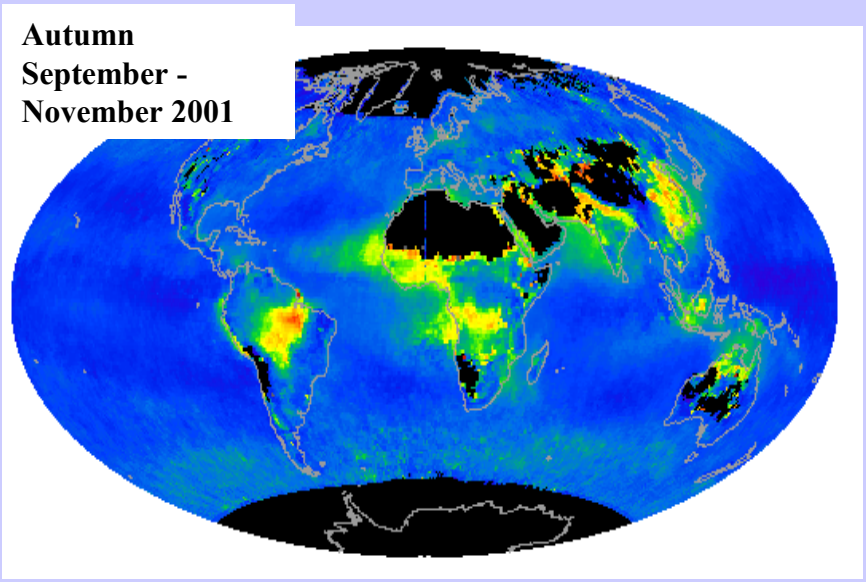

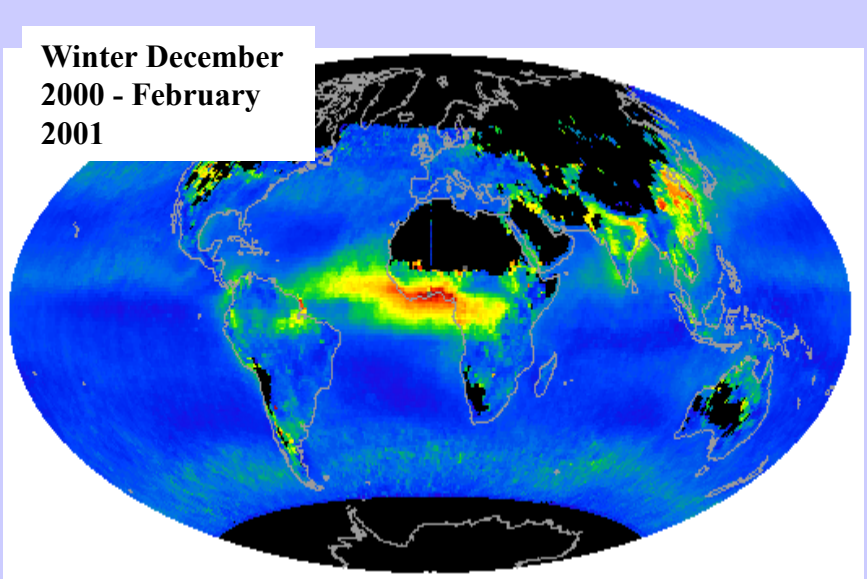

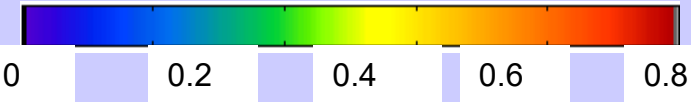

Average optical thickness

Global aerosol AOT trends

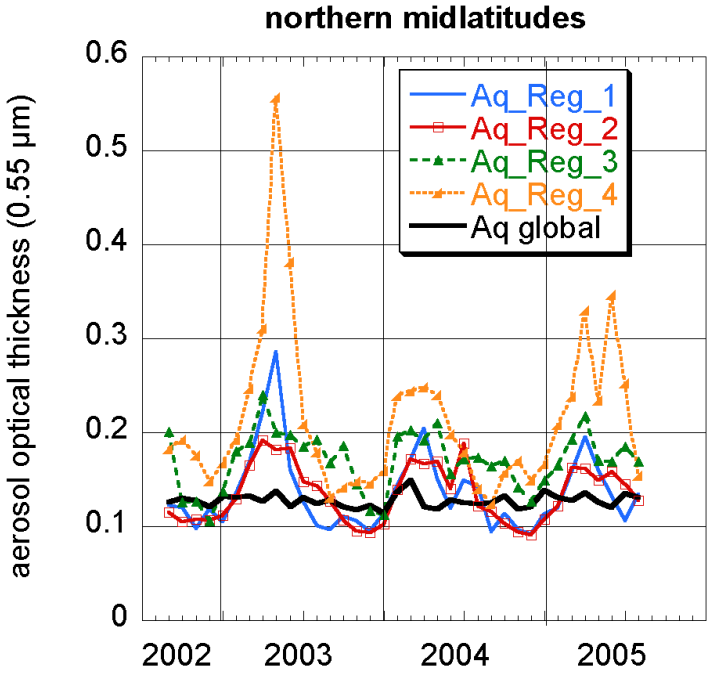

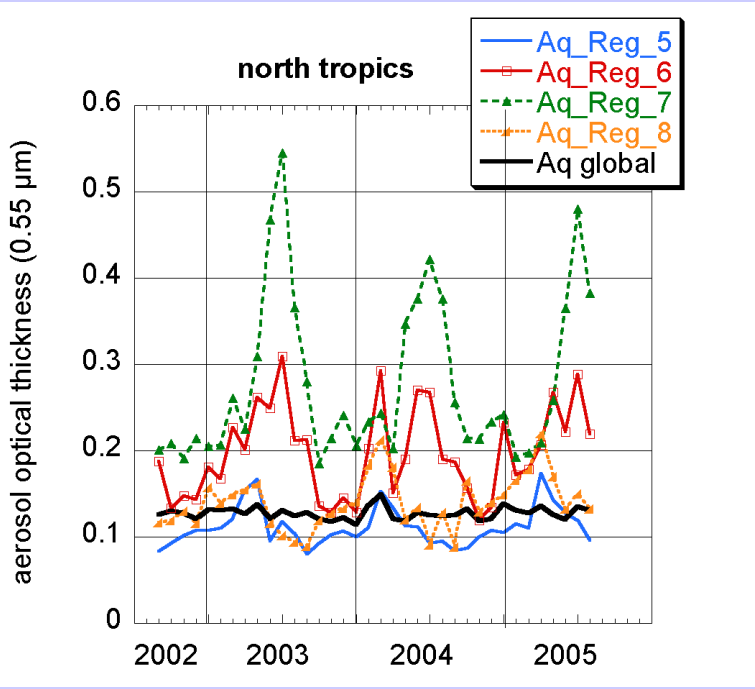

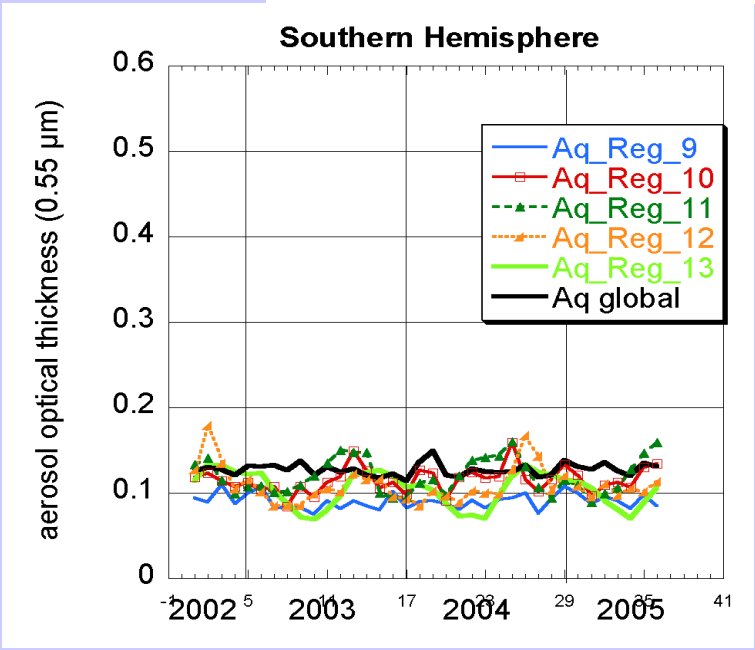

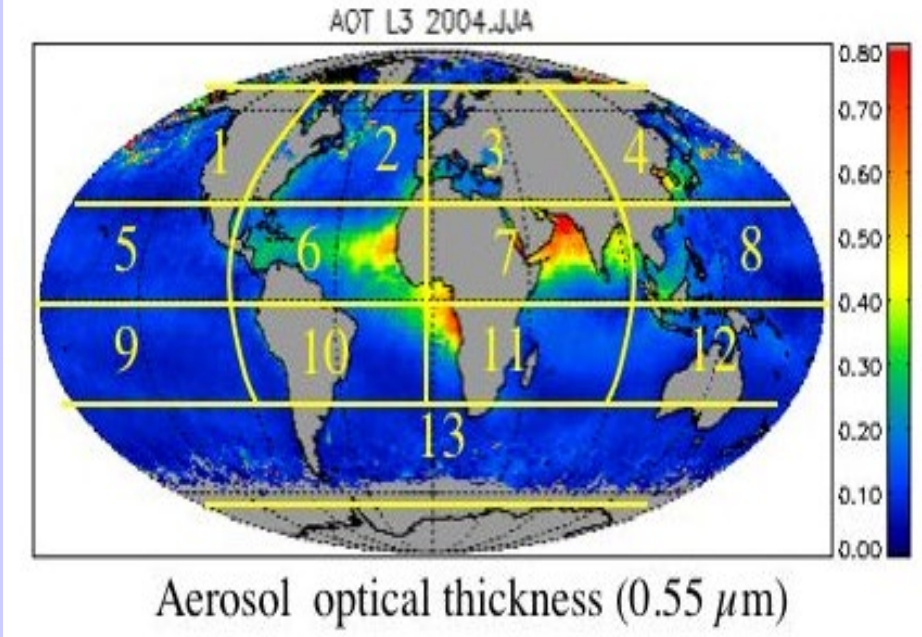

Aerosol effects on cloud cover over the Atlantic Ocean - several aerosol types interact with clouds

June-Aug 2002

Pollution zone

Dust zone

Smoke zone

Marine aerosol

aerosol forcing increased cloud cover 5% (~ 6 W/m2) and height 40 hPa (~ 400 m) in June-Aug 02 over Atlantic Ocean

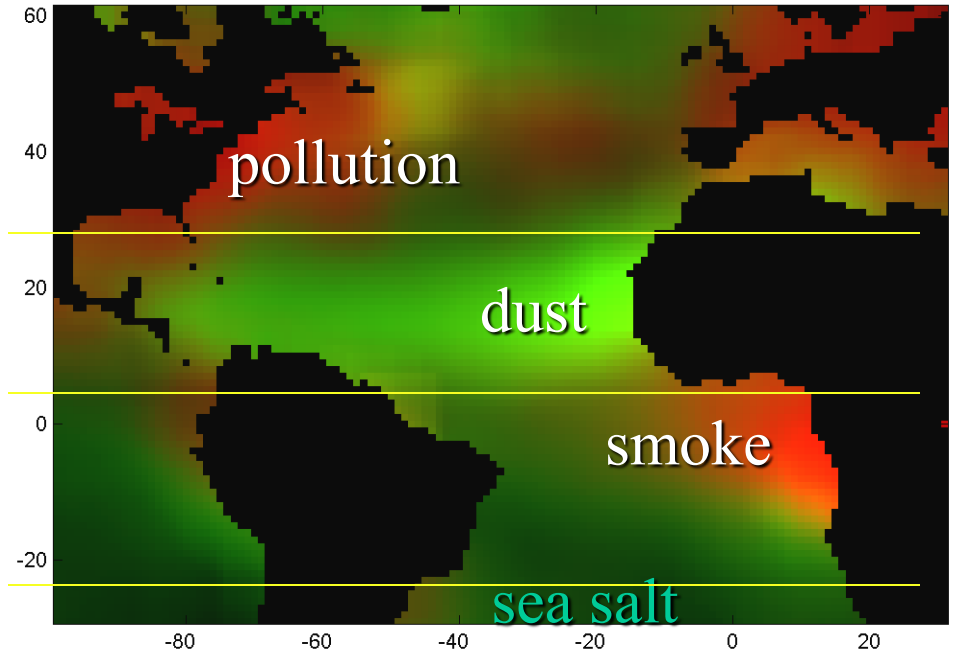

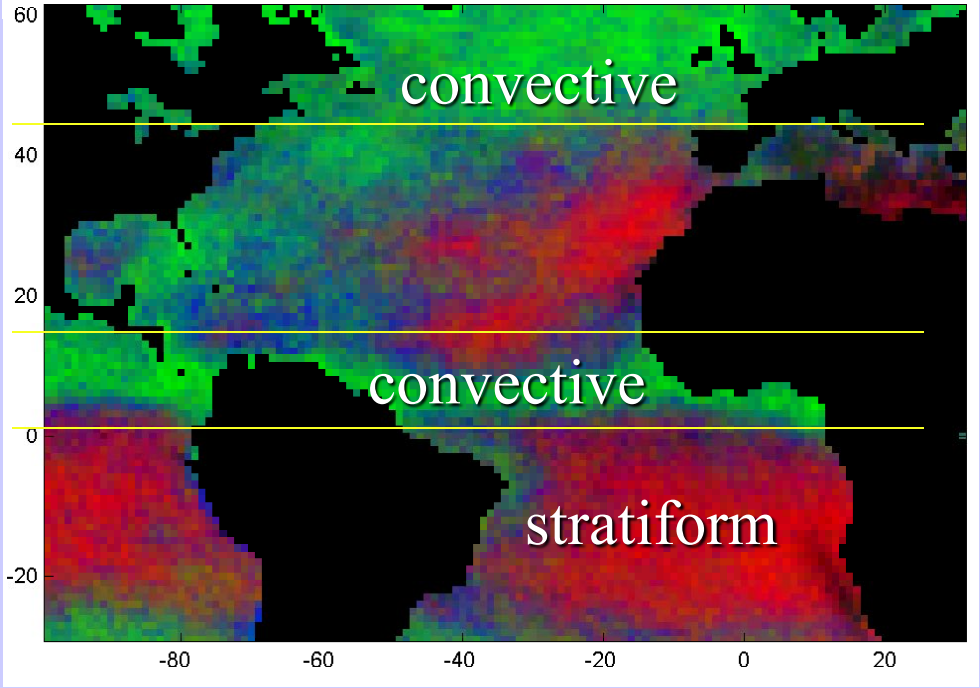

clean

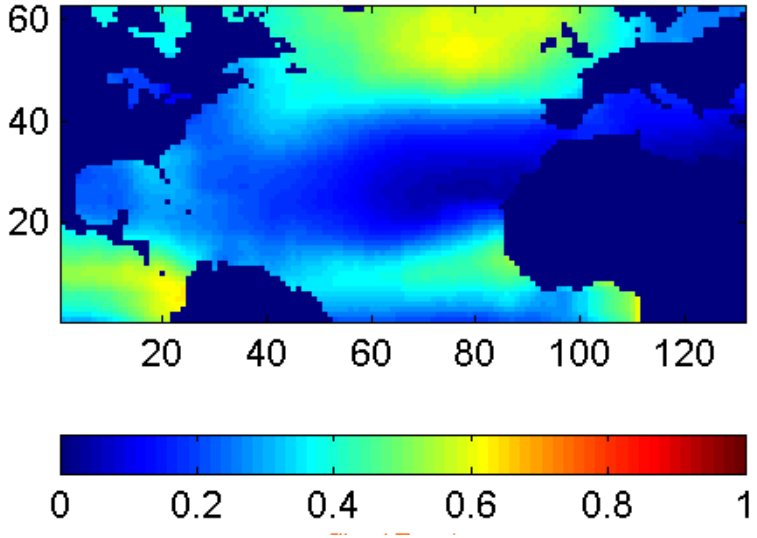

Cloud fraction

hazy

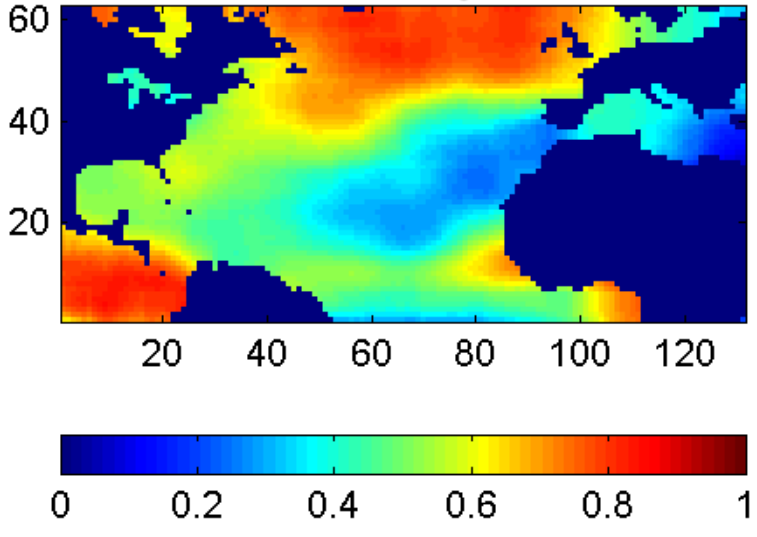

Cloud fraction

clean

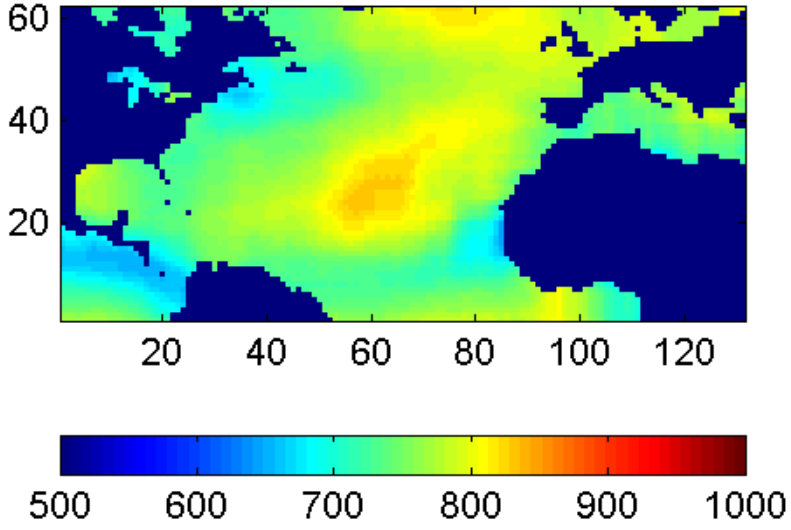

Cloud top pressure

hazy

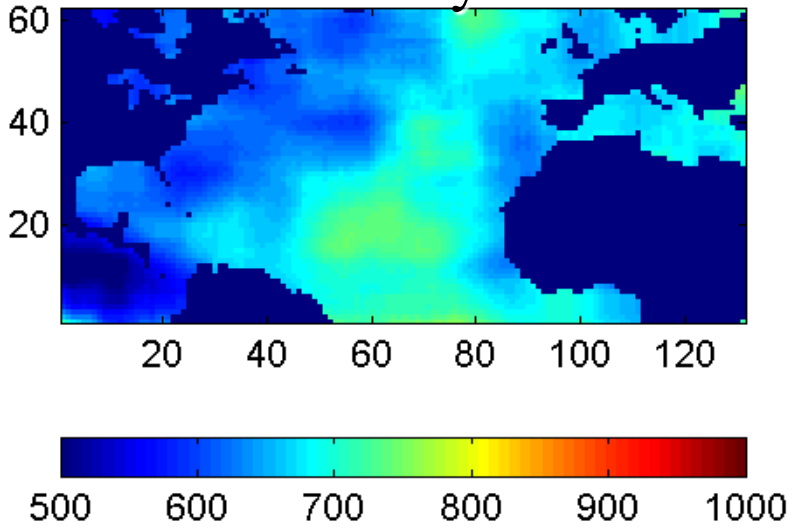

Cloud top pressure

Active Fire Detection

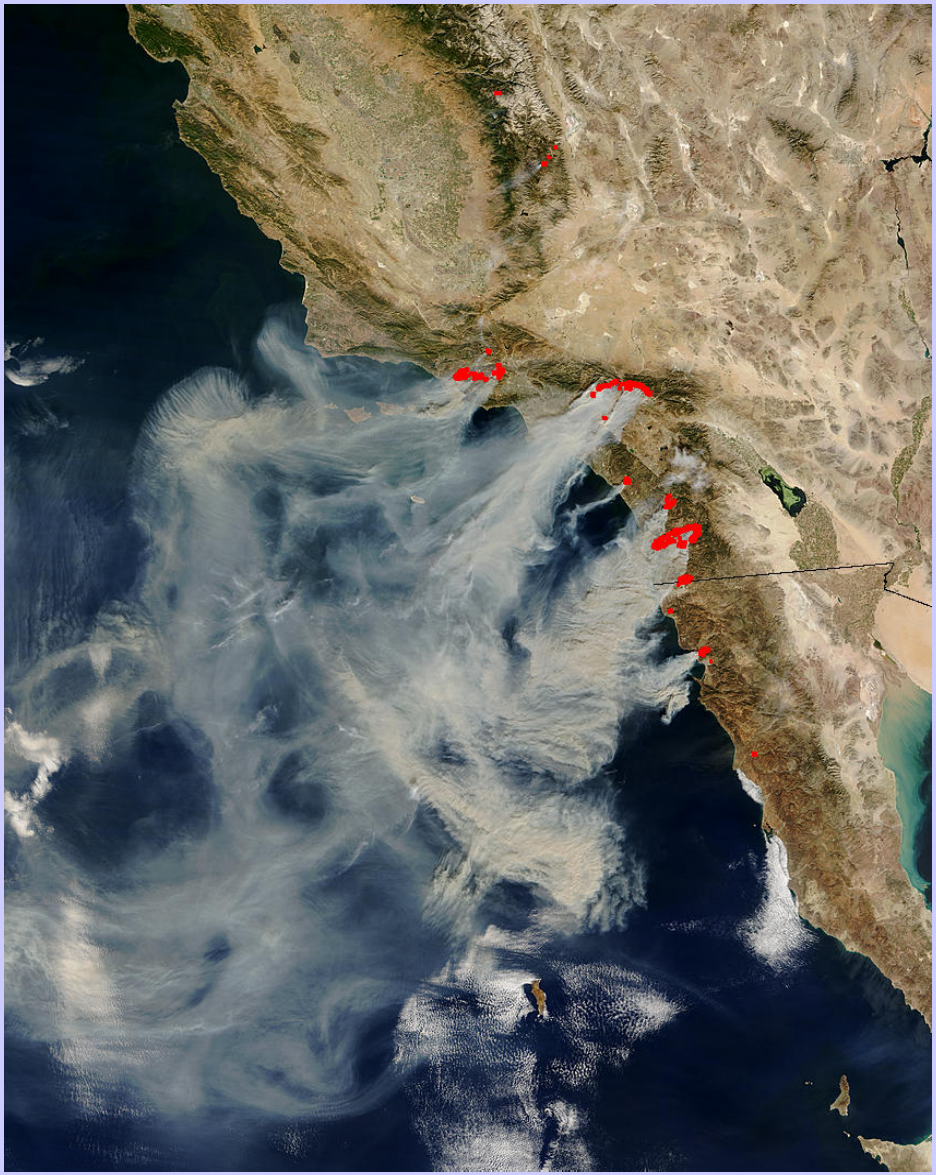

California – 10/26/03

- Same code as the "offical" MOD14 thermal anomalies product
- Contextual algorithm (Giglio et al., 2003)
- The algorithm considers the spectral signature (in middle and thermal infrared) of each pixel and compares it to the non-burning surrounding pixels
- The natural variability of the surrounding background is taken into account
- Fewer false detections than traditional threshold-based algorithms
- Sensitive enough to detect small fires
- Current version: v4.3.2 (March 2003)

Biscuit and Tiller Fires in California and Oregon (08/14/02)

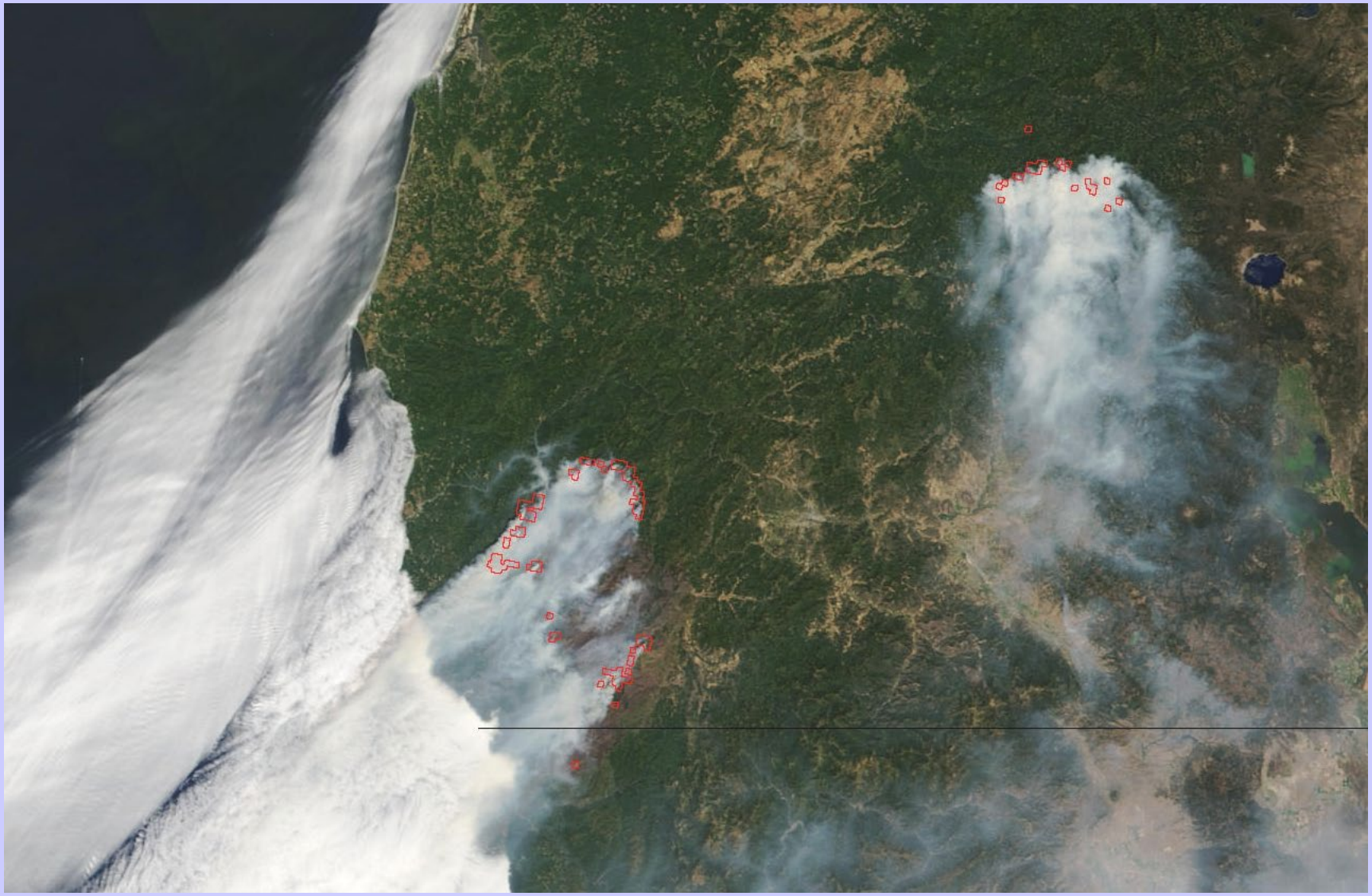

Fire Monitoring: http://rapidfire.sci.gsfc.nasa.gov/realtime

Cooperative Development of Advanced Products

Mapping Burn Severity With MODIS

The Devil Fire Susanville, California May 2001

These MODIS images were obtained shortly after containment of the 4,200 acre Devil Fire on June 3, 2001.

Two models were run on the subset area using Erdas Imagine:

- NDVI (Normalized Difference Vegetation Index)
- NDBR (Normalized Difference Burn Ratio), developed by the USGS.

Unsupervised classifications were then performed on these 2 images as well as on the false color NIR image.

Ground truthing would be required to determine the accuracy of each technique as well as the burned severity of the perimeter area.

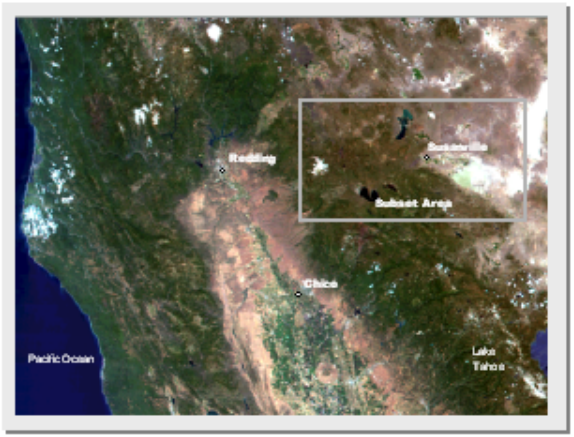

True Color MODIS Image of Northern California June 3, 2001

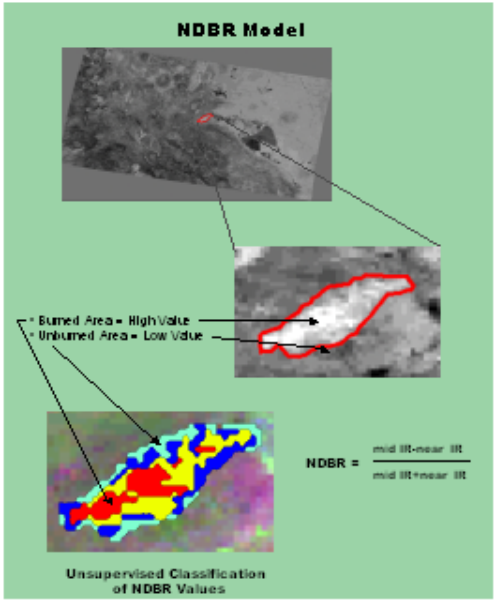

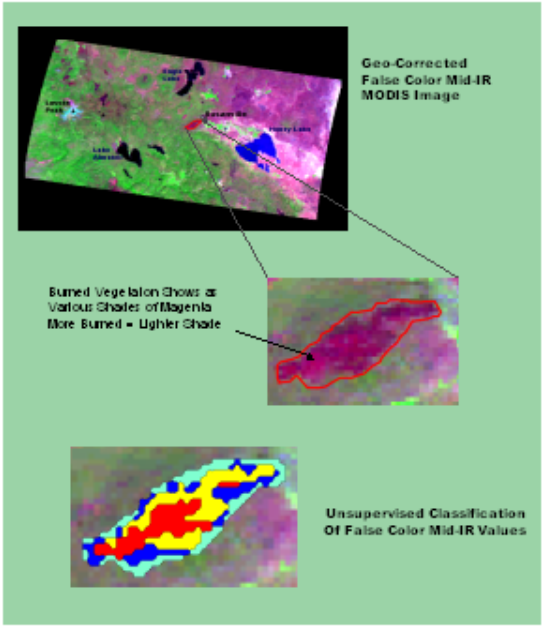

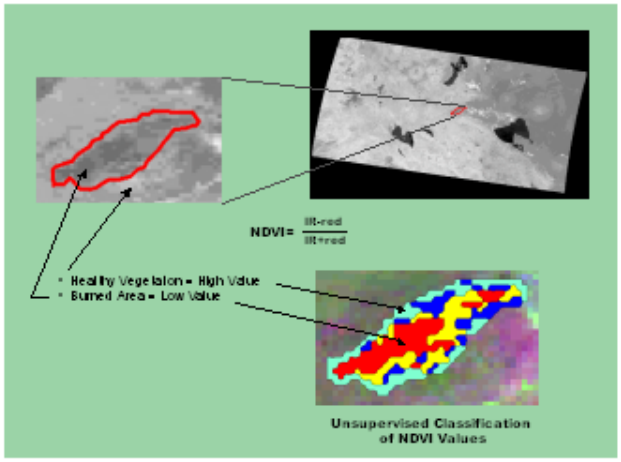

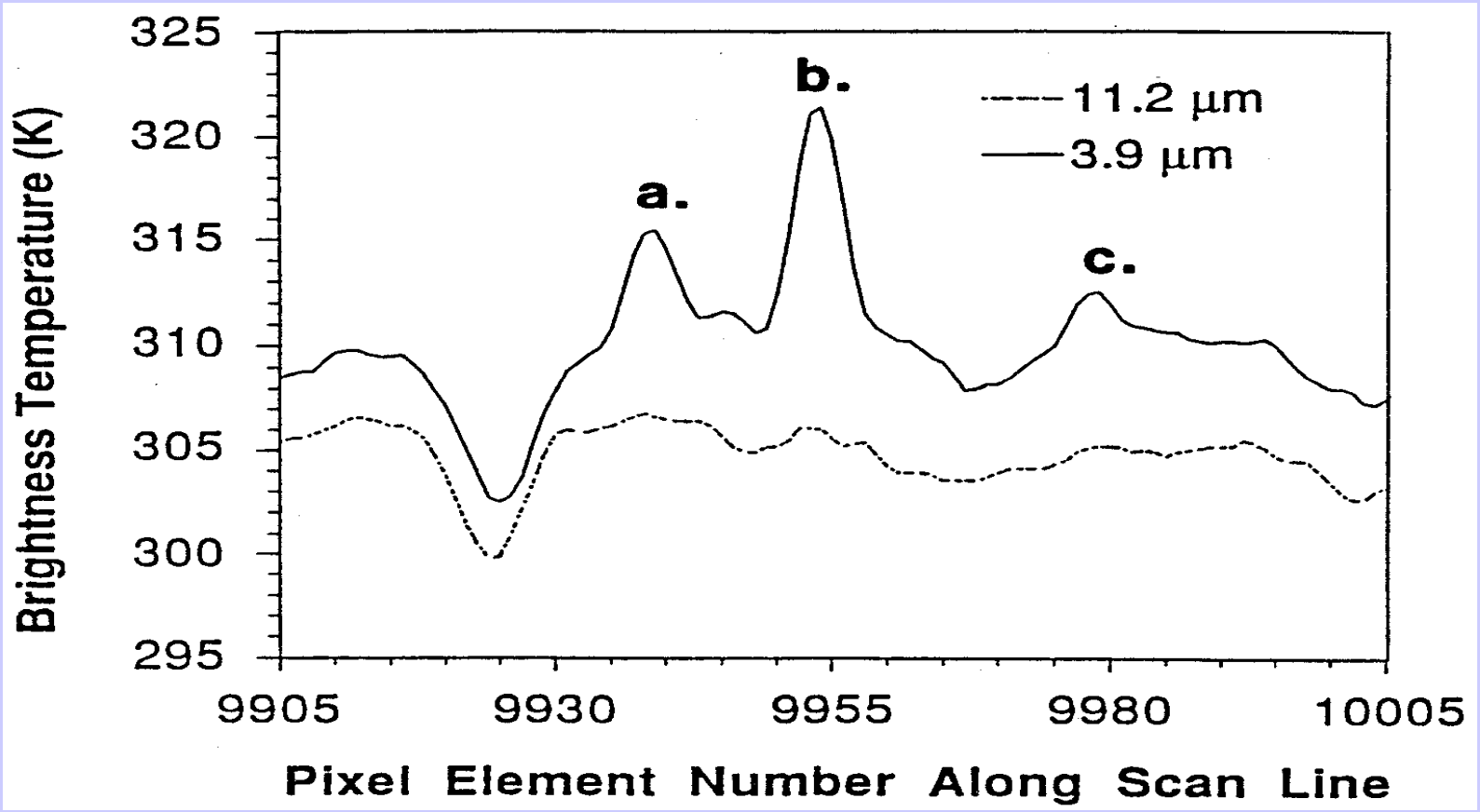

3.9 and 11.2 microns plotted for one scan line over grassland burning in South America; fires are likely at a, b, and c.

The fire extent and temperature within a field of view can be determined by considering the upwelling thermal radiance values obtained by both channels (Matson and Dozier, 1981; Dozier, 1981). For a given channel, λ, the radiative transfer equation indicates

$$R_\lambda(T) = \varepsilon_\lambda B_\lambda(Ts)\, \tau_\lambda(s) + \int_0^1 B_\lambda(T)\, d\tau_\lambda$$

When the GOES radiometer senses radiance from a pixel containing a target of blackbody temperature T_t occupying a portion p (between zero and one) of the pixel and a background of blackbody temperature T_b occupying the remainder of the pixel (1-p), the following equations represent the radiance sensed by the instrument at 4 and 11 micron.

$$R_4(T_4) = p\, R_4(T_t) + \varepsilon_4\, (1-p)\, R_4\, (T_b) + (1-\varepsilon_4)\, \tau_4(s)\, R_4(solar)$$

$$R_{11}(T_{11}) = p\, R_{11}(T_t) + \varepsilon_{11}\, (1-p)\, R_{11}(T_b)$$

The observed short wave window radiance also contains contributions due to solar reflection that must be distinguished from the ground emitted radiances; solar reflection is estimated from differences in background temperatures in the 4 and 11 micron channels. Once T_b is estimated from nearby pixels, these two nonlinear equations can be solved for T_t and p. In this study, the solution to the set of equations is found by applying a globally convergent bisection technique followed by Newton's method.

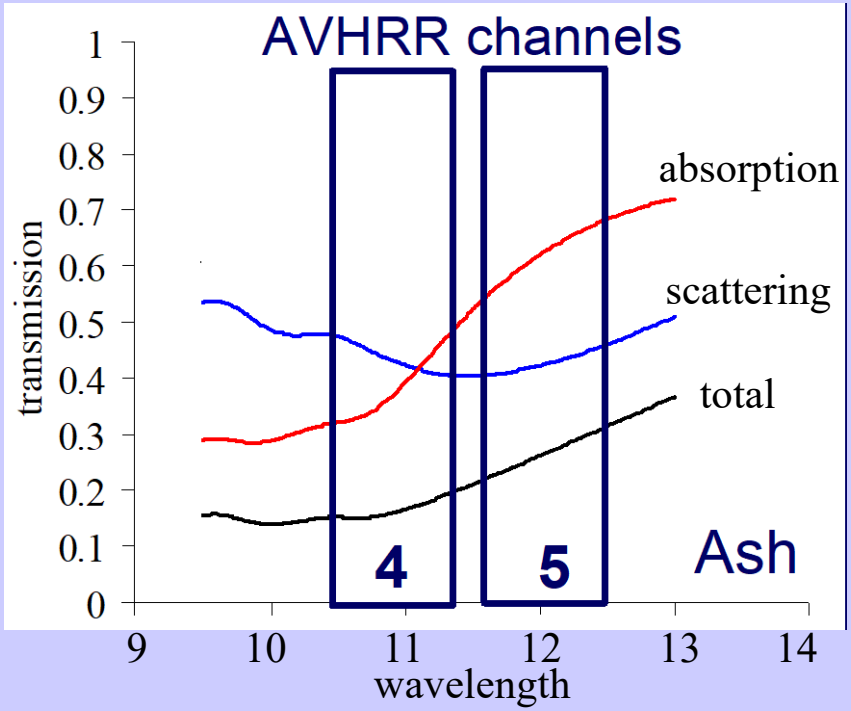

Investigating with Multi-spectral Combinations

Given the spectral response of a surface or atmospheric feature

Select a part of the spectrum where the reflectance or absorption changes with wavelength

e.g. transmission through ash

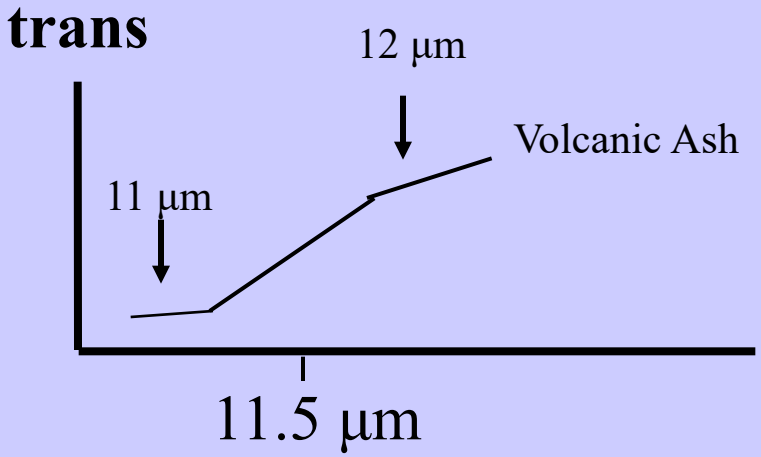

If 11 μm sees the same or higher BT than 12 μm the atmosphere viewed does not contain volcanic ash; if 12 μm sees considerably higher BT than 11 μm then the atmosphere probably contains volcanic ash

Ash Plume Detection

Mt. Cleveland Eruption 19 Feb 2001

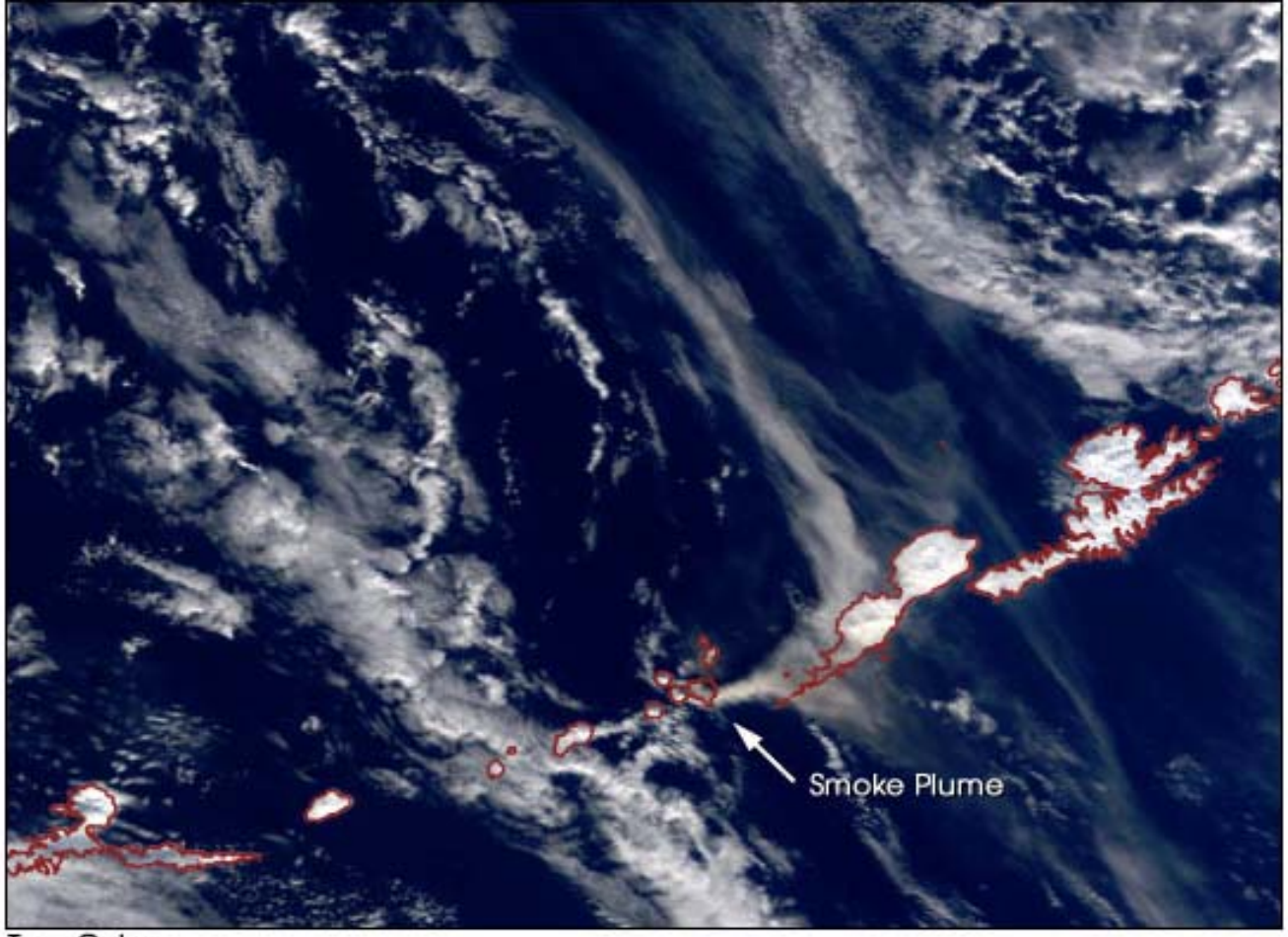

True Color

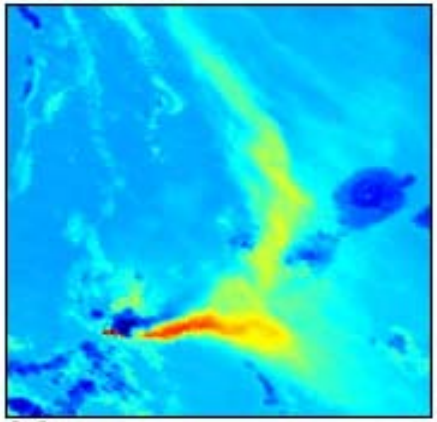

3.9μm

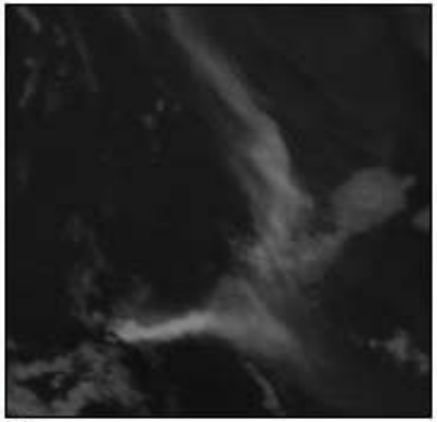

11μm

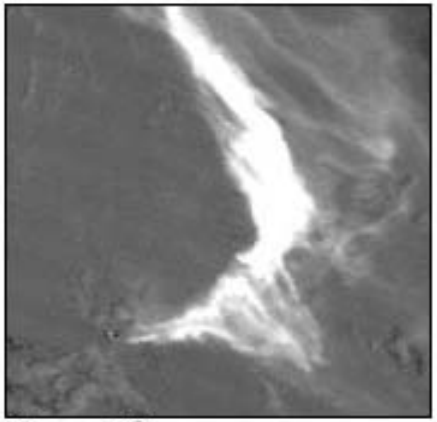

11μm - 12μm

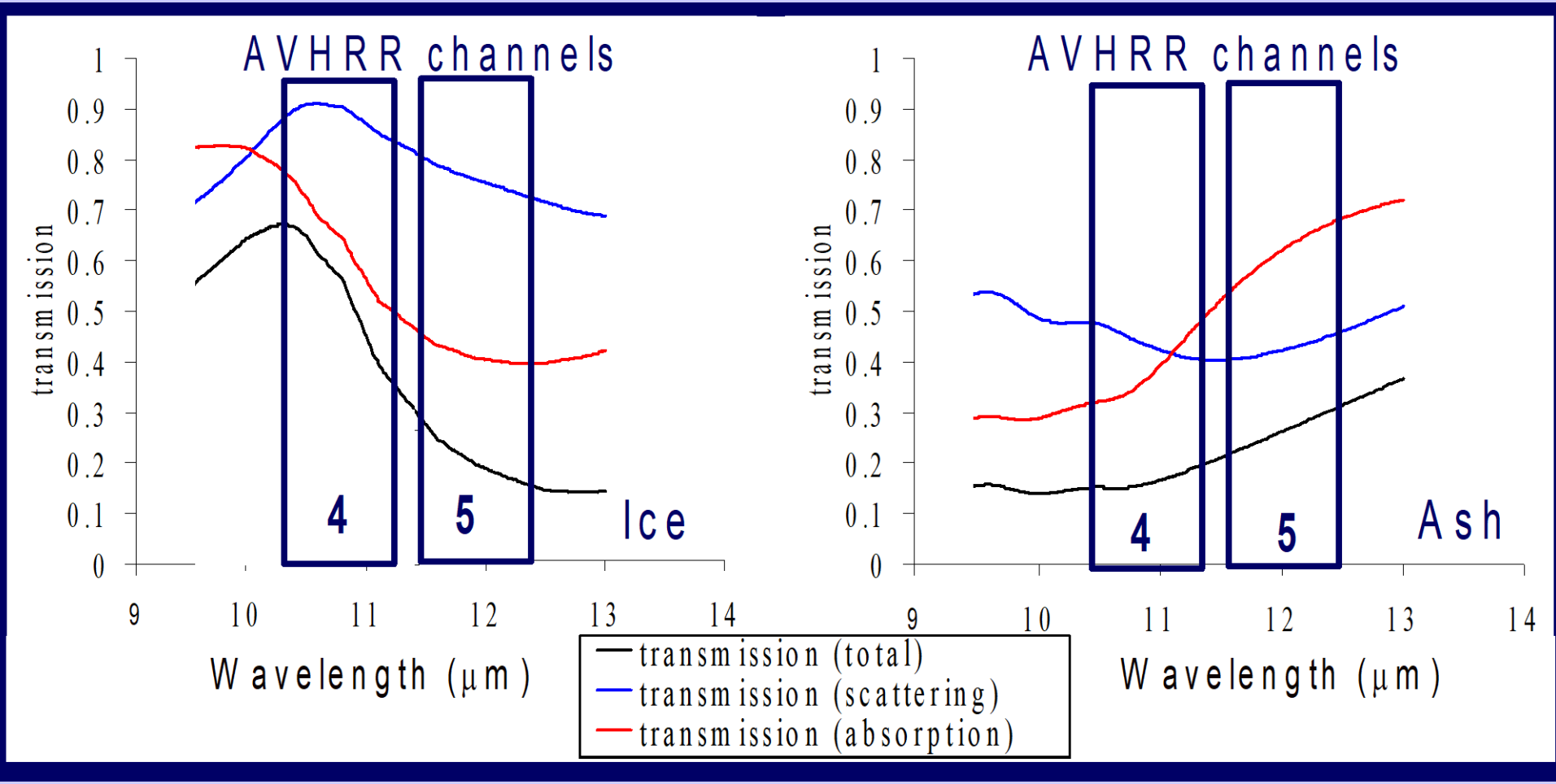

BT11-BT12 > 0 for ice
BT11-BT12 < 0 for volcanic ash

Frank Honey 1980s

Dust and Cirrus Signals

Imaginary Index of Refraction of Ice and Dust

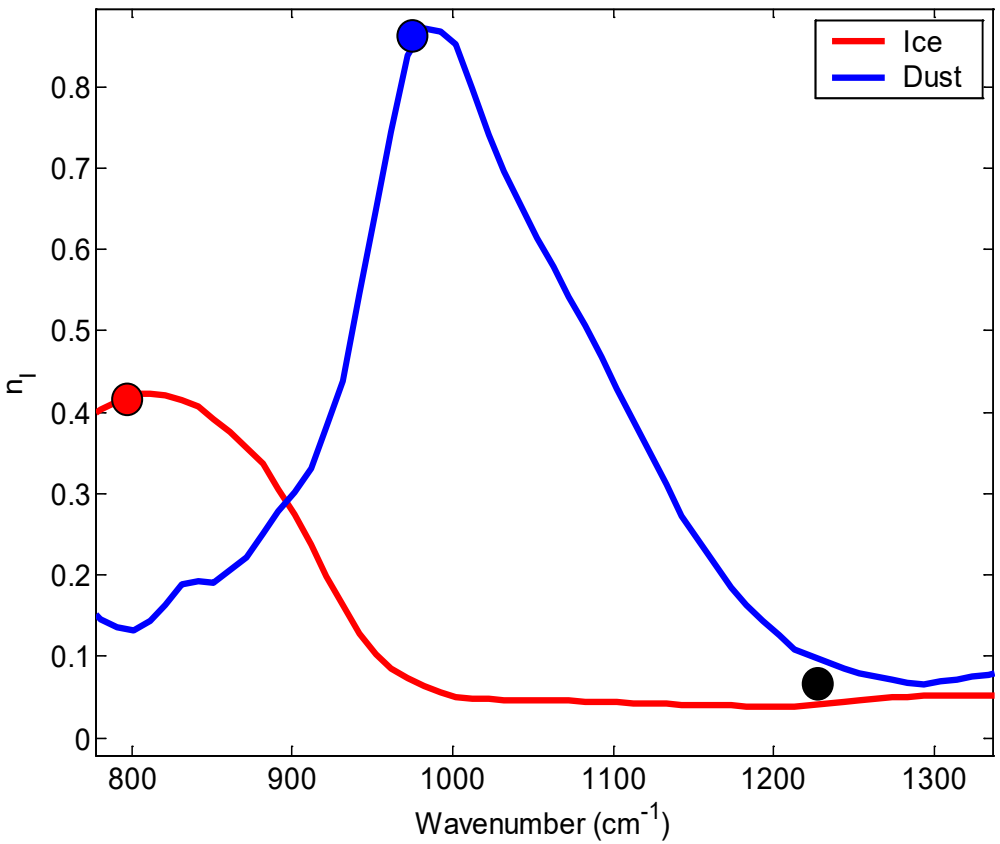

- Both ice and silicate absorption small in 1200 cm^{-1} window
- In the 800-1000 cm^{-1} atmospheric window:

  Silicate index *increases*

  Ice index *decreases*

  with wavenumber

Volz, F.E. : Infrared optical constant of ammonium sulphate, Sahara Dust, volcanic pumice and flash, Appl Opt 12 564-658 (1973)

BT11-BT12 (BT1000-BT800) > 0 for ice
BT11-BT8.6 (BT1000-BT1200)< 0 for dust

MODIS detects ship tracks

Ship Tracks occur in marine stratocumulus regions of the globe

- California, Azores, Namibia, and Peru

Conditions for formation

- High humidity
- Small air-sea temperature difference
- Low wind speed
- Boundary layer between 300 and 750 m deep

Enhanced reflectance of clouds at 3.7 μm

- Larger number of small droplets arising from particulate emission from ships

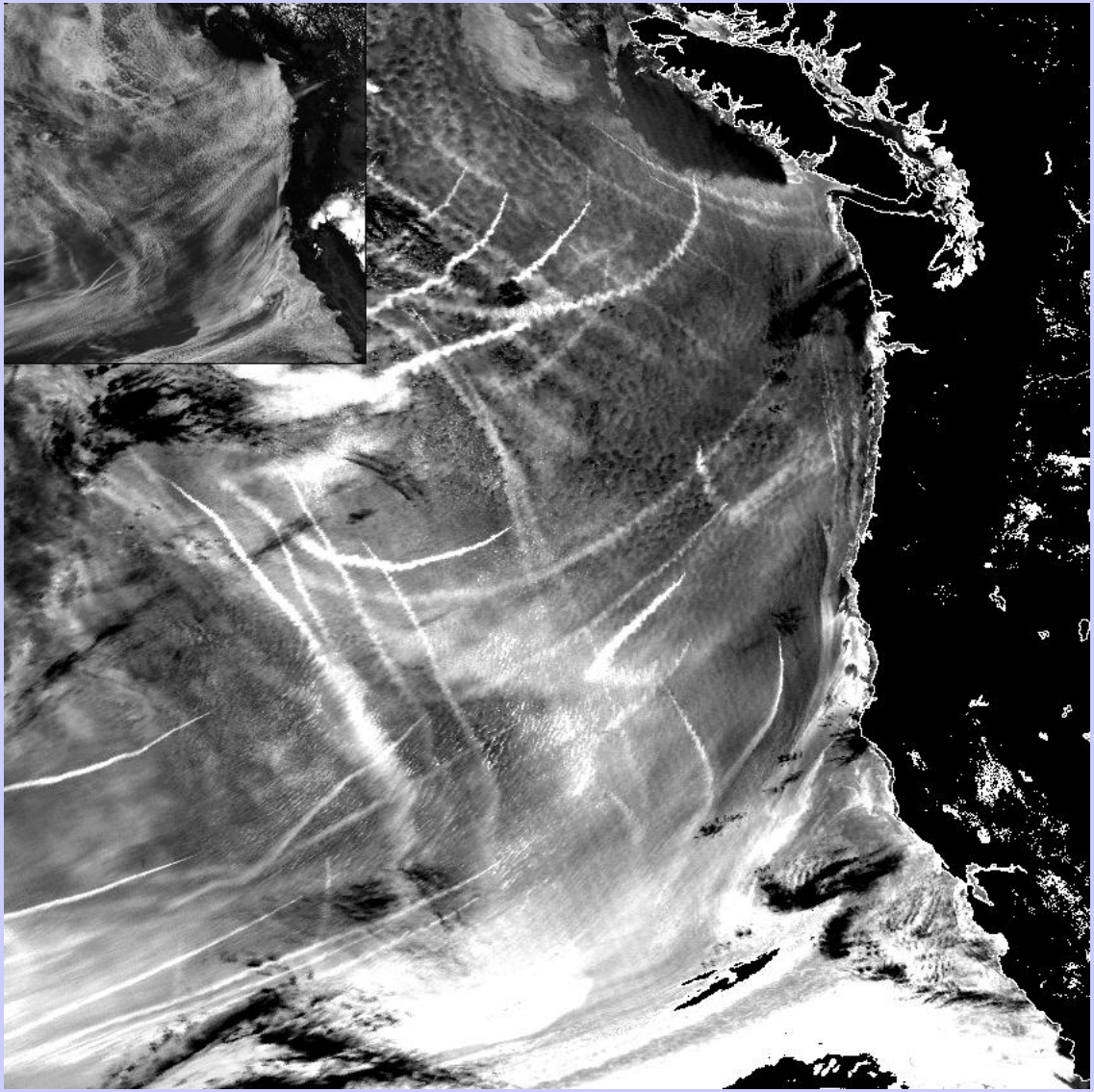

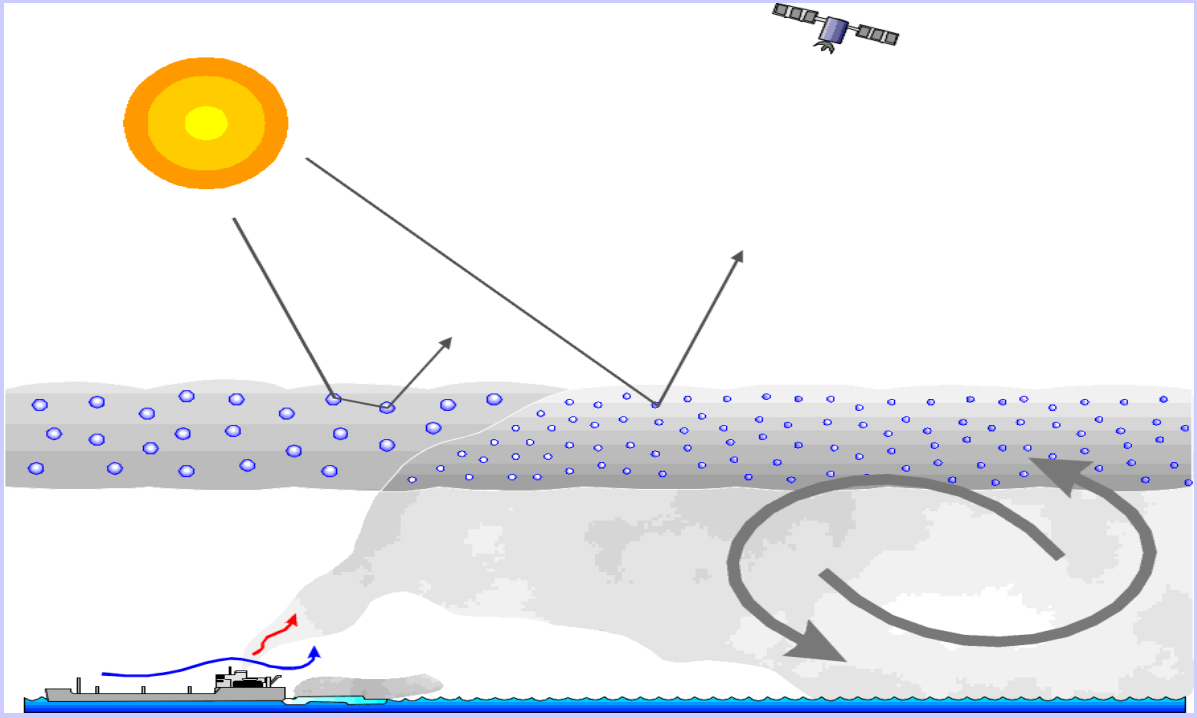

* Particles emitted by ships increase concentration of cloud condensation nuclei (CCN) in the air
* Increased CCN increase concentration of cloud droplets and reduce average size of the droplets
* Increased concentration and smaller particles reduce production of drizzle (100 μm radius) droplets in clouds
* Liquid water content increases because loss of drizzle particles is suppressed
* Clouds are *optically thicker* and brighter along ship track

Ship tracks off France (01/27/03)

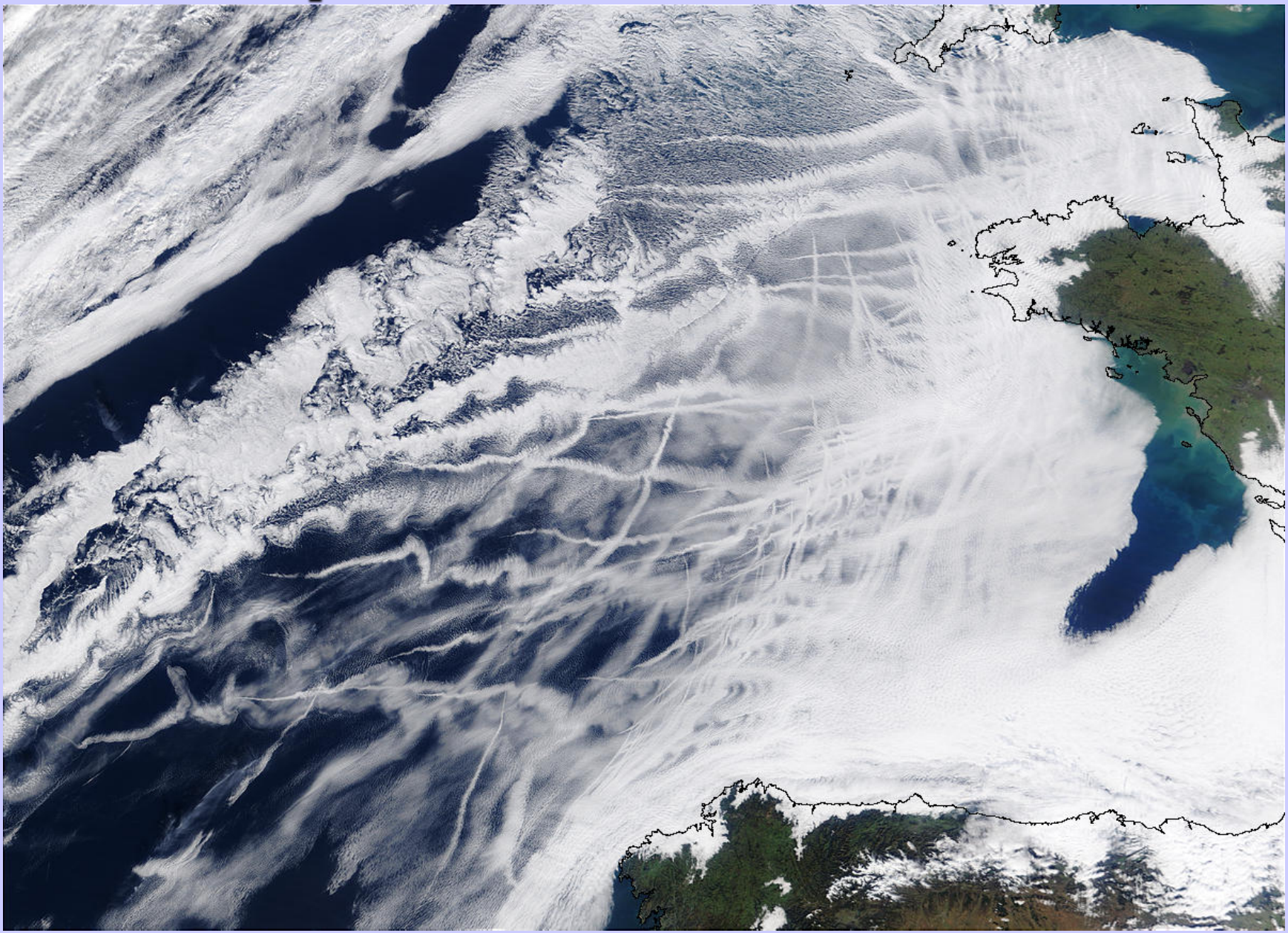

Application Opportunities with Multispectral Remote Sensing Data

Satellite Remote Sensing
Energy Balance
VIS, IR, and MW Radiative Transfer
EOS Terra & Aqua MODIS
Multispectral Applications
(Ocean Color, Snow/Ice, Vegetation, Aerosols, Fires, Volcanic Ash, Clouds, Moisture)
Detecting Climate Trends

Relevant Material in Applications of Meteorological Satellites

ATMOSPHERE-SOLAR RADIATION

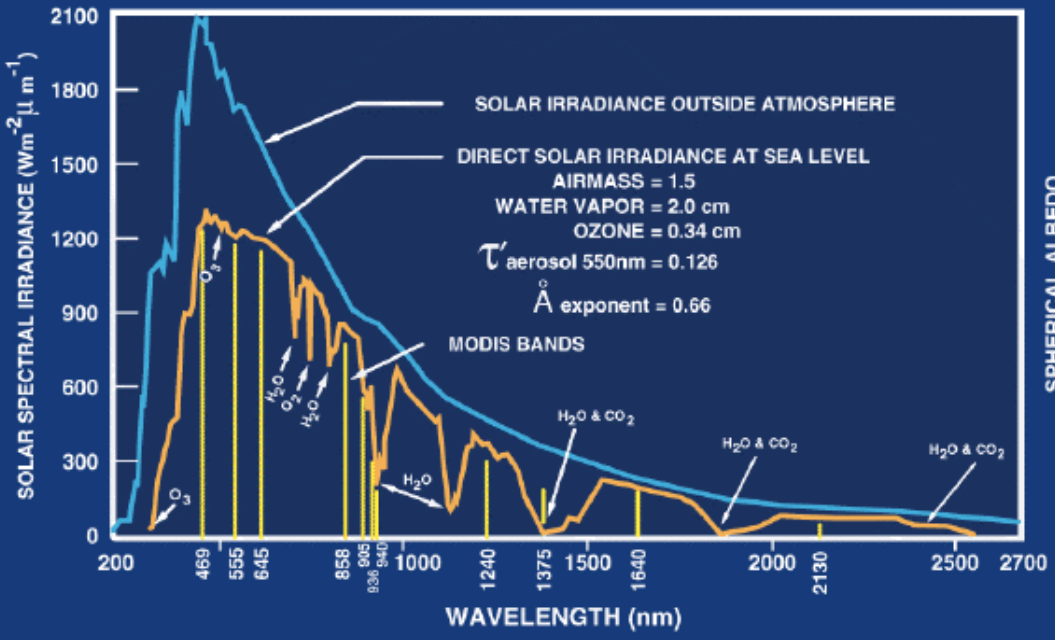

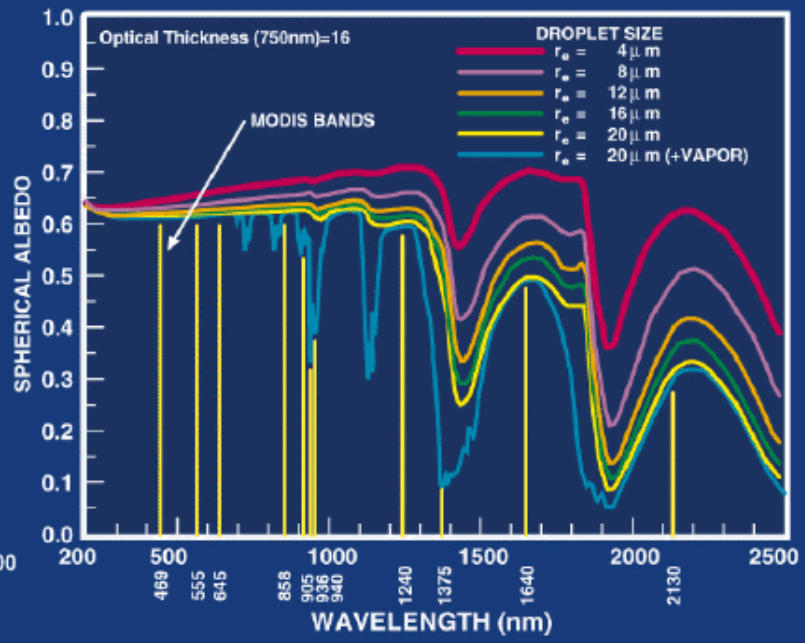

ATMOSPHERE - CLEAR SKY
THERMAL EMISSION

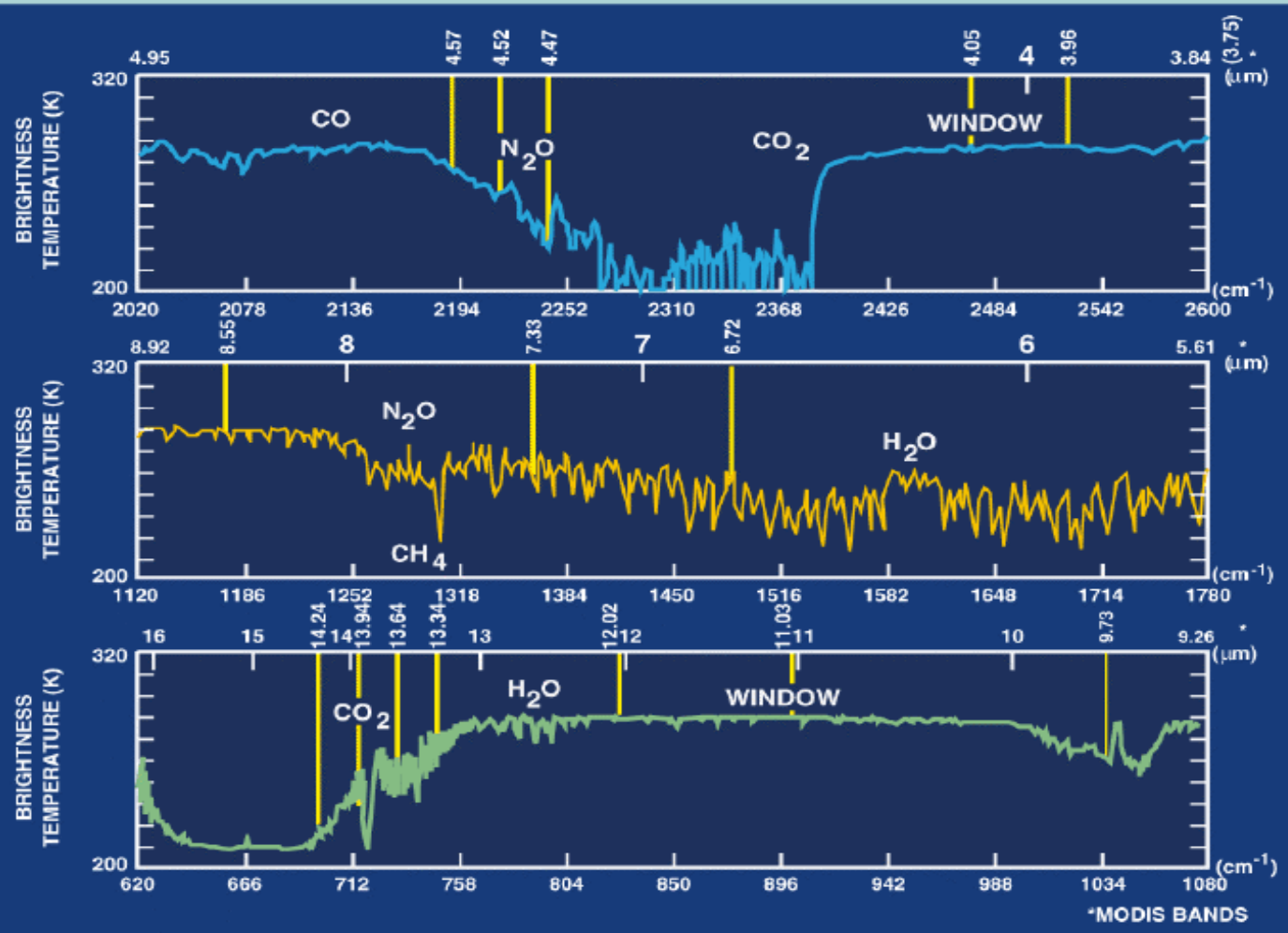

002 11/92

ATMOSPHERE - THERMAL RADIATION

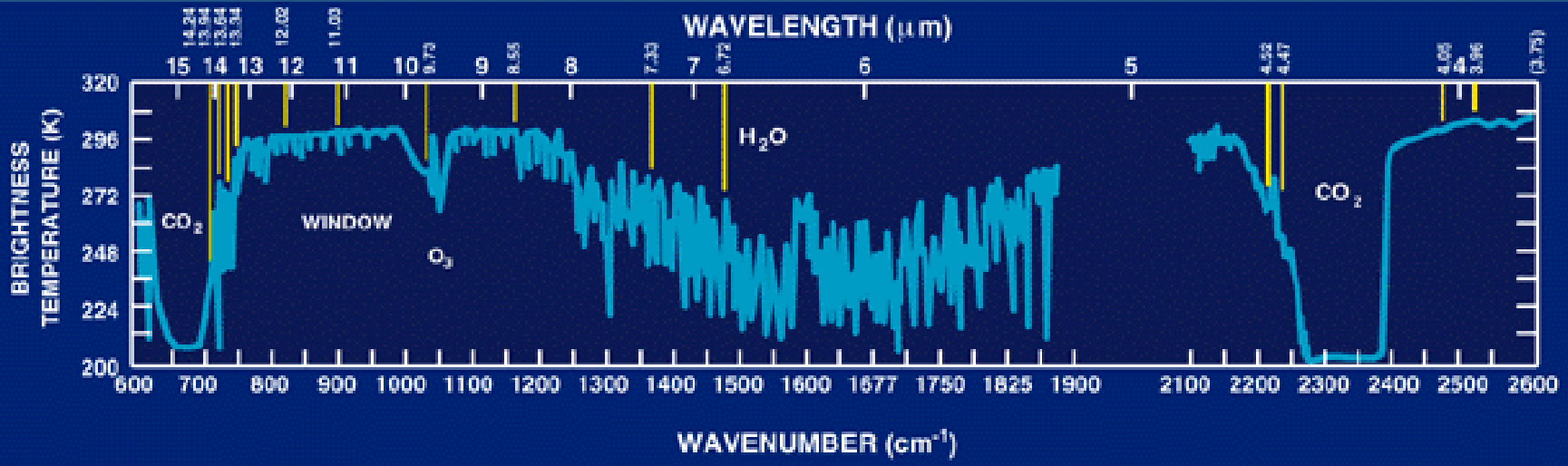

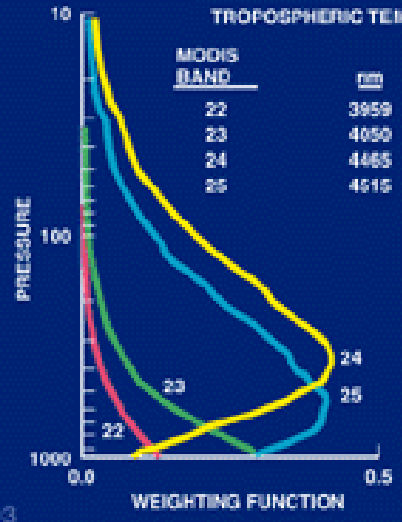

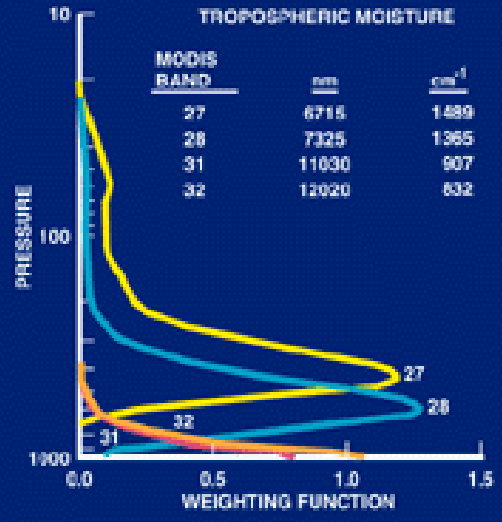

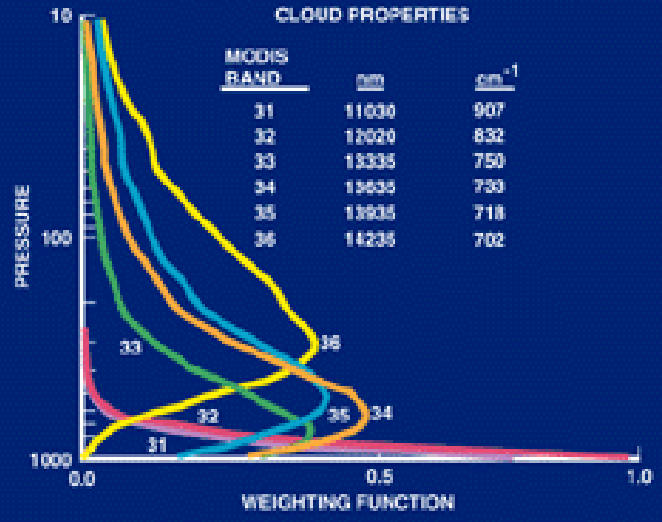

E351.002 5/93

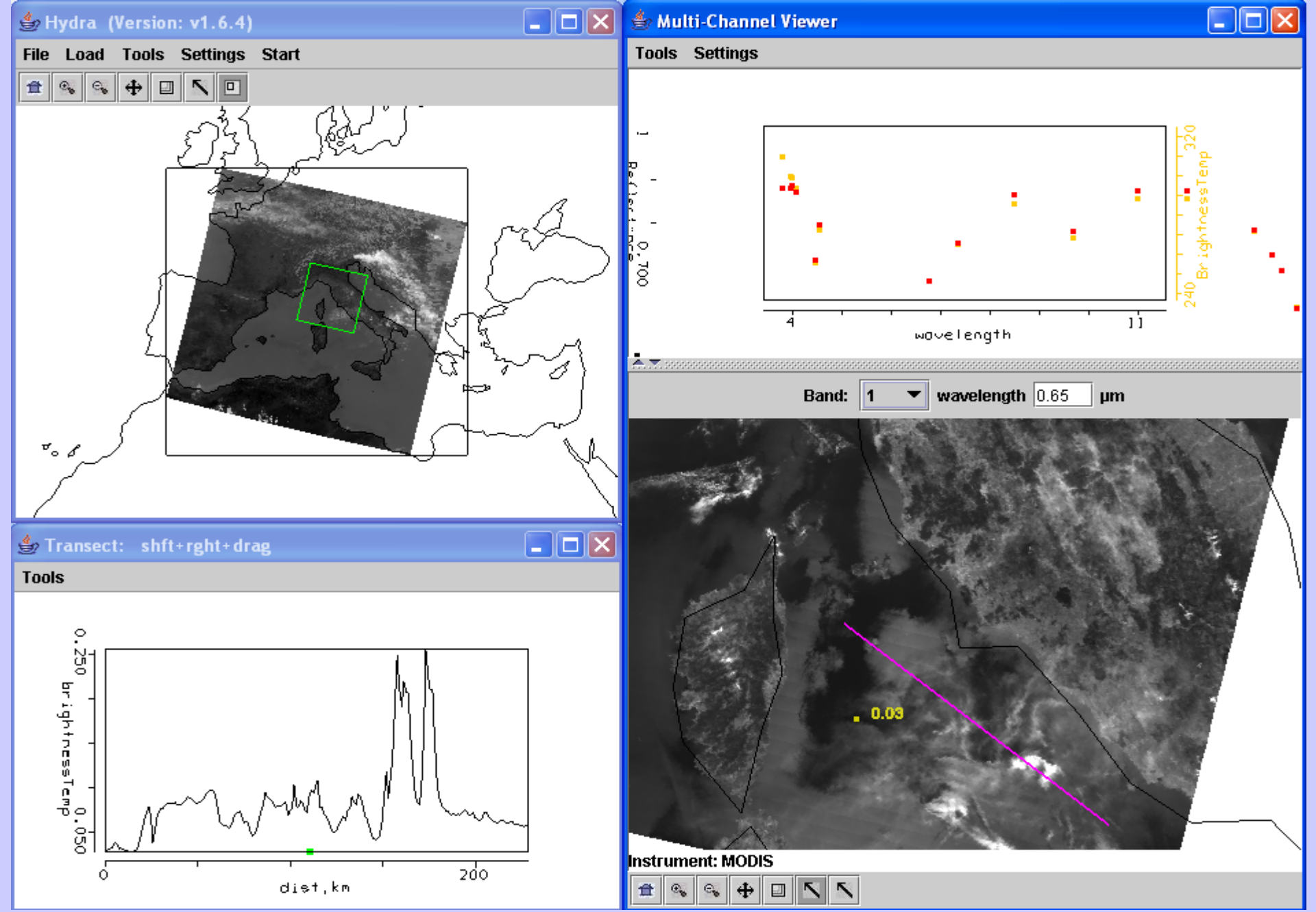

High clouds reflect more than surface at 0.65 µm

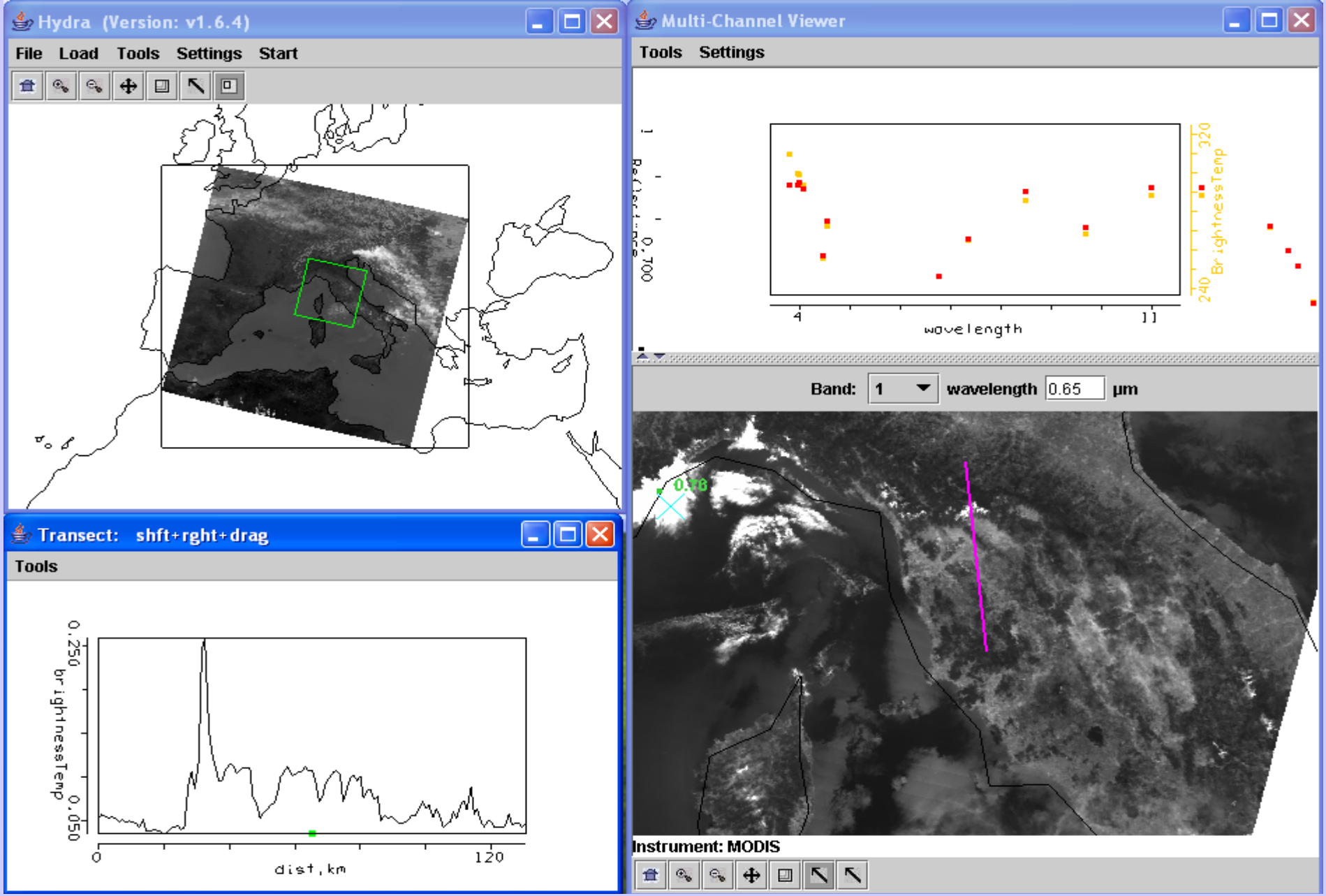

High clouds reflect more than surface at 0.65 µm, even over vegetation

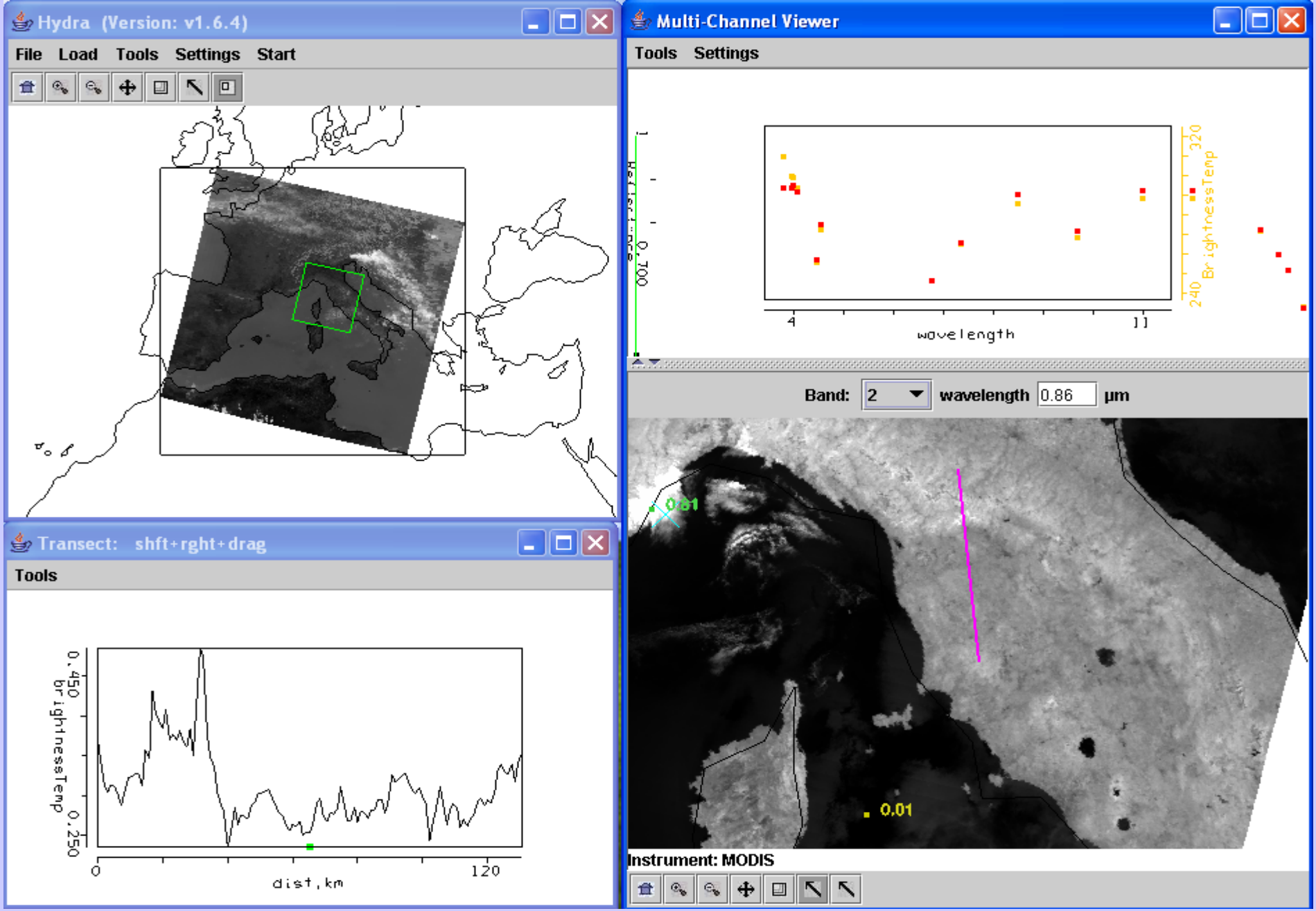

High clouds are more difficult to detect at 0.86 µm over vegetation

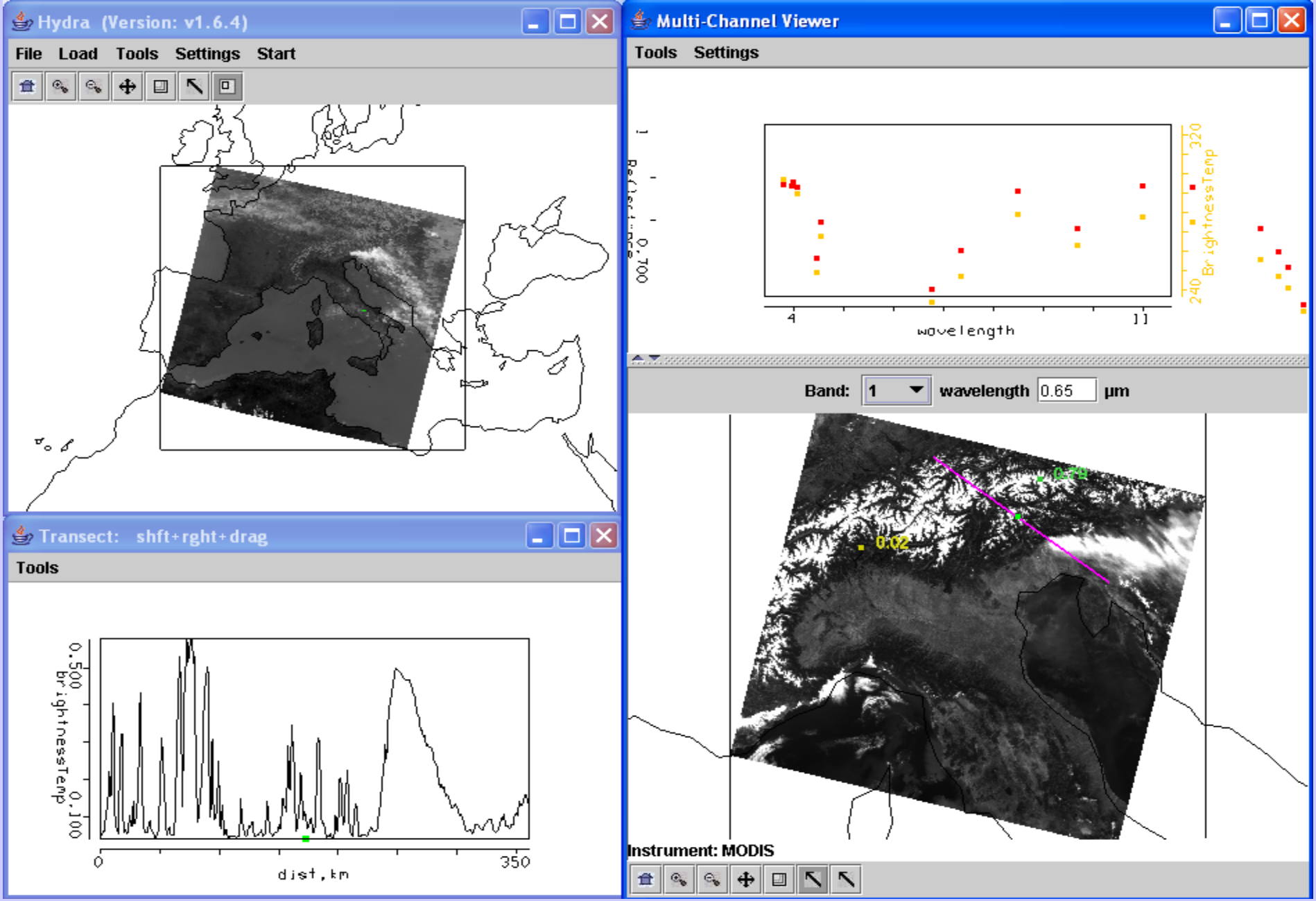

High clouds and snow both reflect a lot at 0.65 µm

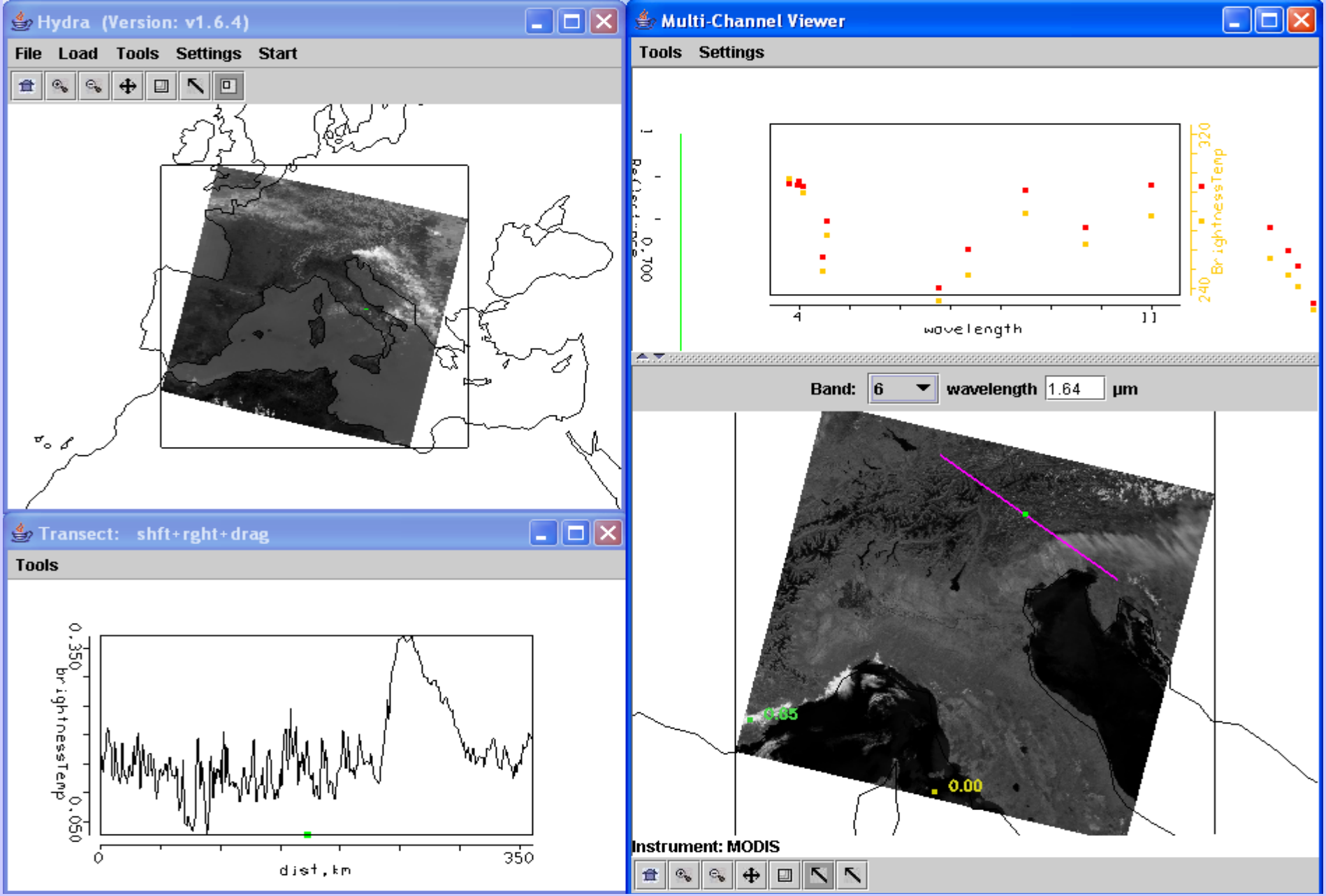

High clouds reflect but snow doesn't at 1.64 µm

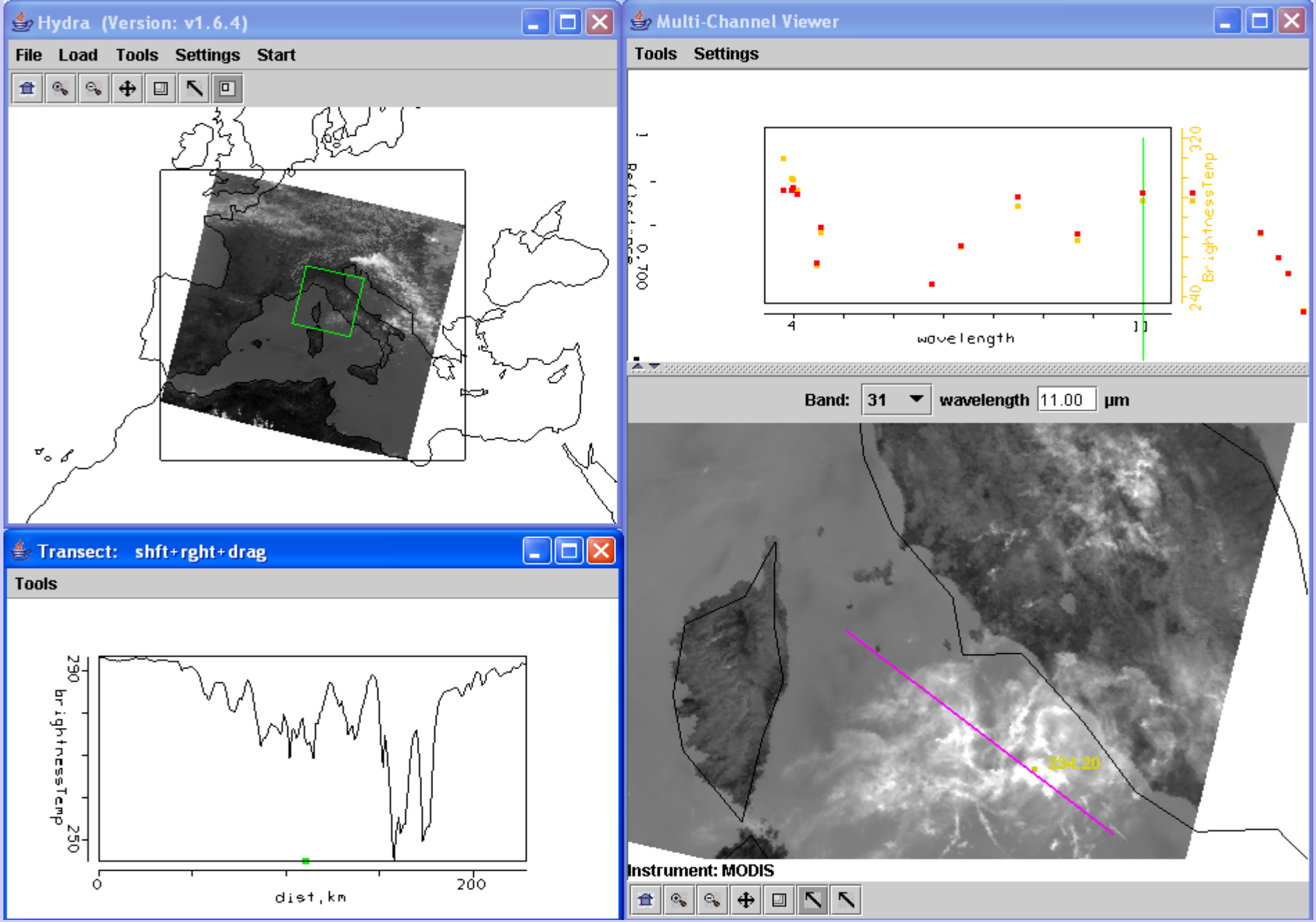

High clouds, cooler than surface, create lower 11 µm BTs

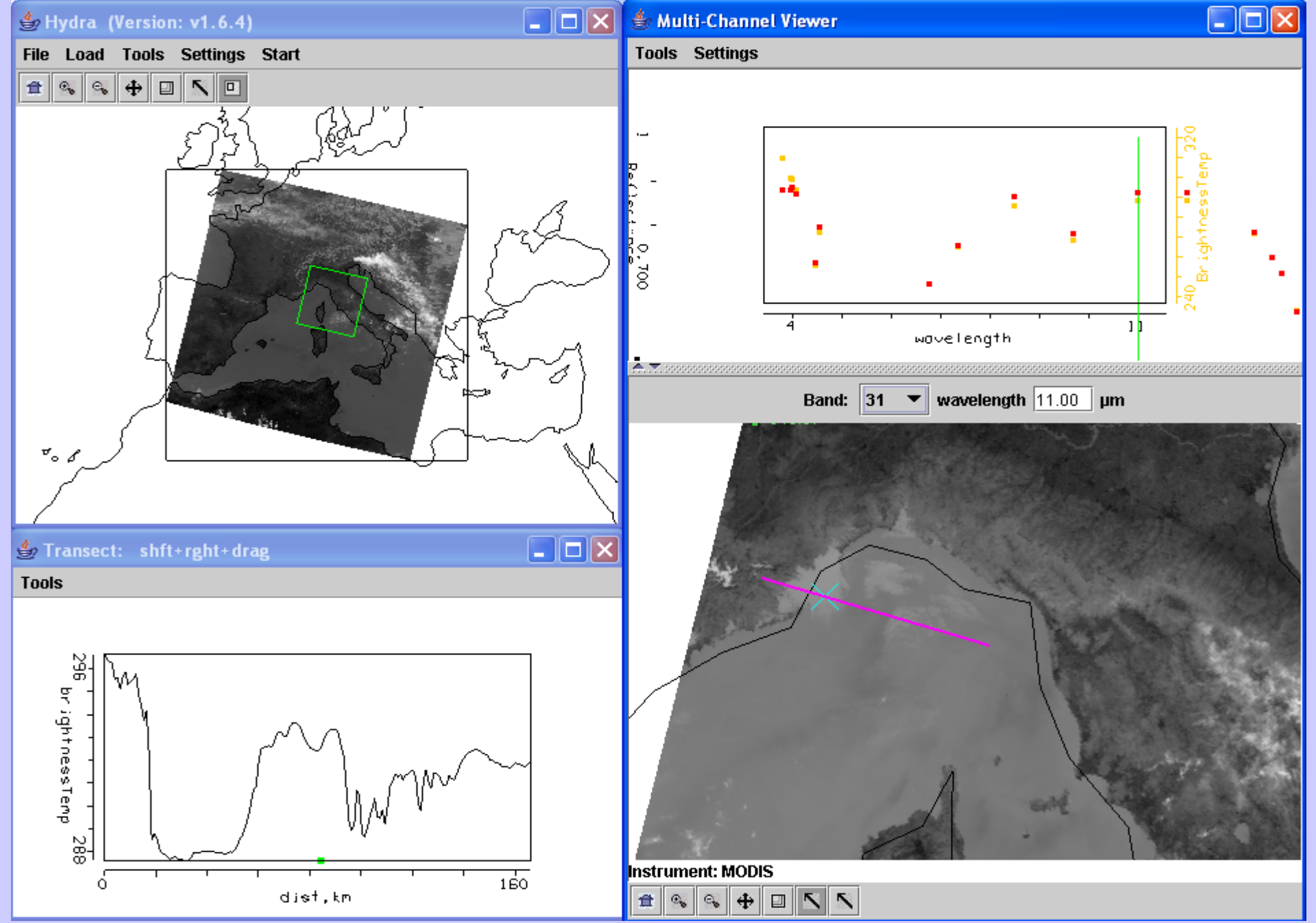

Low clouds, cooler than surface, create lower 11 µm BTs

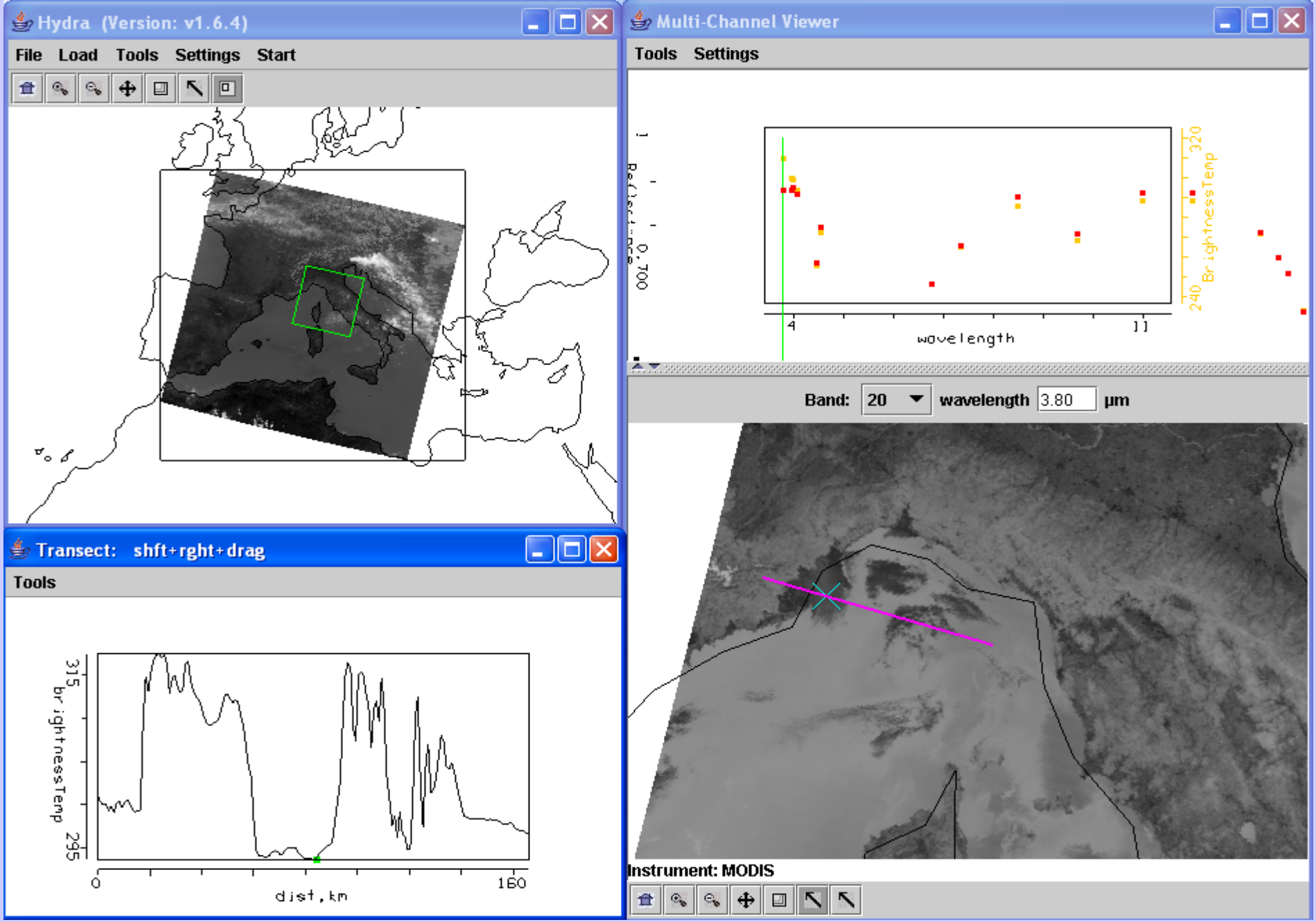

Low clouds reflecting create larger 4 µm brightness temperatures

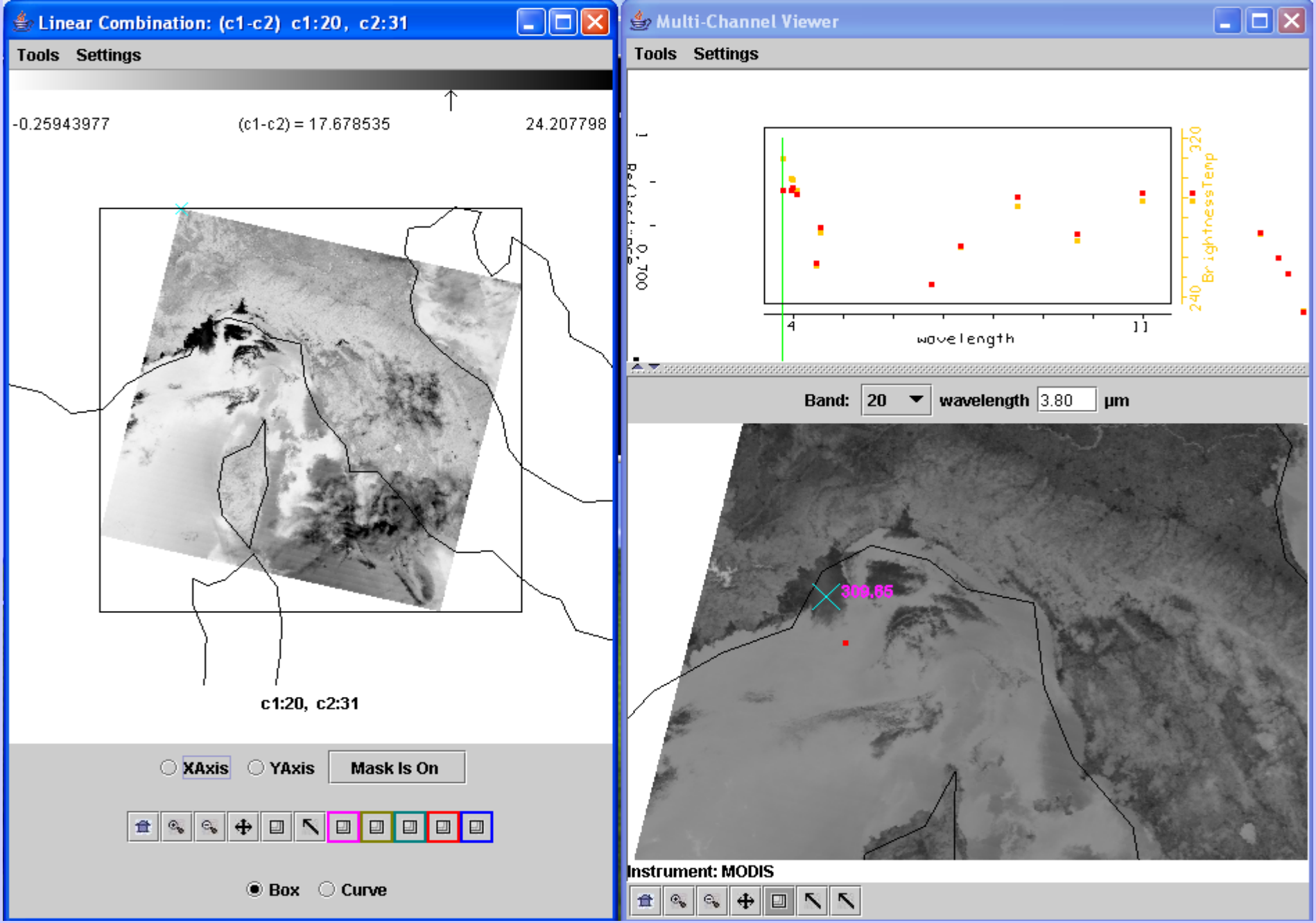

Detecting low clouds in 4-11 µm brightness temperature differences

Fog and Low Stratus

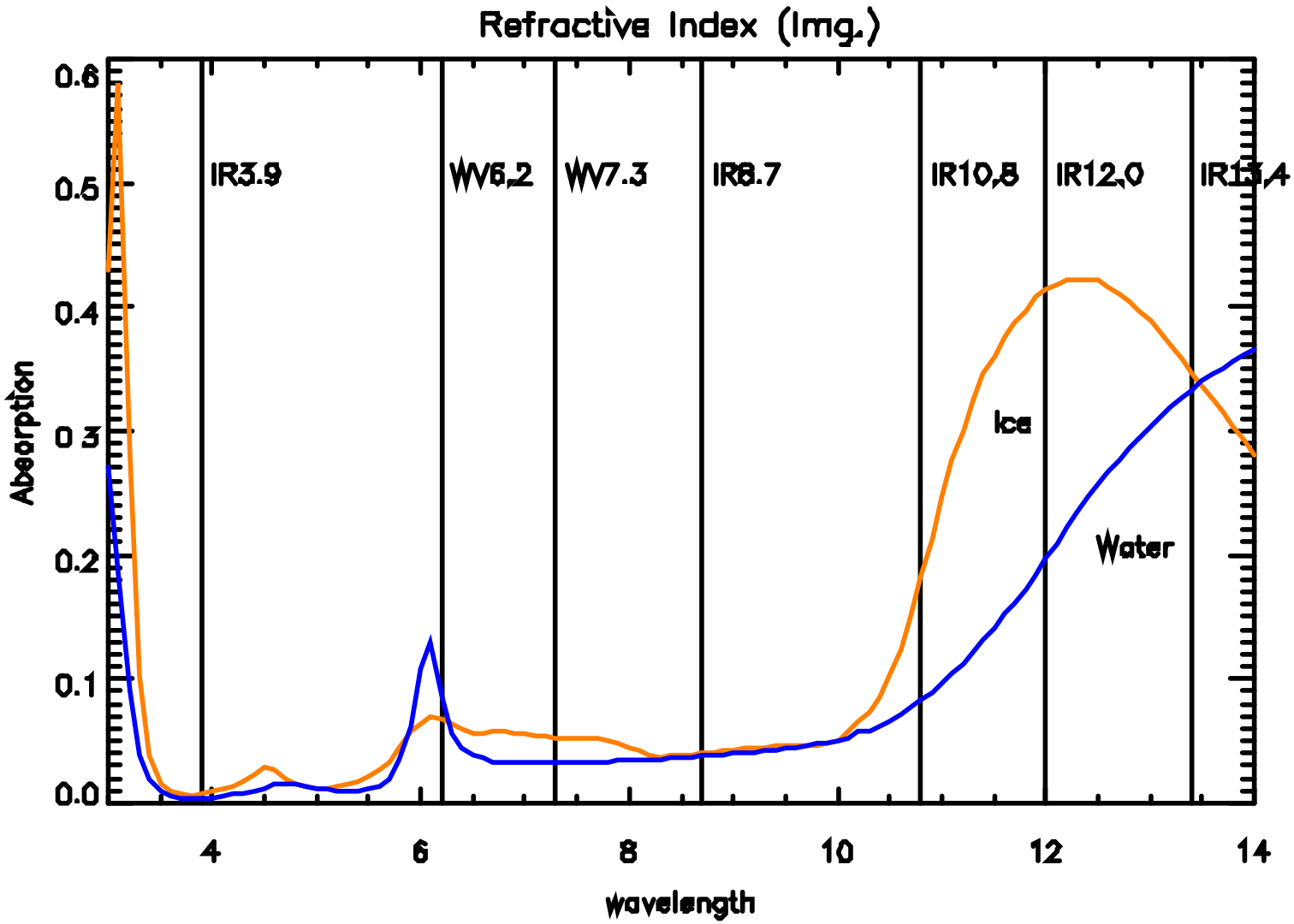

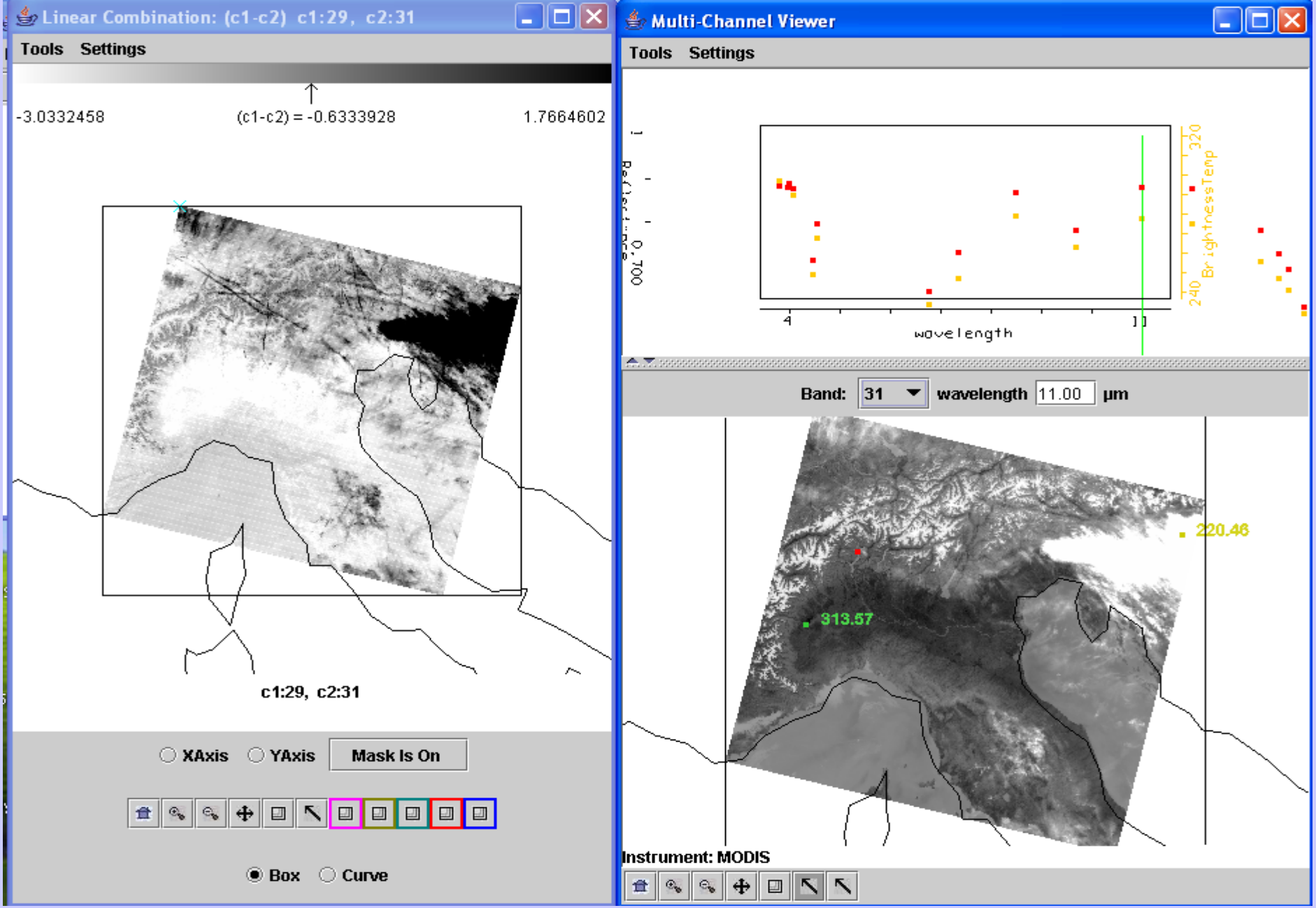

Detecting ice clouds in 8.6-11 μm brightness temperature differences

Optical properties of cloud particles: imaginary part of refraction index

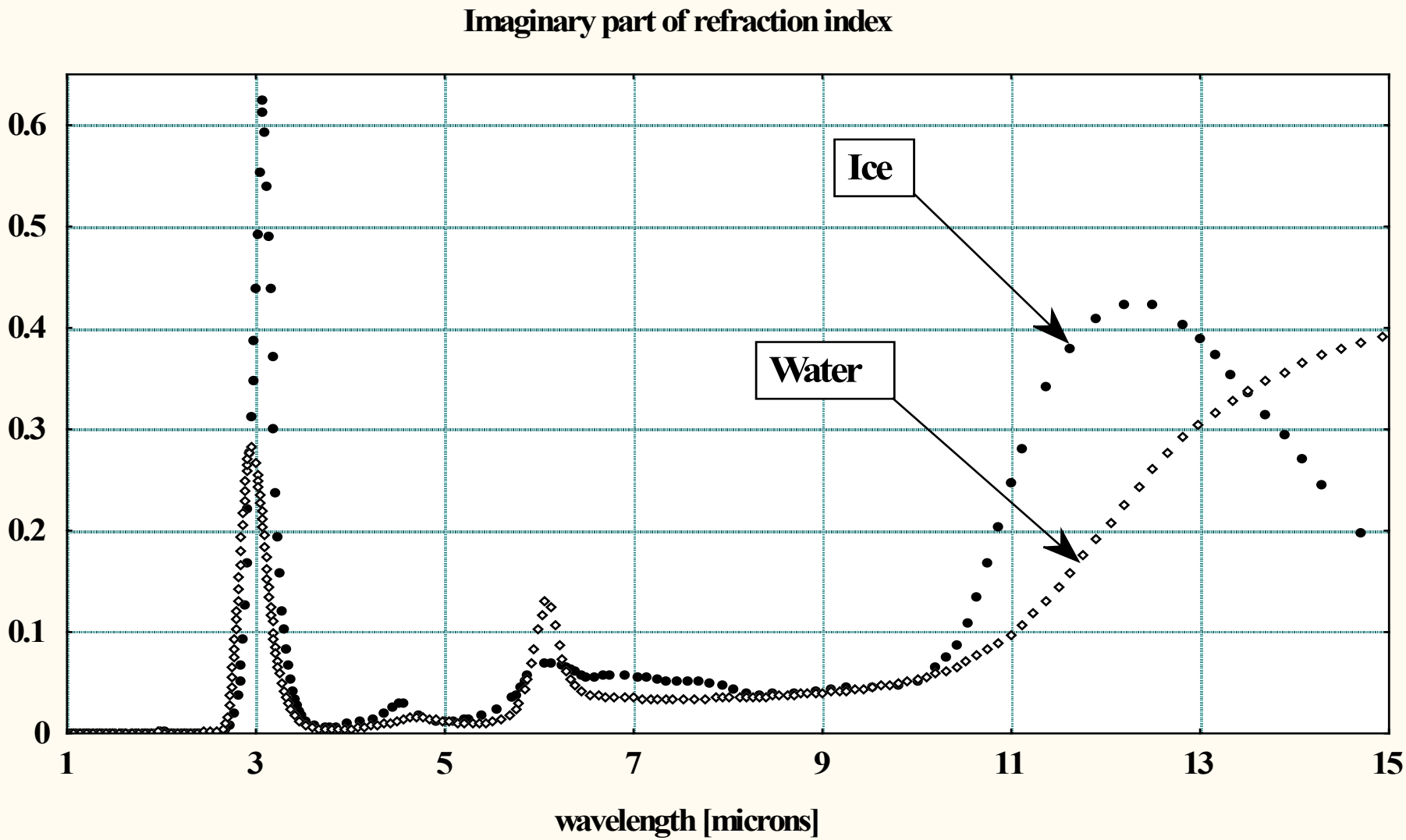

BT[8.6] – BT[11] will be positive for ice clouds

MODIS identifies cloud classes

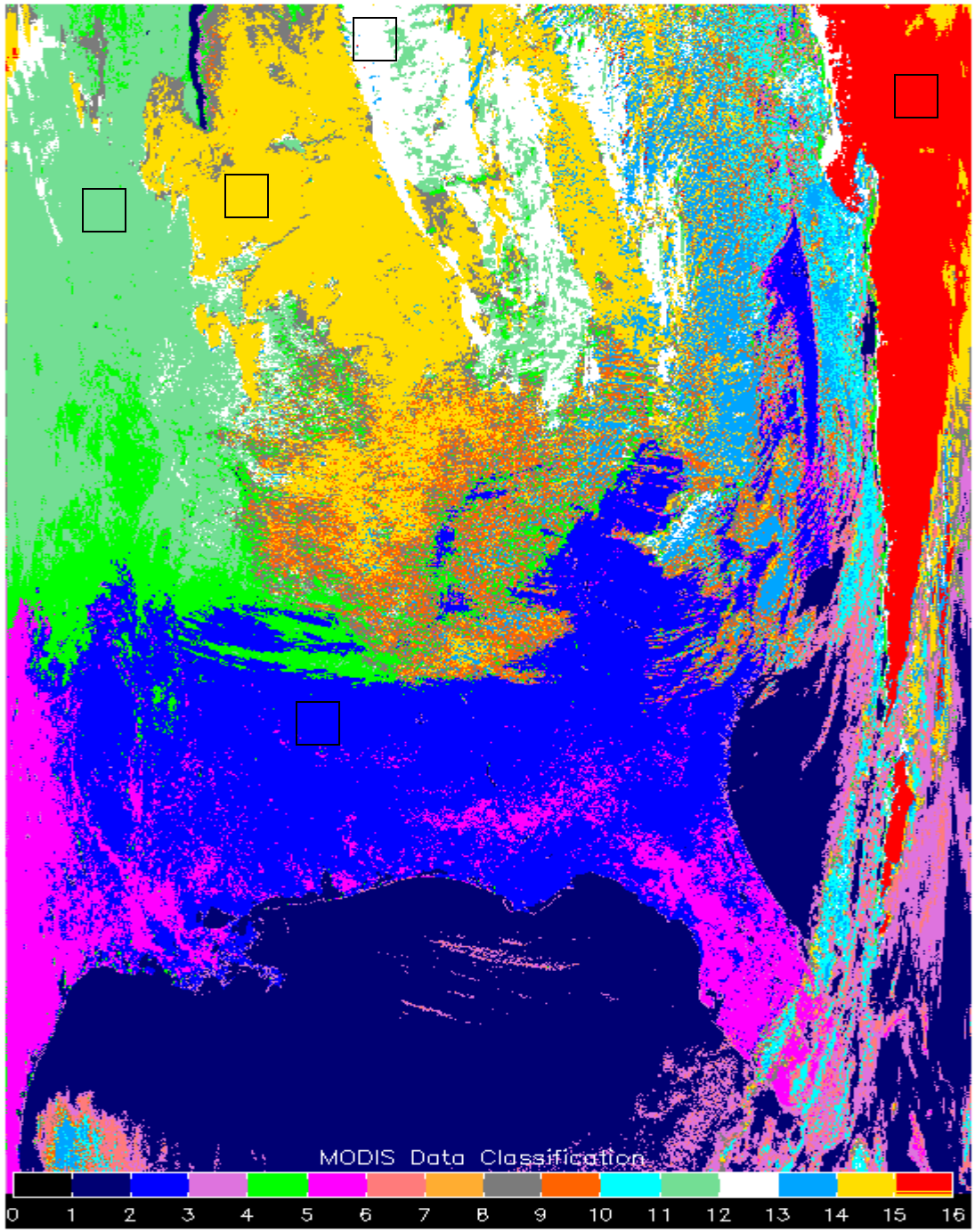

Hi cld

Mid cld

Lo cld

Snow

clr

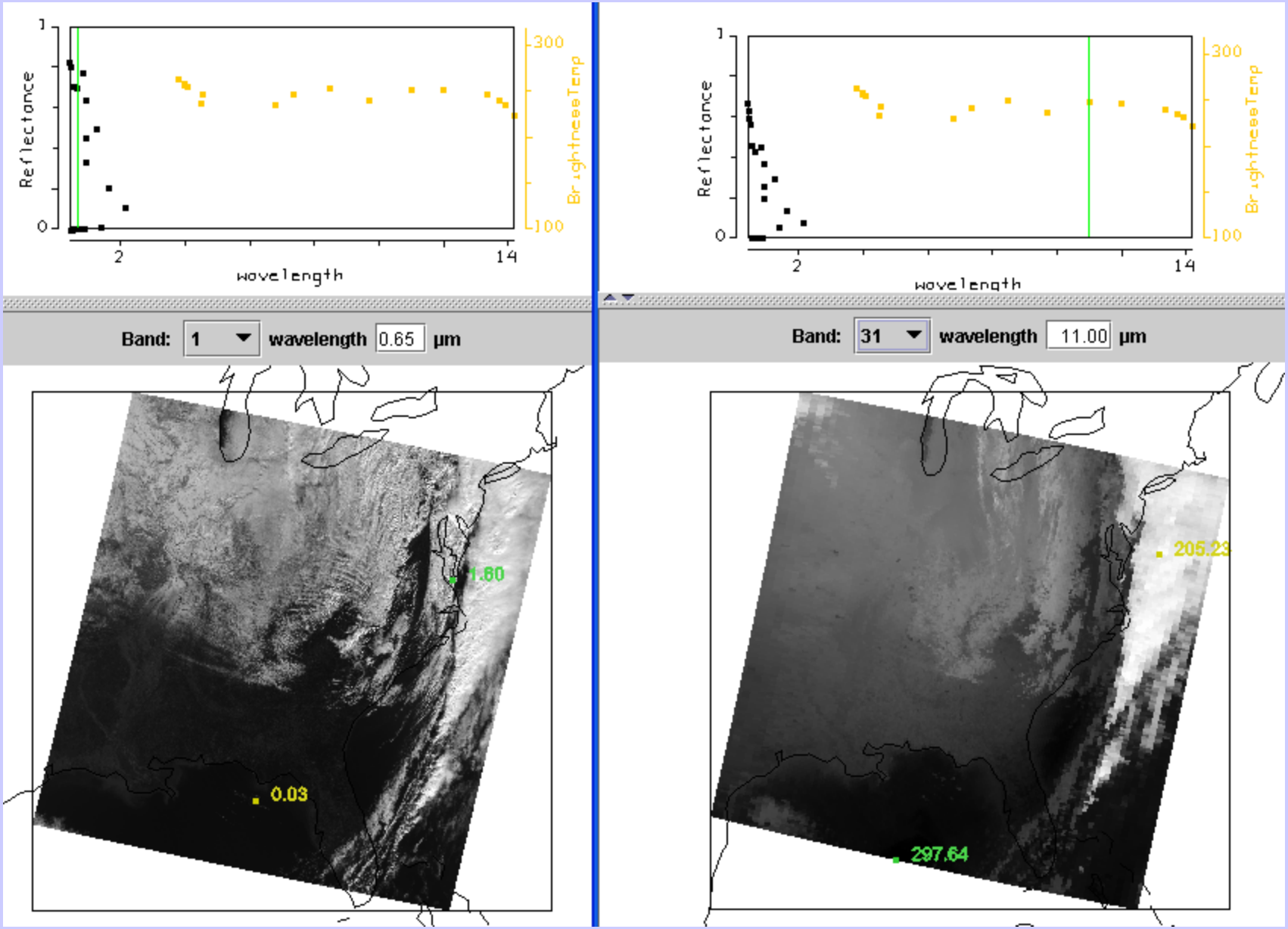

Visible (left) and IRW (right) do not discriminate cloud from clear

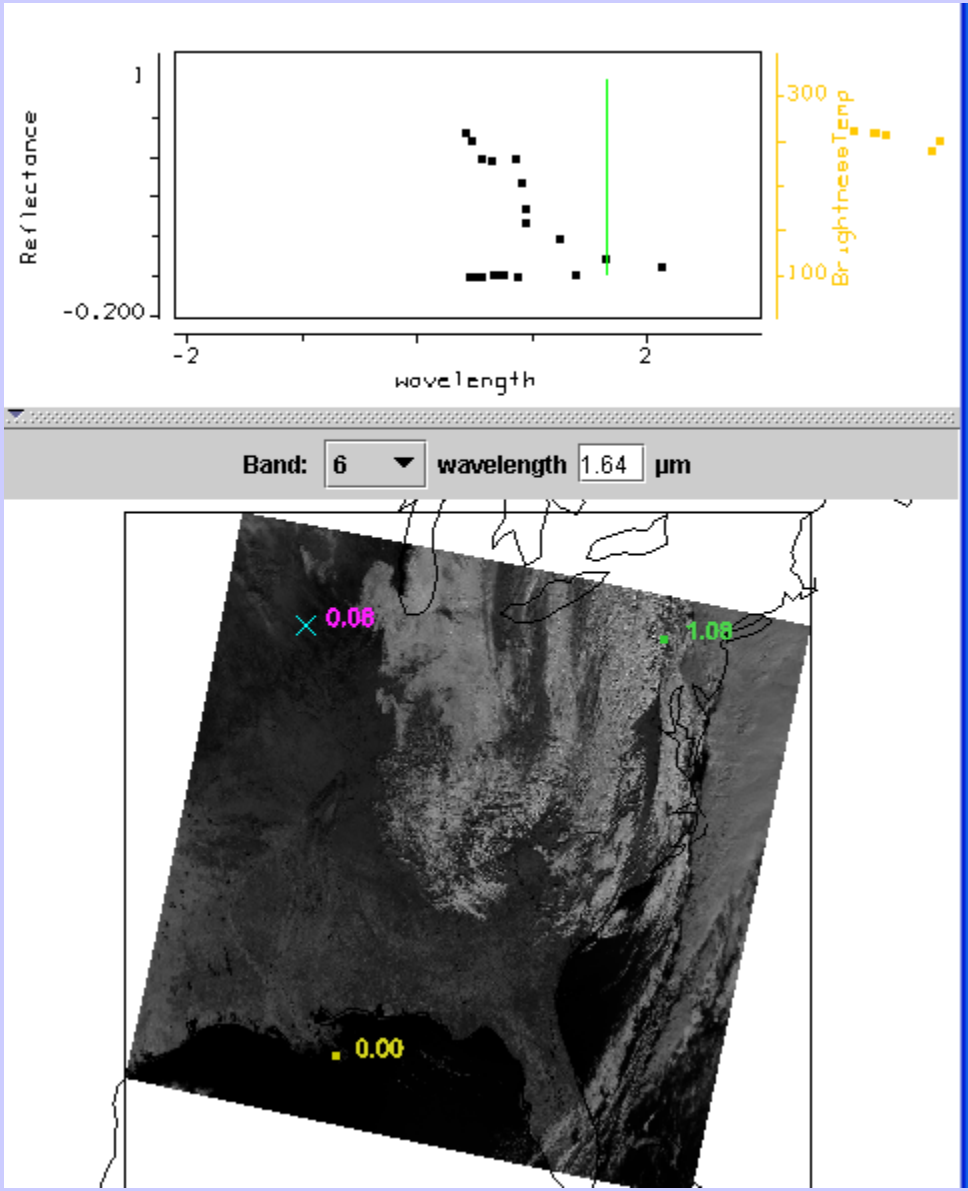

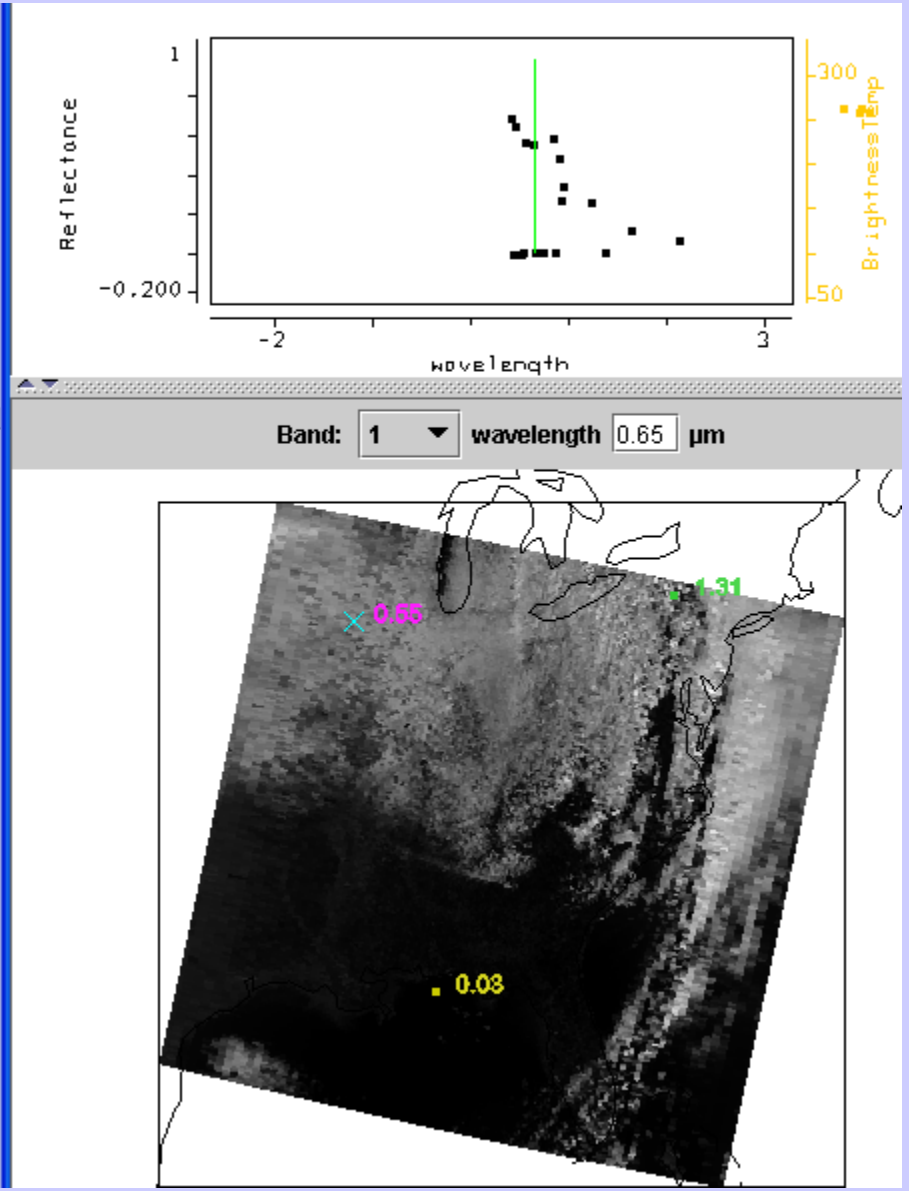

1.6 micron (left) and visible (right) discriminate cloud from snow

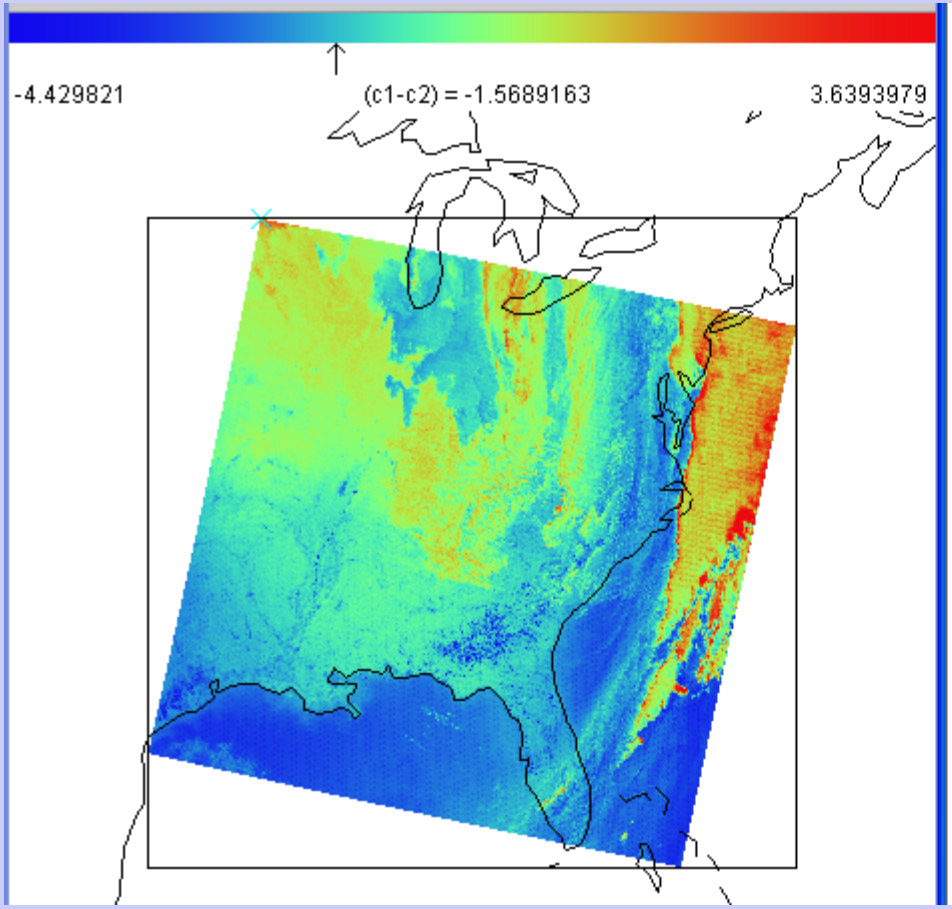

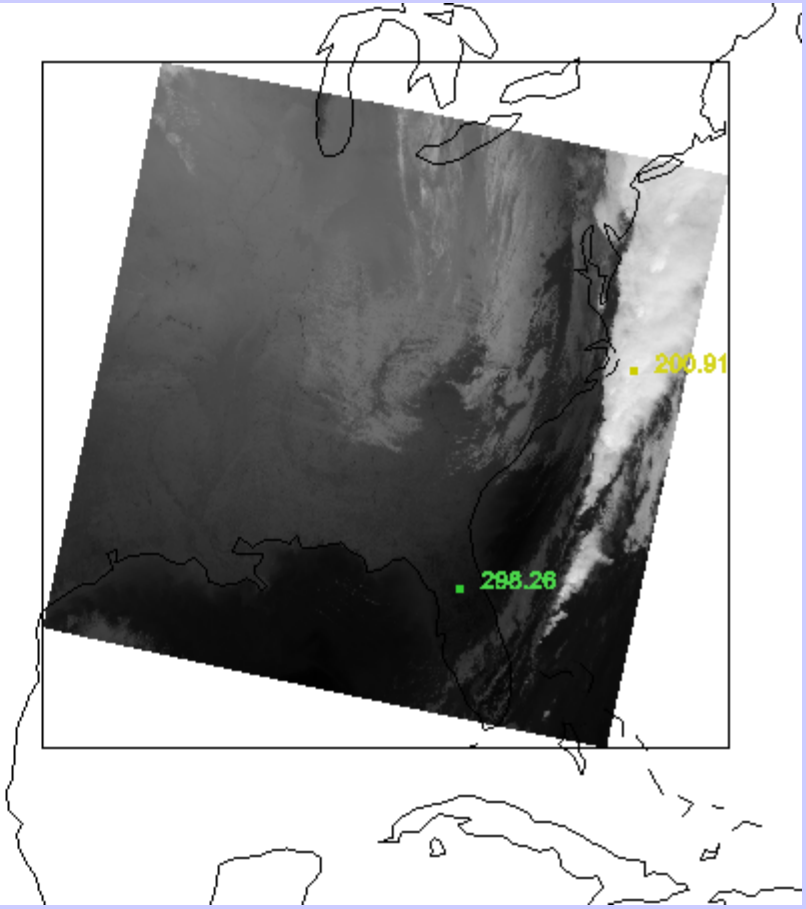

8.6-11 micron (left) & IRW (right) discriminate ice from water cloud

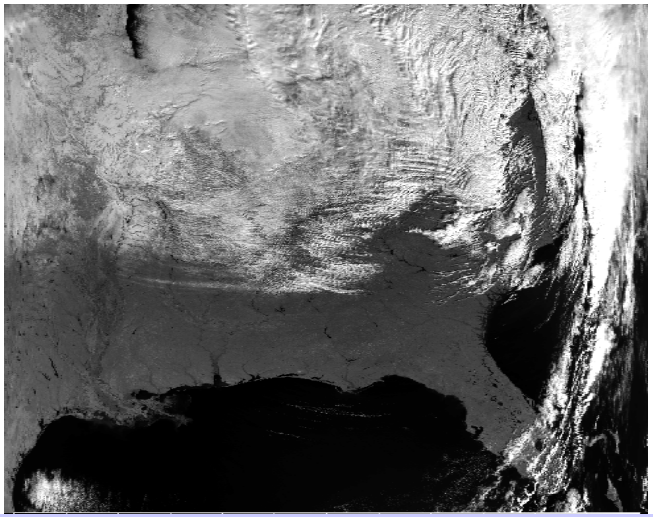

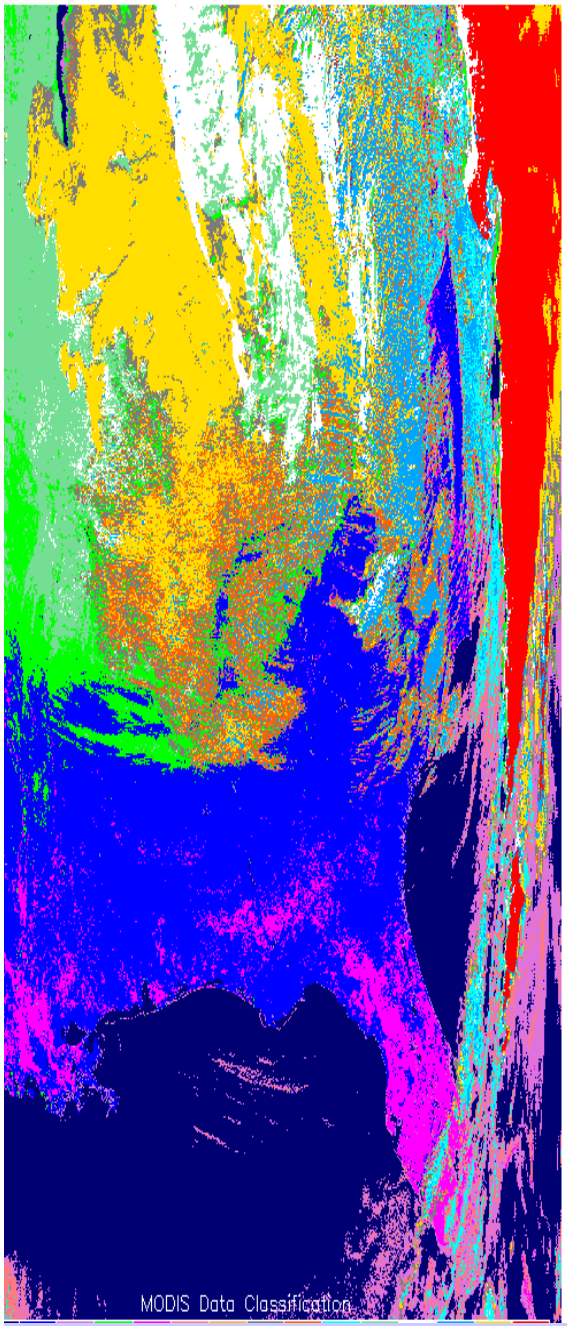

0.86 um **1.6 um** **cld class**

Clouds separate into classes when multispectral radiance information is viewed

vis

LSD 1.6 um

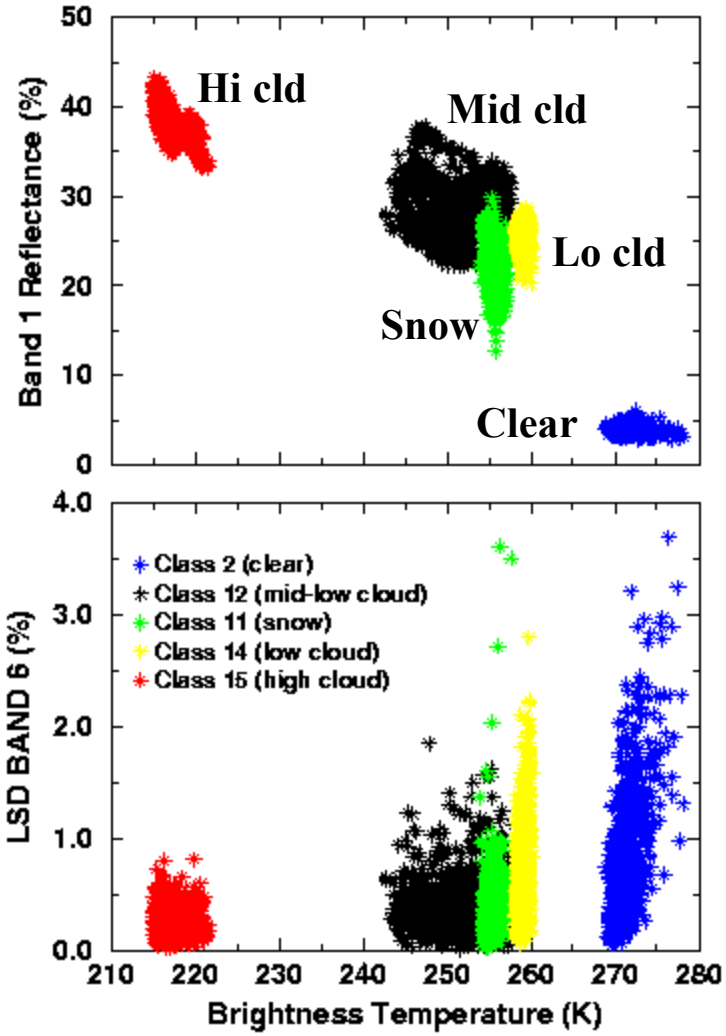

11 um

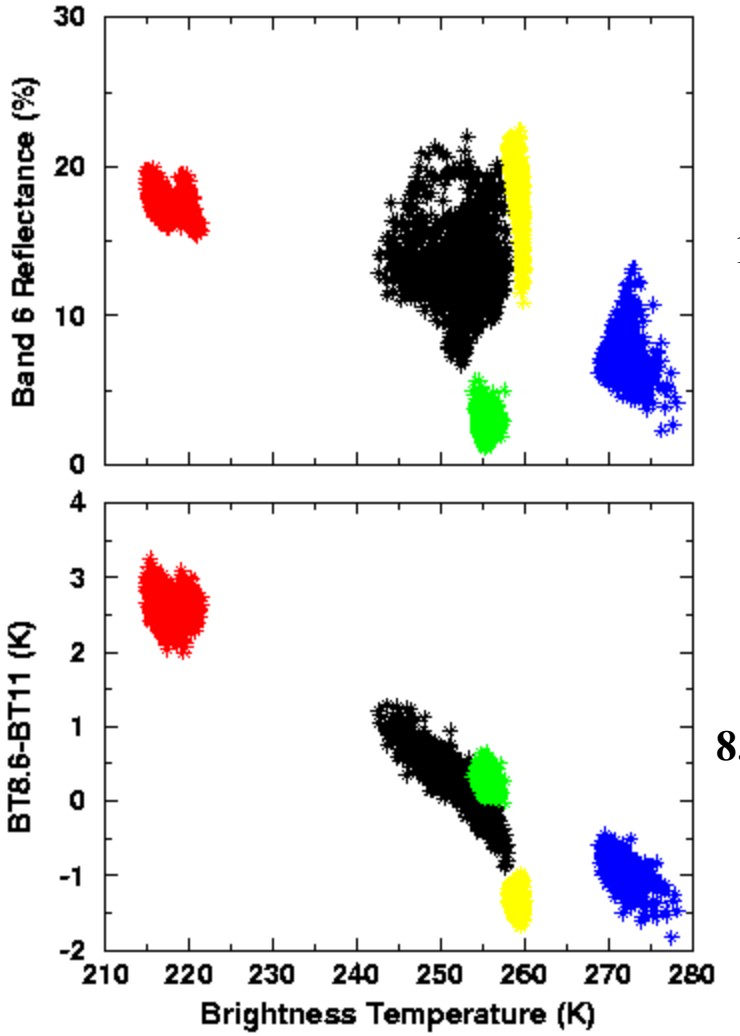

1.6 um

8.6-11 um

11 um

Radiance from a partly cloudy FOV

Cloud Parameter Determinations from Satellite Measured Radiances
for a given field of view (FOV) partly clear and partly cloudy

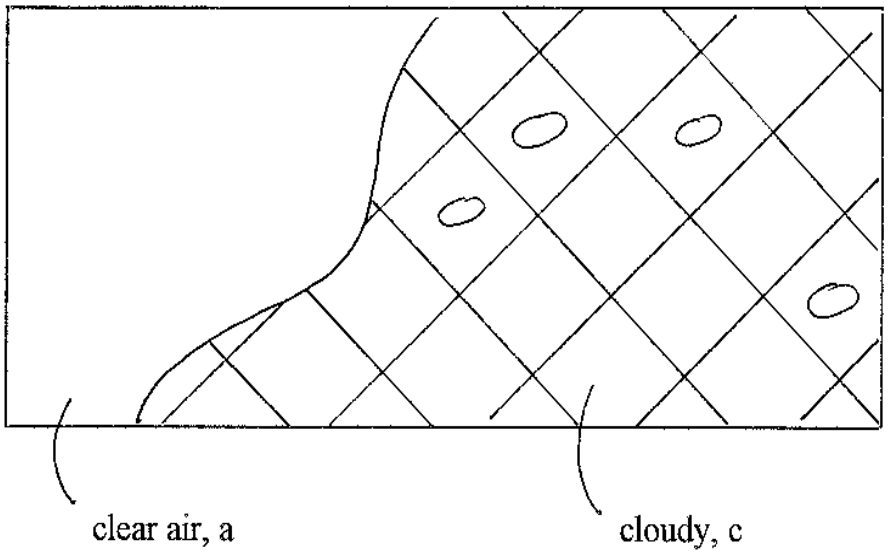

$$R = [1 - N] R_a + N R_c$$

but if b indicates opaque "black" cloud

$$R_c = [1 - \varepsilon] R_a + \varepsilon R_b(p_c)$$

so together

$$R = [1 - N\varepsilon] R_a + N\varepsilon R_b(p_c)$$

Two unknowns, ε and Pc, require two measurements

RTE in Cloudy Conditions

$$I_\lambda = \eta\, I^{cd}_\lambda + (1 - \eta)\, I^{clr}_\lambda$$ where cd = cloud, clr = clear, η = cloud fraction

$$I^{clr}_\lambda = B_\lambda(T_s)\, \tau_\lambda(p_s) + \int_{p_s}^{o} B_\lambda(T(p))\, d\tau_\lambda \,.$$

$$I^{cd}_\lambda = (1-\varepsilon_\lambda)\, B_\lambda(T_s)\, \tau_\lambda(p_s) + (1-\varepsilon_\lambda) \int_{p_s}^{p_c} B_\lambda(T(p))\, d\tau_\lambda$$

$$+ \varepsilon_\lambda\, B_\lambda(T(p_c))\, \tau_\lambda(p_c) + \int_{p_c}^{o} B_\lambda(T(p))\, d\tau_\lambda$$

ε_λ is emittance of cloud. First two terms are from below cloud, third term is cloud contribution, and fourth term is from above cloud. After rearranging

$$I_\lambda - I_\lambda^{clr} = \eta\varepsilon_\lambda \int_{p_s}^{p_c} \tau_\lambda(p)\, \frac{dB_\lambda}{dp}\, dp \,.$$

CO2 channels see to different levels in the atmosphere

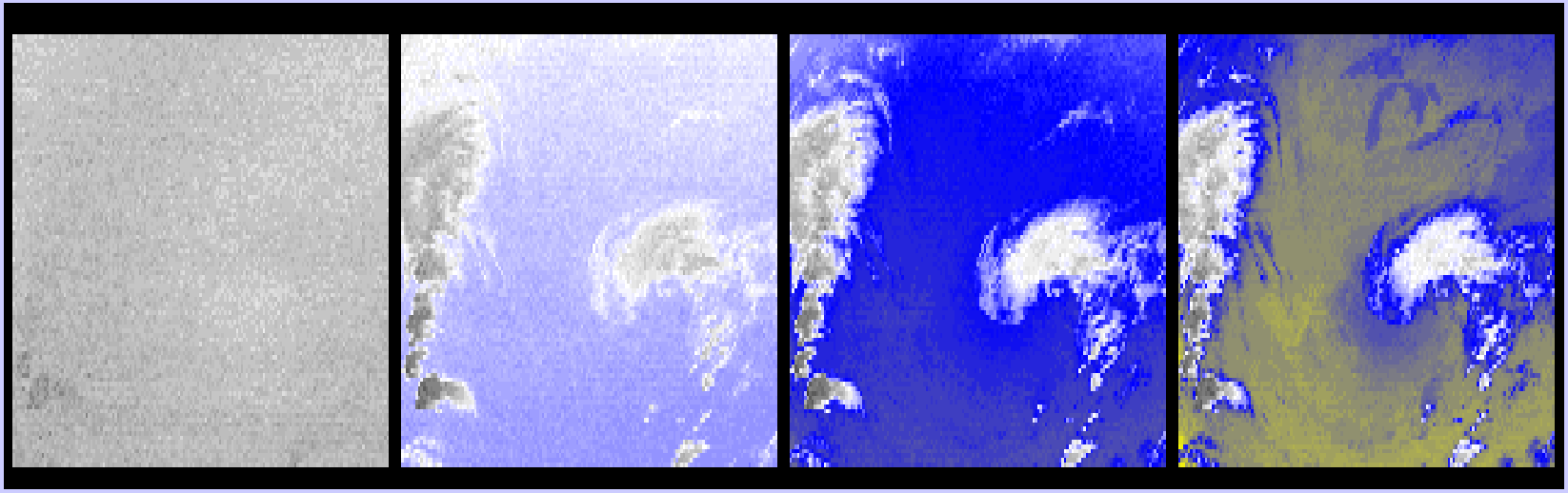

14.2 um 13.9 um 13.6 um 13.3 um

Different ratios reveal cloud properties at different levels

hi - 14.2/13.9
mid - 13.9/13.6
low - 13.6/13.3

Meas **Calc**

$$\frac{(I_{\lambda 1}-I_{\lambda 1}^{clr})}{(I_{\lambda 2}-I_{\lambda 2}^{clr})} = \frac{\eta\varepsilon_{\lambda 1}\int_{p_s}^{p_c}\tau_{\lambda 1}\,dB_{\lambda 1}}{\eta\varepsilon_{\lambda 2}\int_{p_s}^{p_c}\tau_{\lambda 2}\,dB_{\lambda 2}}$$

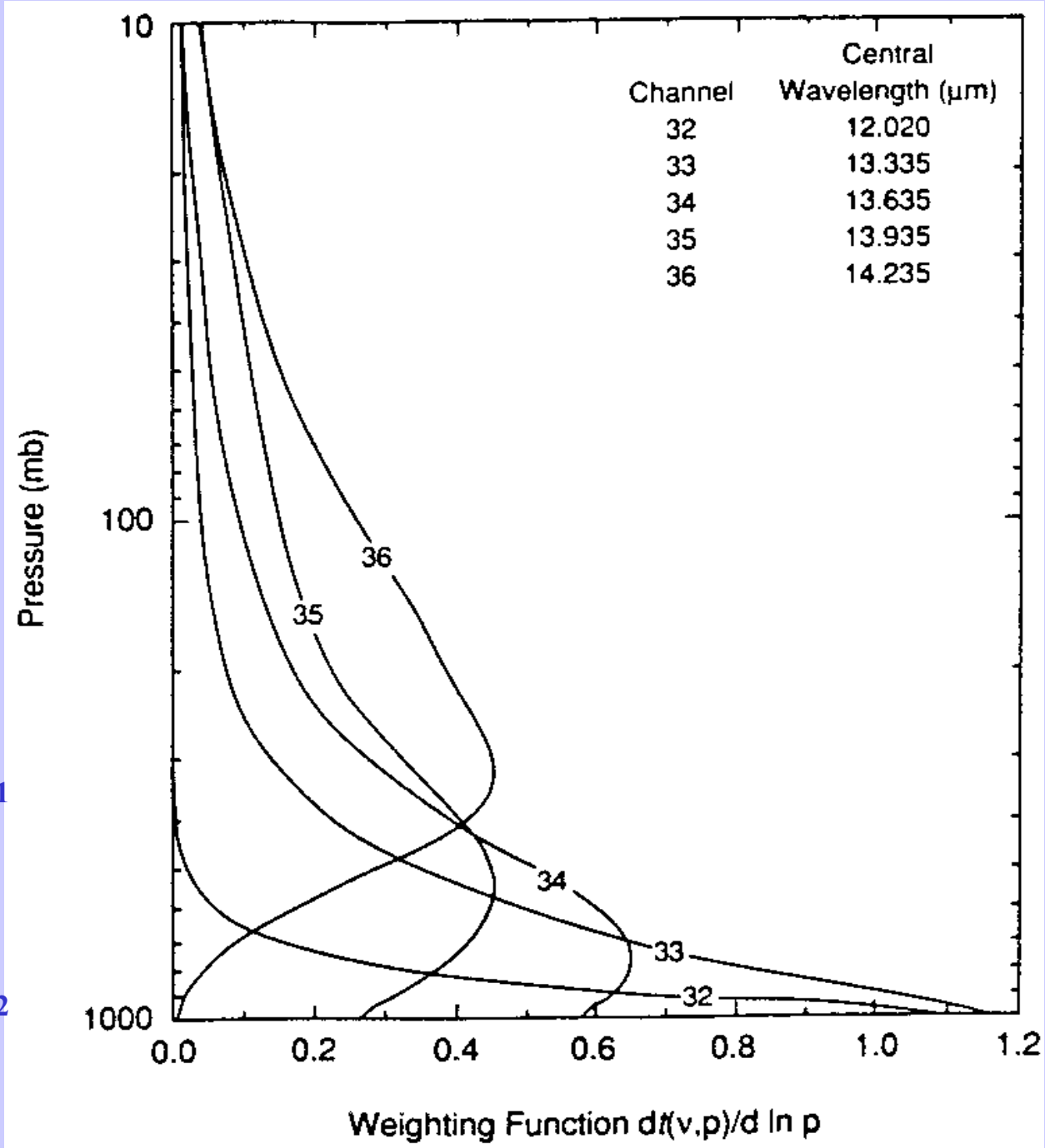

BTs in and out of clouds for MODIS CO_2 bands

demonstrate weighting functions and cloud top algorithm

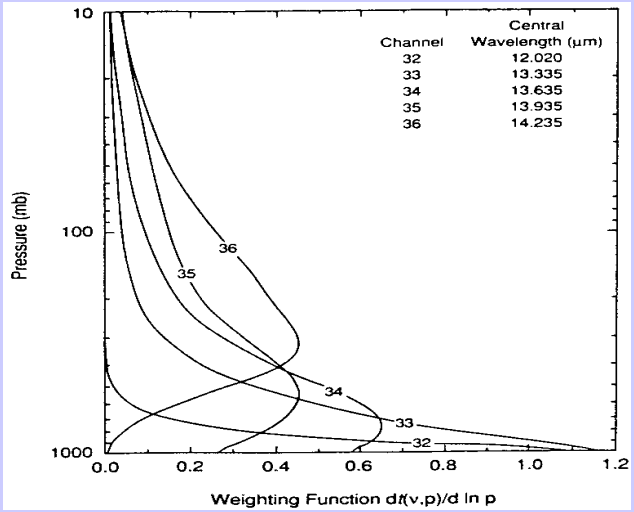

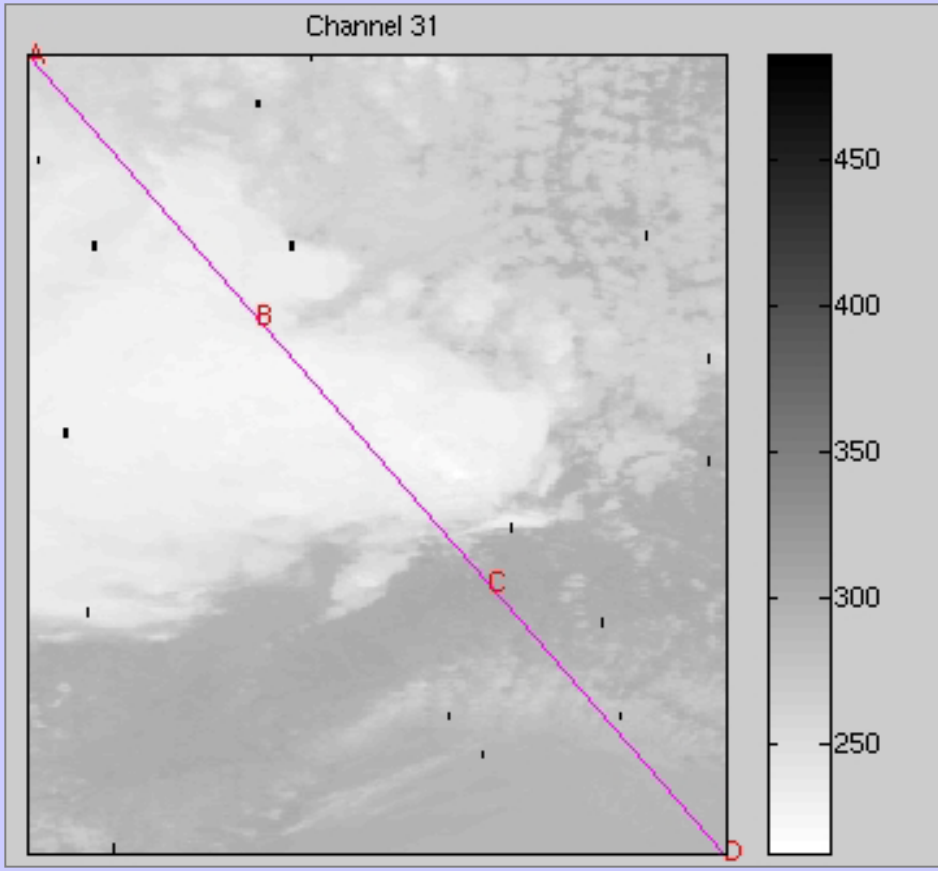

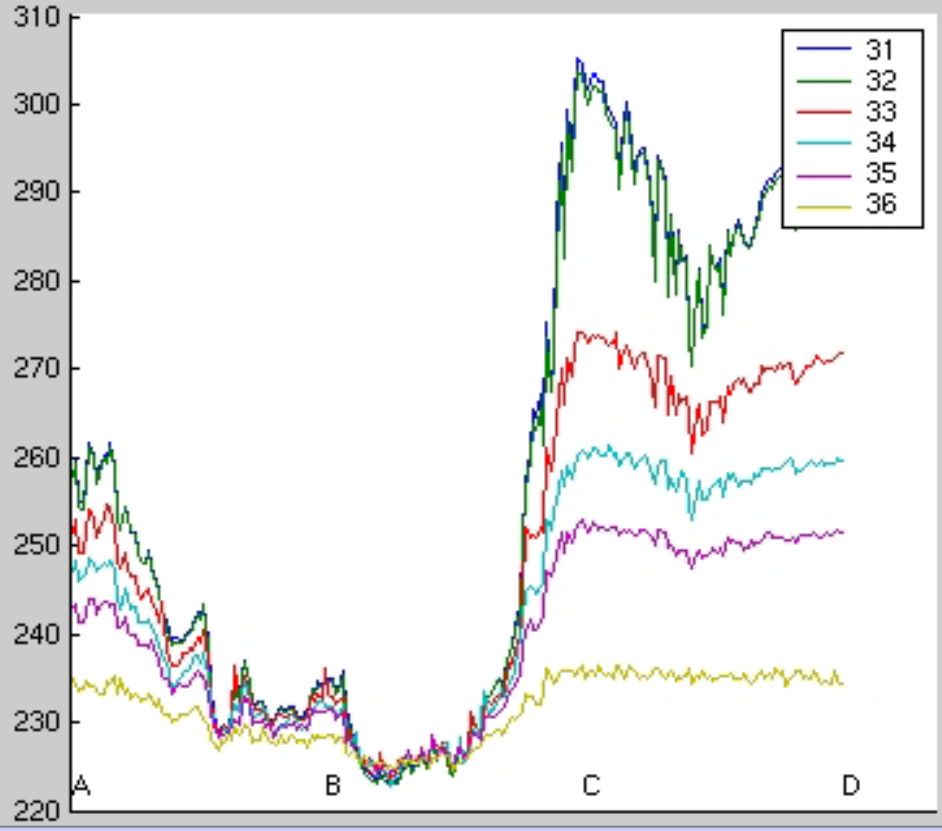

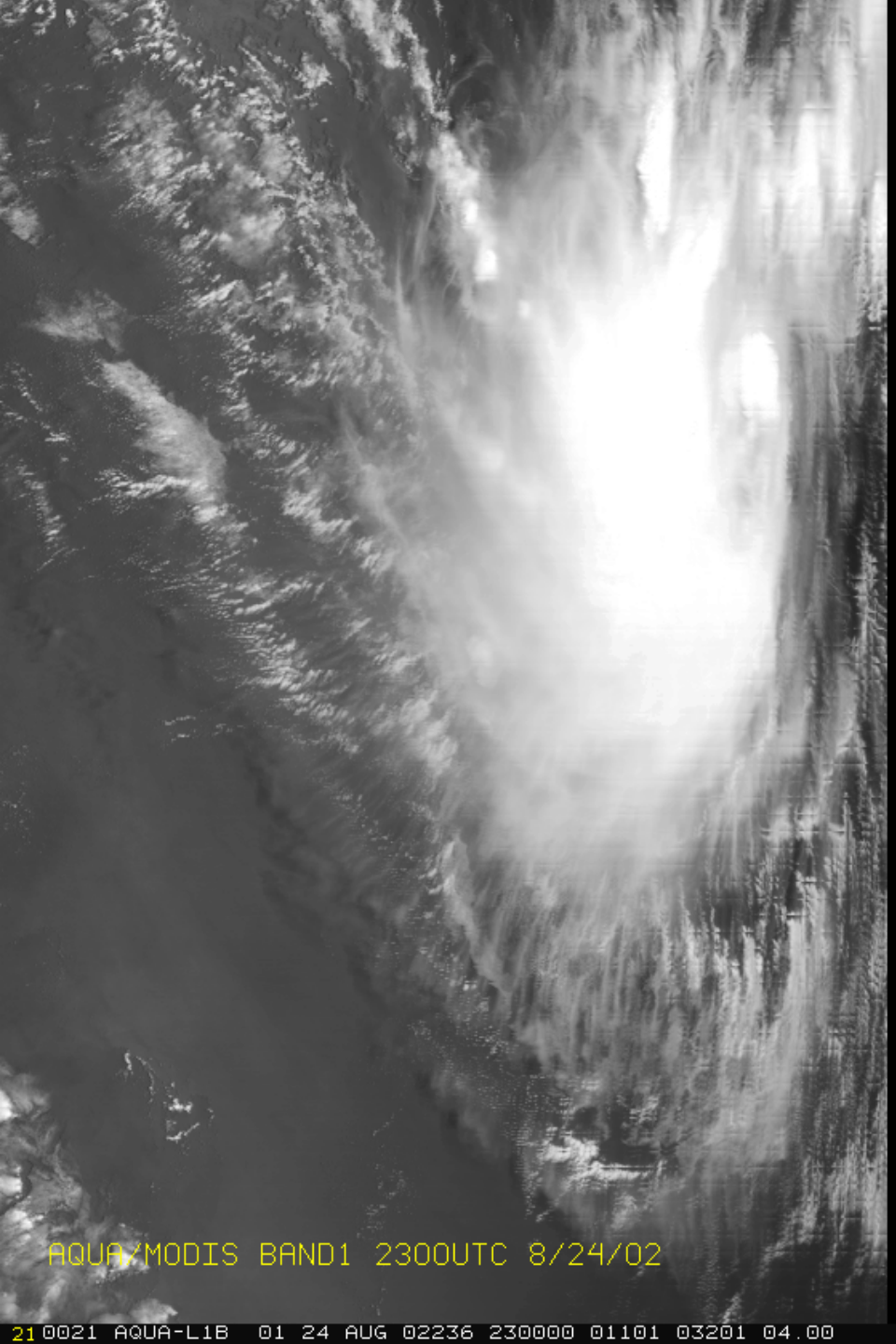

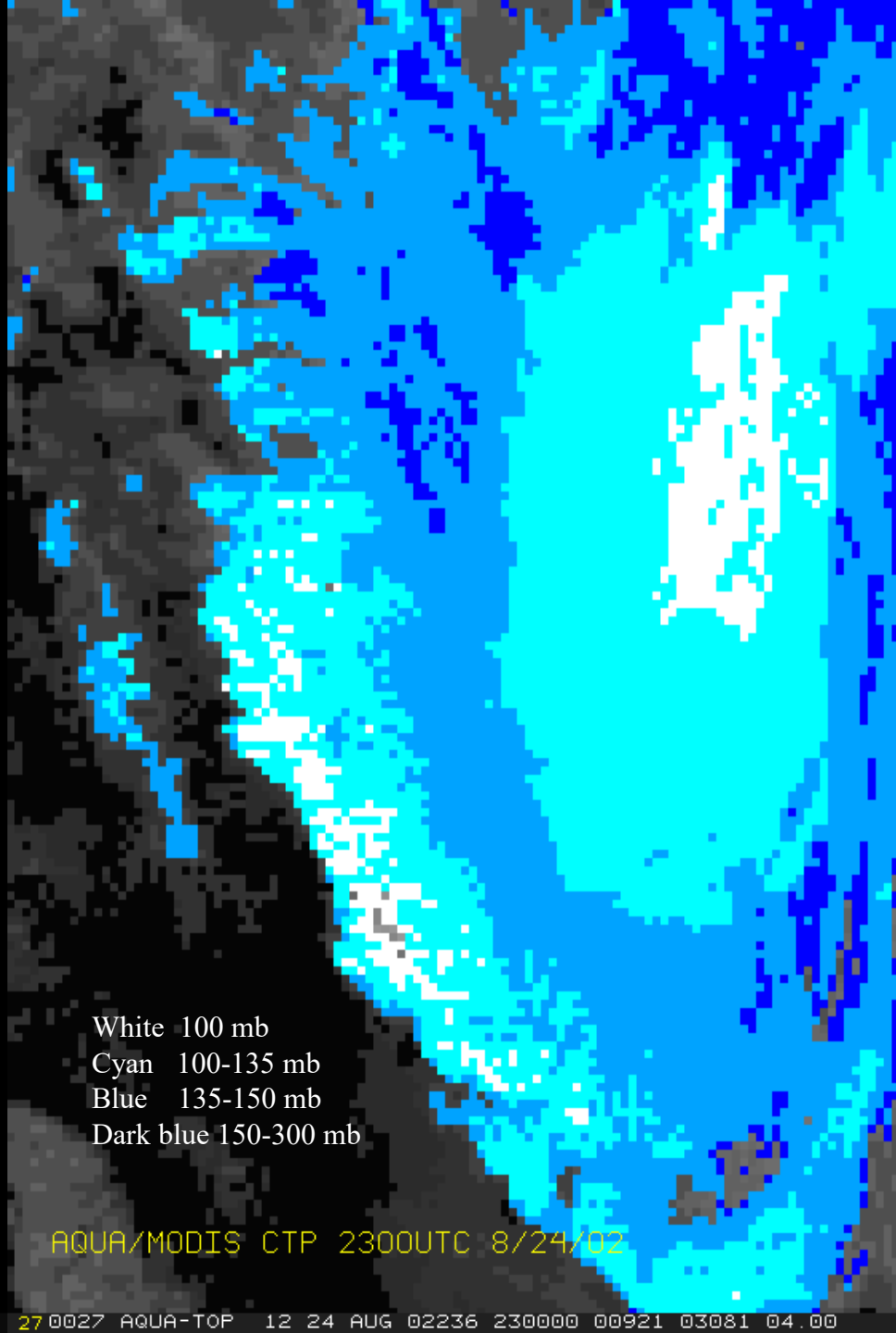

21 0021 AQUA-L1B 01 24 AUG 02236 230000 01101 03201 04.00

27 0027 AQUA-TOP 12 24 AUG 02236 230000 00921 03081 04.00

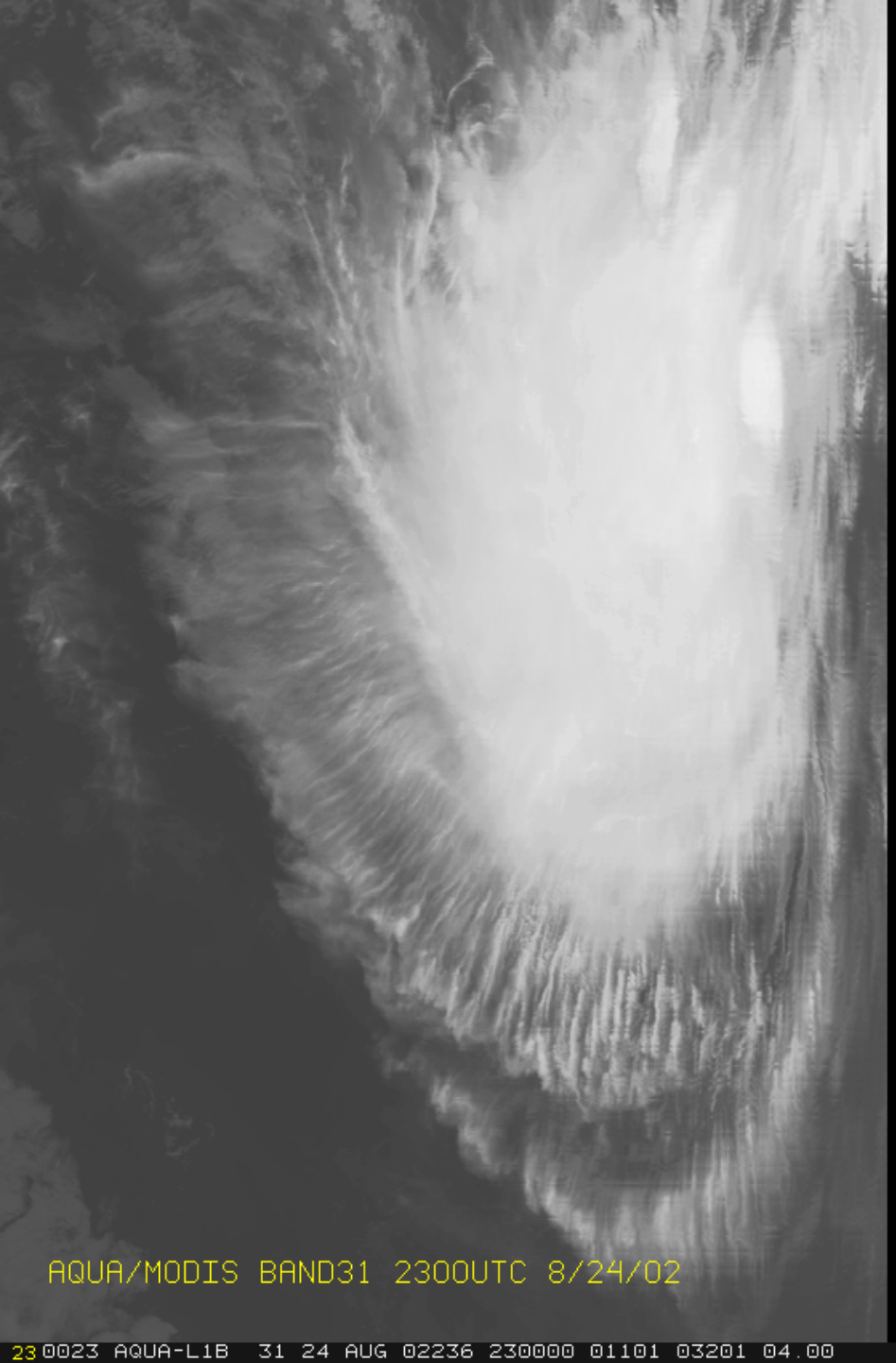

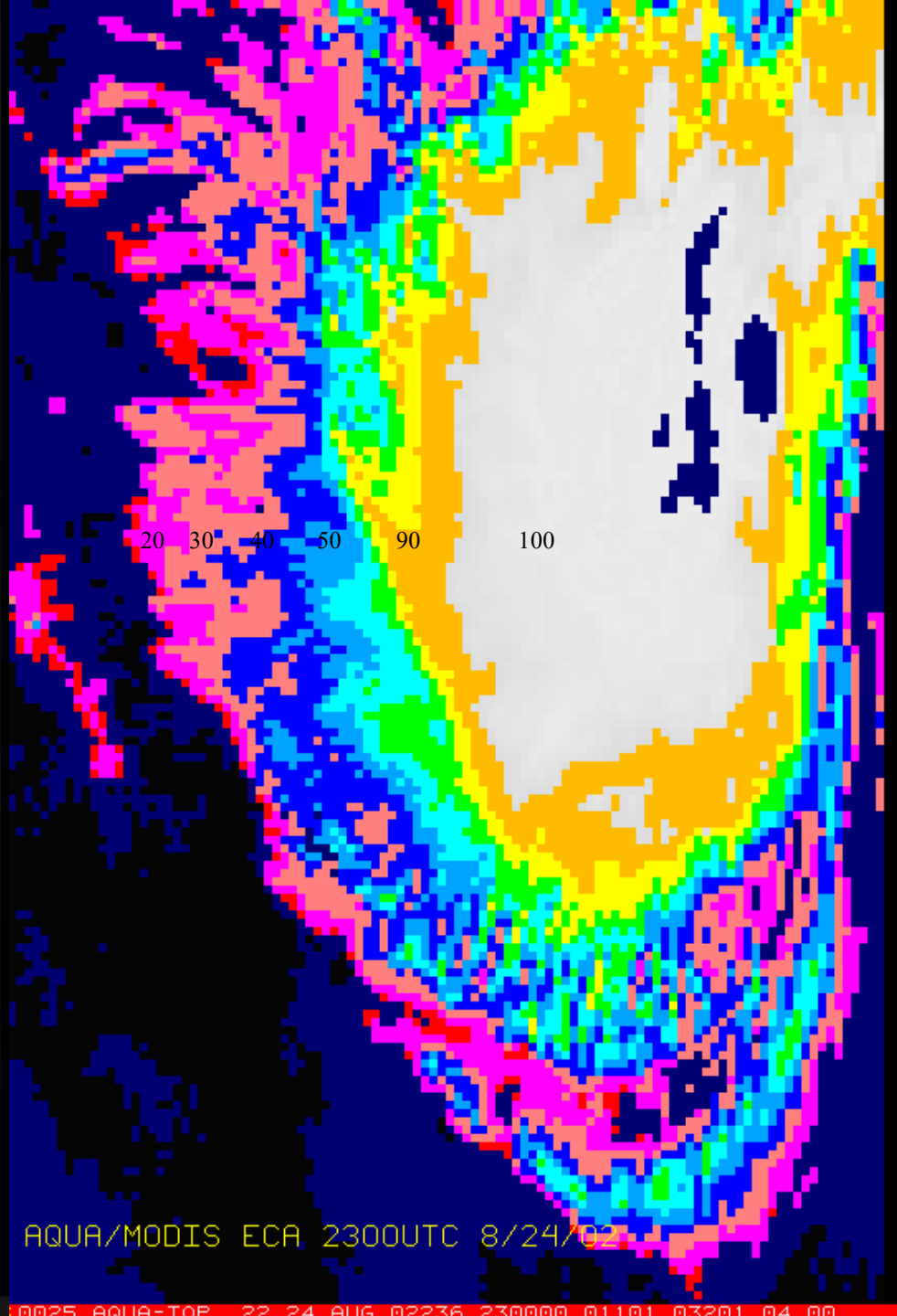

23 0023 AQUA-L1B 31 24 AUG 02236 230000 01101 03201 04.00
0025 AQUA-TOP 22 24 AUG 02236 230000 01101 03201 04.00

January 2001: MODIS High Clouds (0–400 mb)

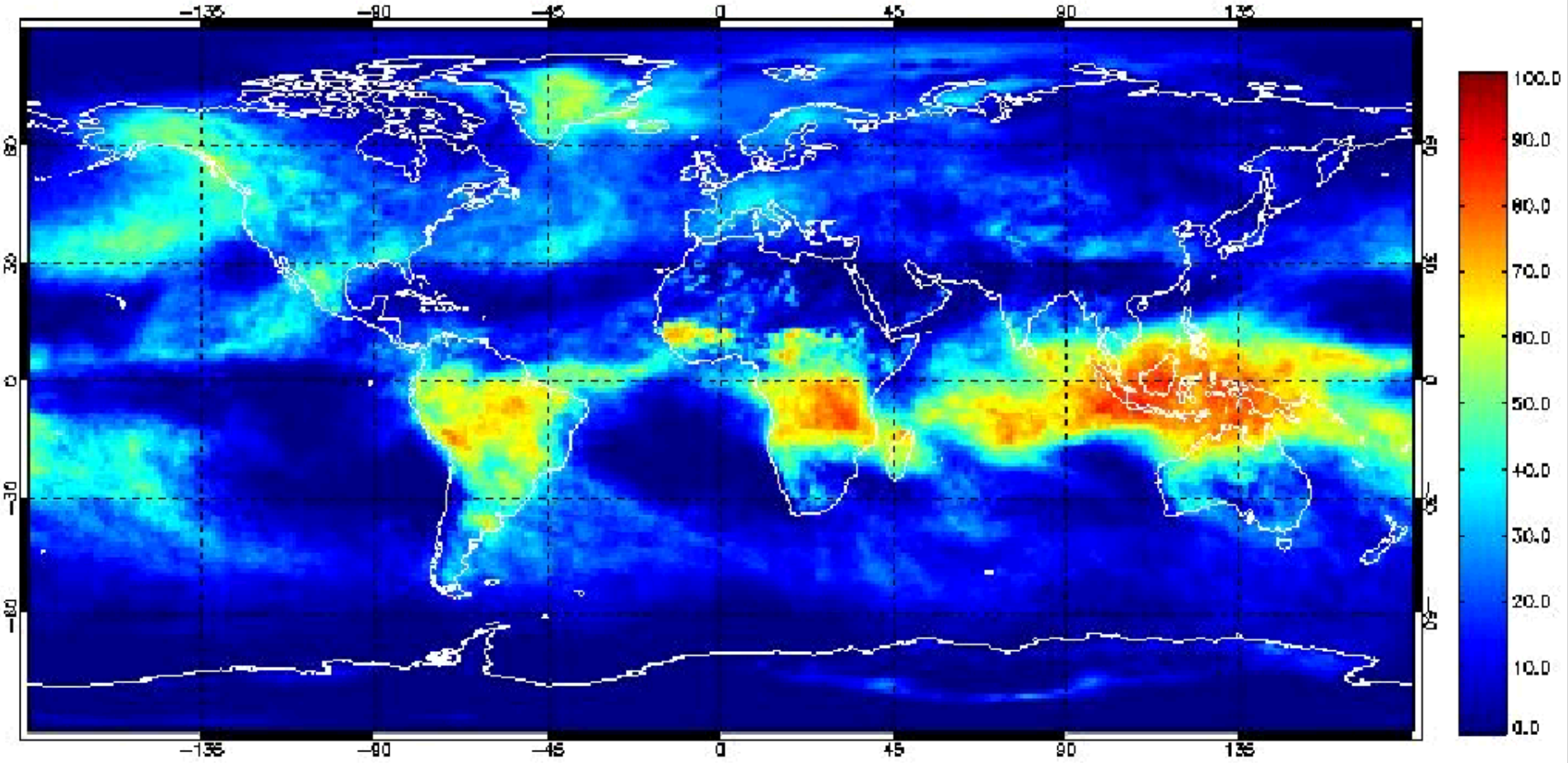

Simulations of Ice and Water Phase Clouds
8.5 - 11 μm BT Differences

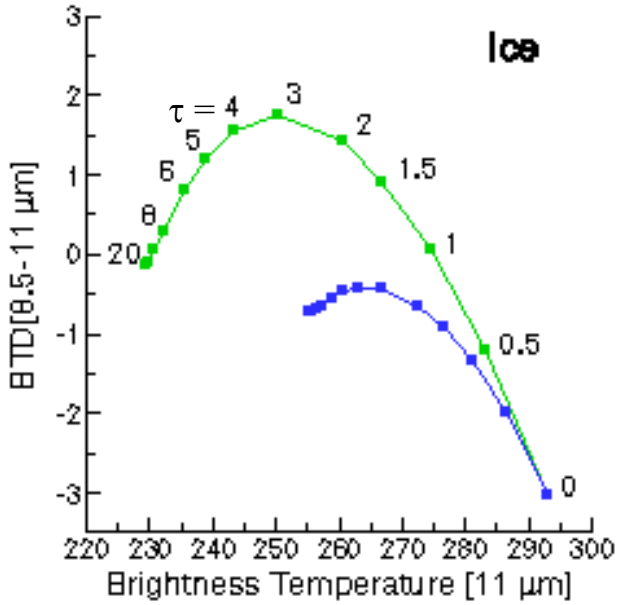

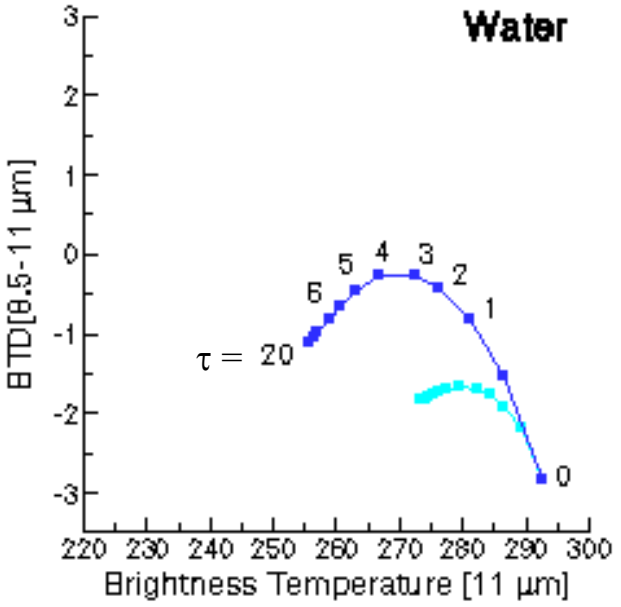

High Ice clouds

- BTD[8.5-11] > 0 over a large range of optical thicknesses τ
- T_{cld} = 228 K

Midlevel clouds

- BTD[8.5-11] values are similar (*i.e.*, negative) for both water and ice clouds
- T_{cld} = 253 K

Low-level, warm clouds

- BTD[8.5-11] values always negative
- T_{cld} = 273 K

Ice: Cirrus model derived from FIRE-I in-situ data (Nasiri et al, 2002)
Water: r_e=10 μm
Angles: θ_o = 45°, θ = 20°, and ϕ = 40°
Profile: midlatitude summer

MODIS Direct Broadcast

May 14, 2003 at 1458 UTC (Terra)
1-km resolution

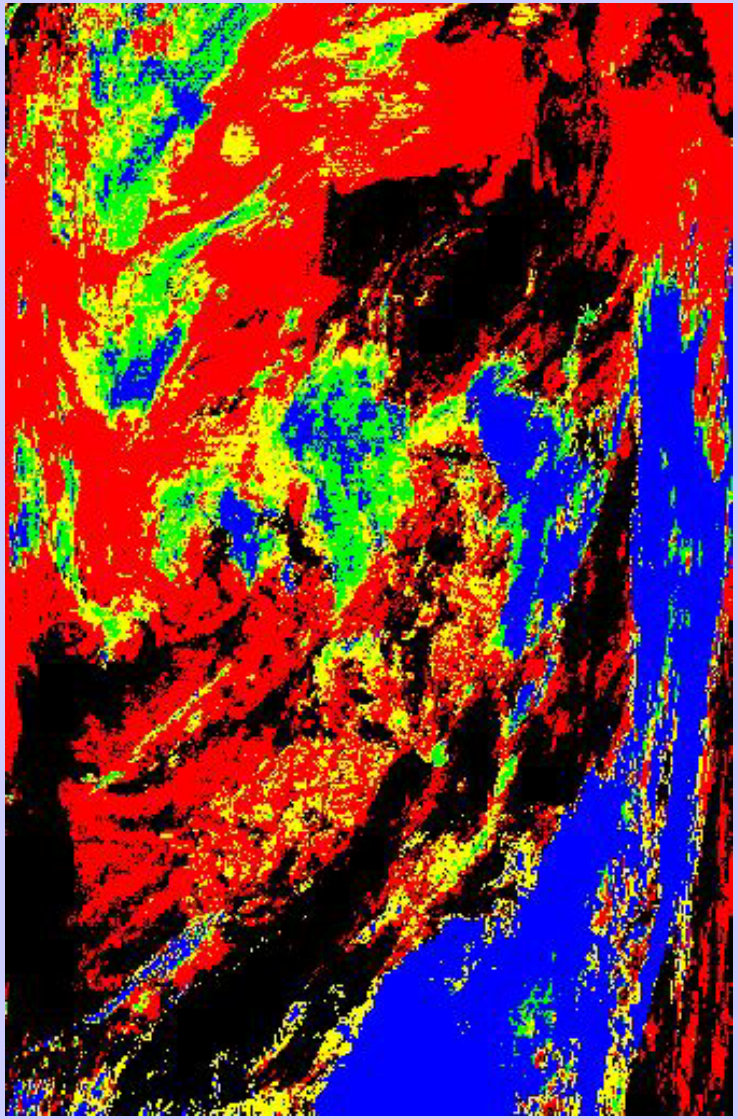

Cloud Clearing

For a single layer of clouds, radiances in one spectral band vary linearly with those of another as cloud amount varies from one field of view (fov) to another

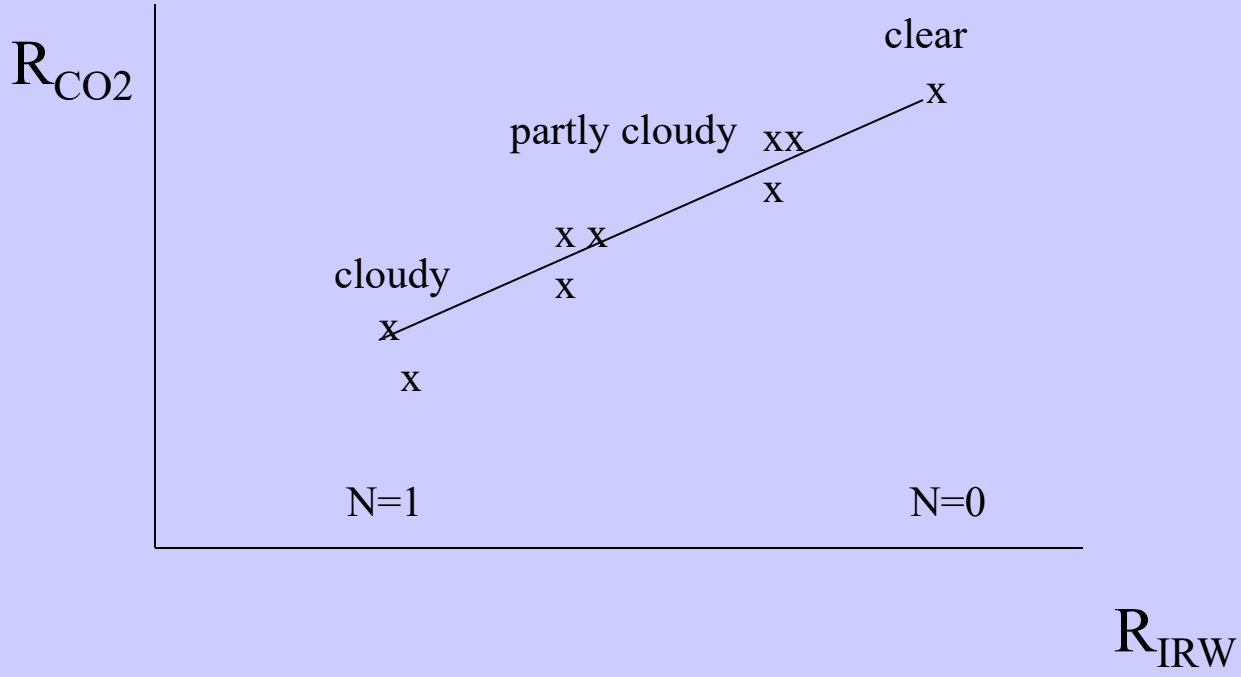

Clear radiances can be inferred by extrapolating to cloud free conditions.

First Order Estimation of TPW

Moisture attenuation in atmospheric windows varies linearly with optical depth.

$$\tau_\lambda = e^{-k_\lambda u} = 1 - k_\lambda u$$

For same atmosphere, deviation of brightness temperature from surface temperature is a linear function of absorbing power. Thus moisture corrected SST can inferred by using split window measurements and extrapolating to zero k_λ

$$T_s = T_{bw1} + [\, k_{w1} / (k_{w2} - k_{w1}) \,] \, [T_{bw1} - T_{bw2}] \; .$$

Moisture content of atmosphere inferred from slope of linear relation.

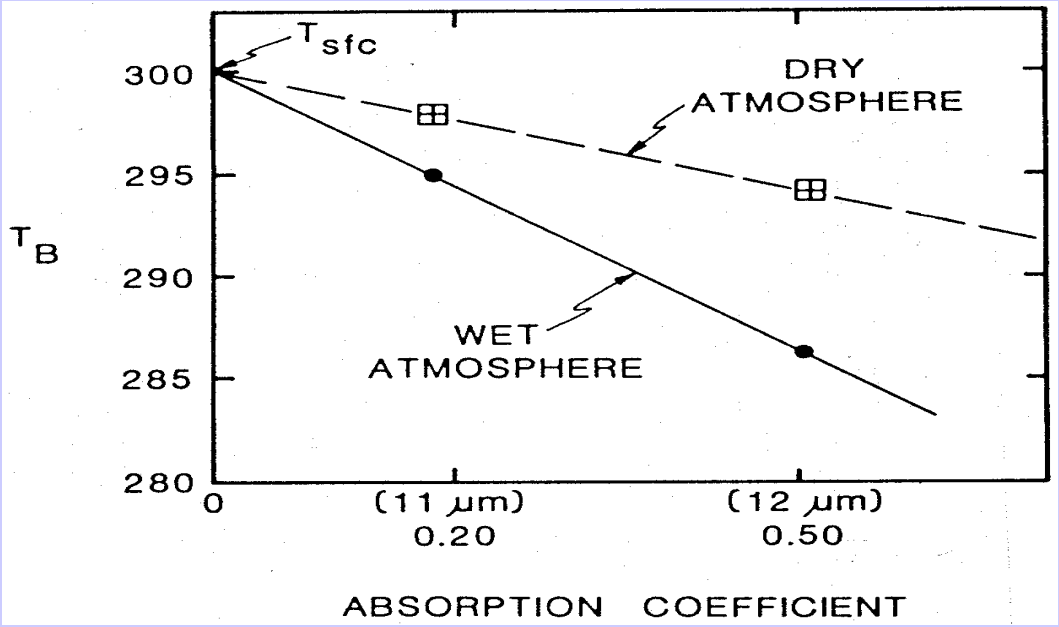

Water vapour evaluated in multiple infrared window channels where absorption is weak, so that

$$\tau_w = \exp[-k_w u] \sim 1 - k_w u \text{ where w denotes window channel}$$

and

$$d\tau_w = -k_w du$$

What little absorption exists is due to water vapour, therefore, u is a measure of precipitable water vapour. RTE in window region

$$I_w = B_{sw}(1-k_w u_s) + k_w \int_o^{u_s} B_w du$$

u_s represents total atmospheric column absorption path length due to water vapour, and s denotes surface. Defining an atmospheric mean Planck radiance, then

$$I_w = B_{sw}(1-k_w u_s) + k_w u_s \bar{B}_w \text{ with } \bar{B}_w = \int_o^{u_s} B_w du \Big/ \int_o^{u_s} du$$

Since B_{sw} is close to both I_w and B_w, first order Taylor expansion about the surface temperature T_s allows us to linearize the RTE with respect to temperature, so

$T_{bw} = T_s(1-k_w u_s) + k_w u_s \bar{T}_w$, where T_w is mean atmospheric temperature corresponding to B_w.

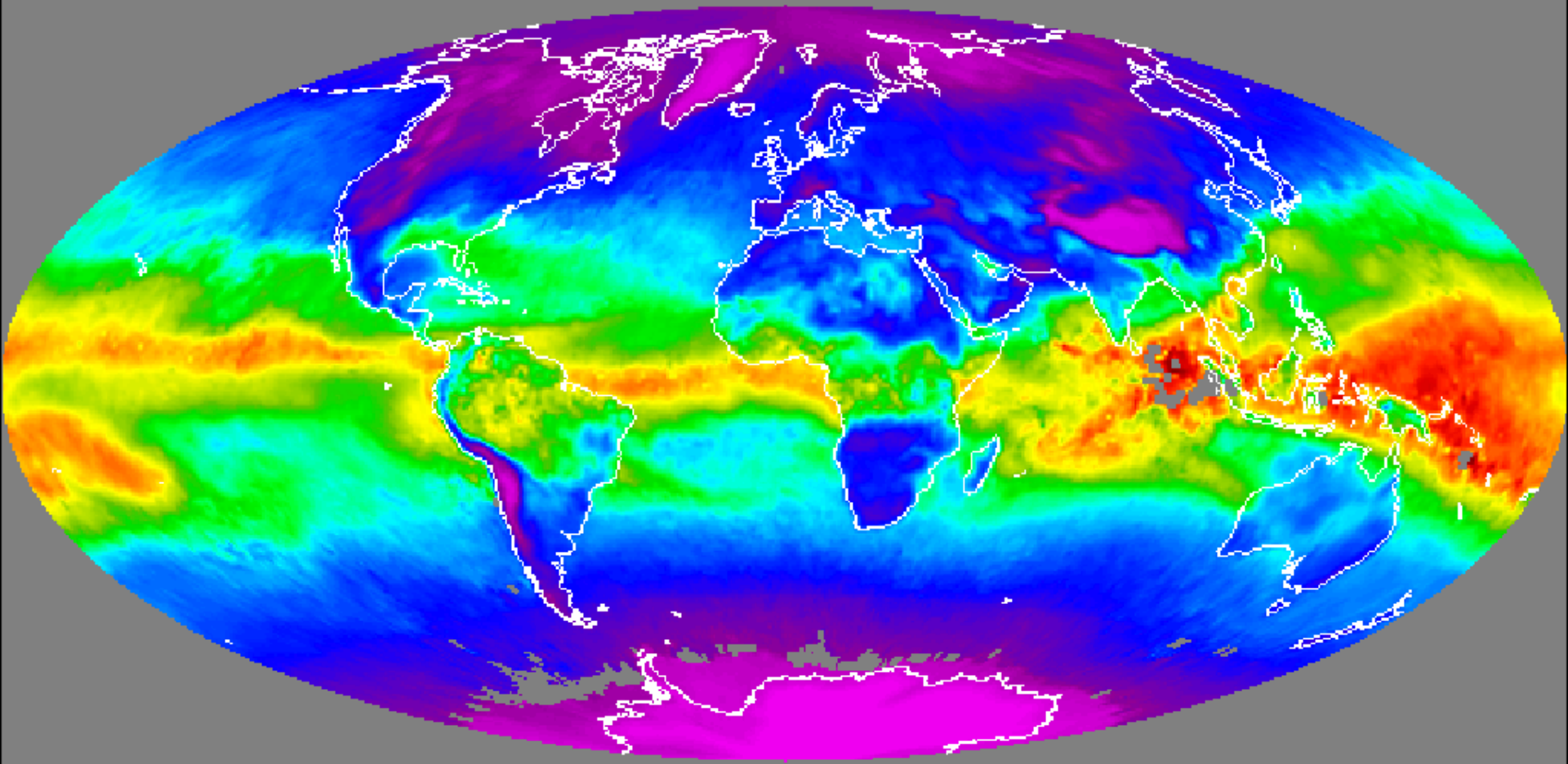

Global TPW from Seemann

T(p)

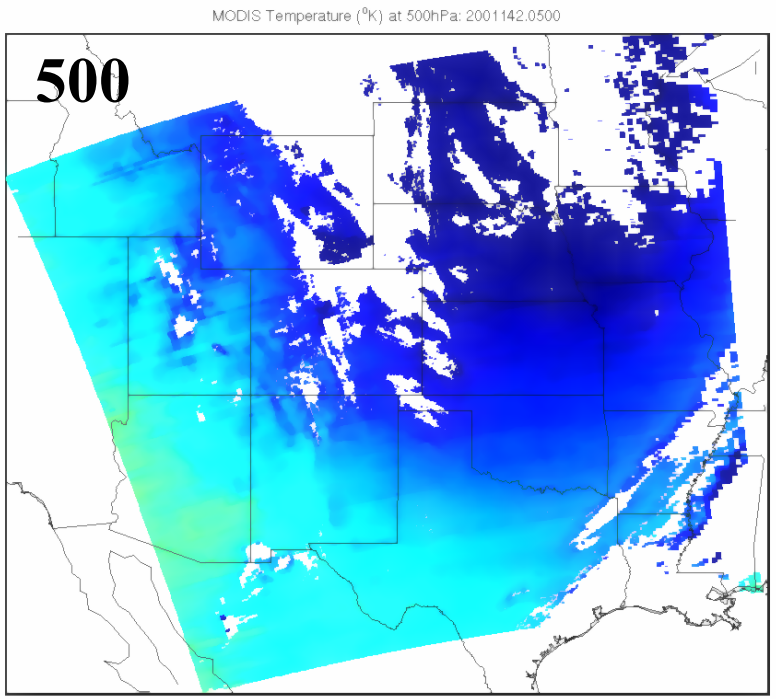
MODIS Temperature (°K) at 500hPa: 2001142.0500
500

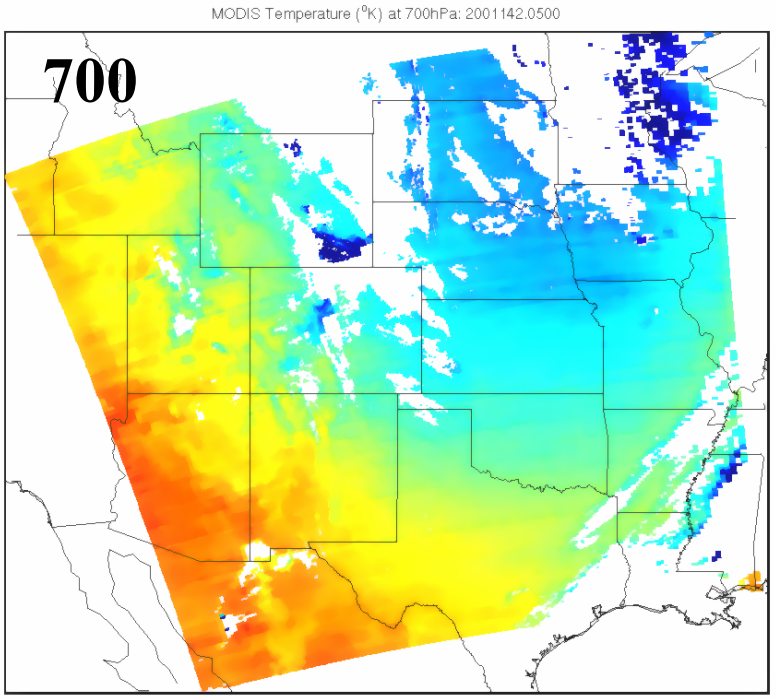
MODIS Temperature (°K) at 700hPa: 2001142.0500
700

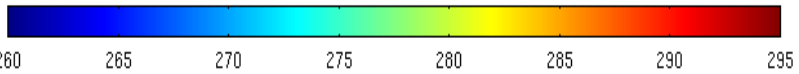
260
265
270
275
280
285
290
295

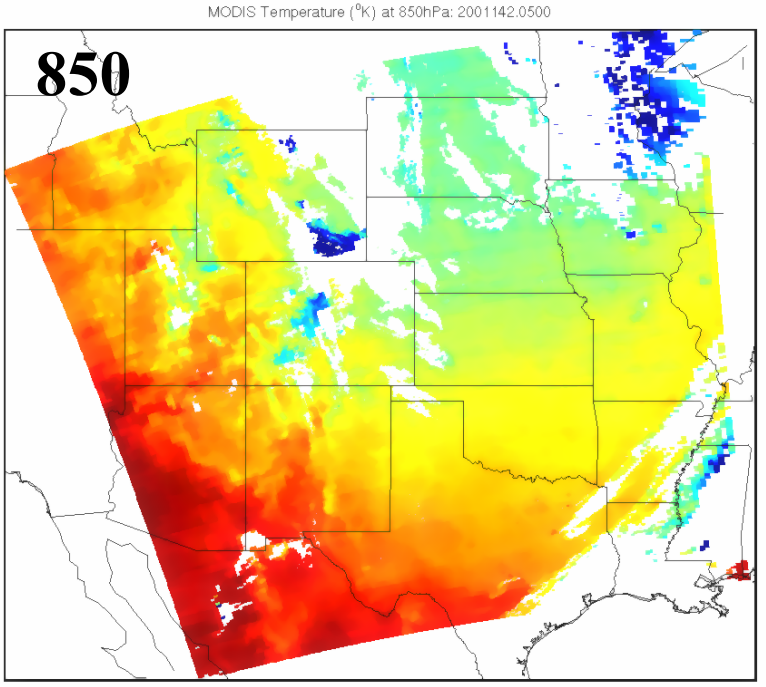
MODIS Temperature (°K) at 850hPa: 2001142.0500
850

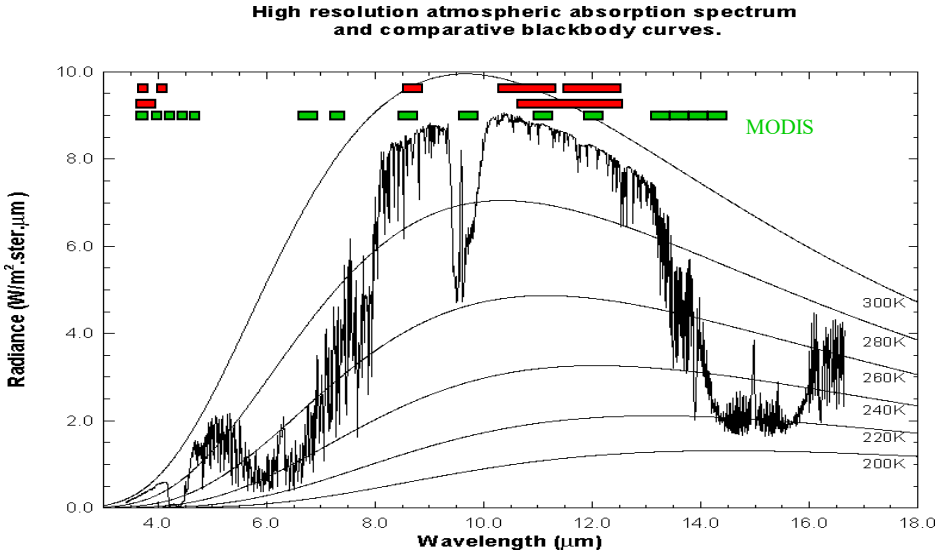
High resolution atmospheric absorption spectrum
and comparative blackbody curves.
MODIS
300K
280K
260K
240K
220K
200K
Radiance (W/m².ster.μm)
Wavelength (μm)
0.0
2.0
4.0
6.0
8.0
10.0
4.0
6.0
8.0
10.0
12.0
14.0
16.0
18.0

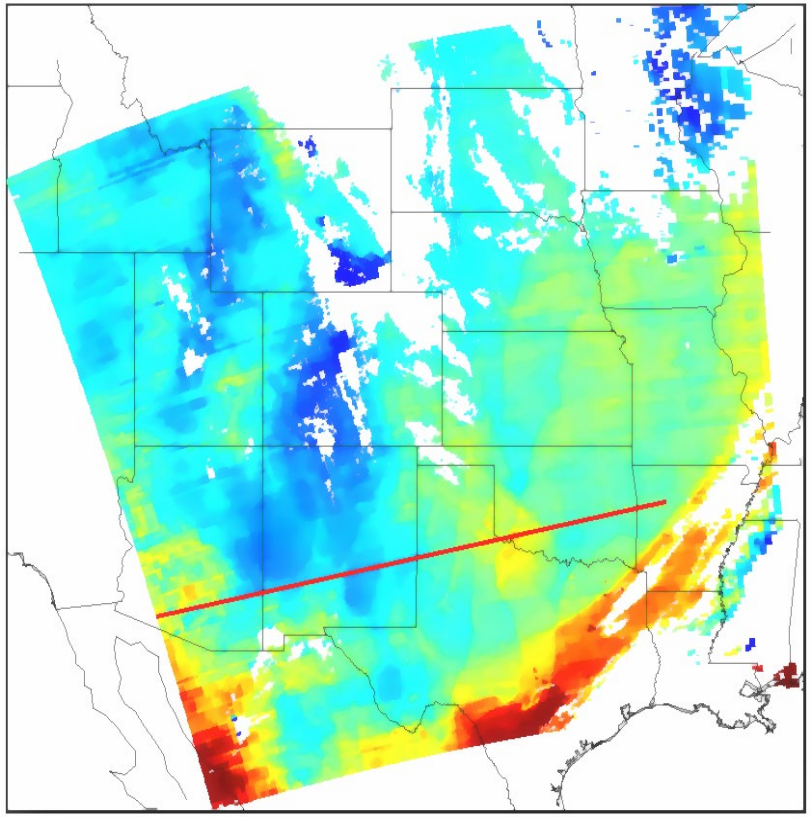

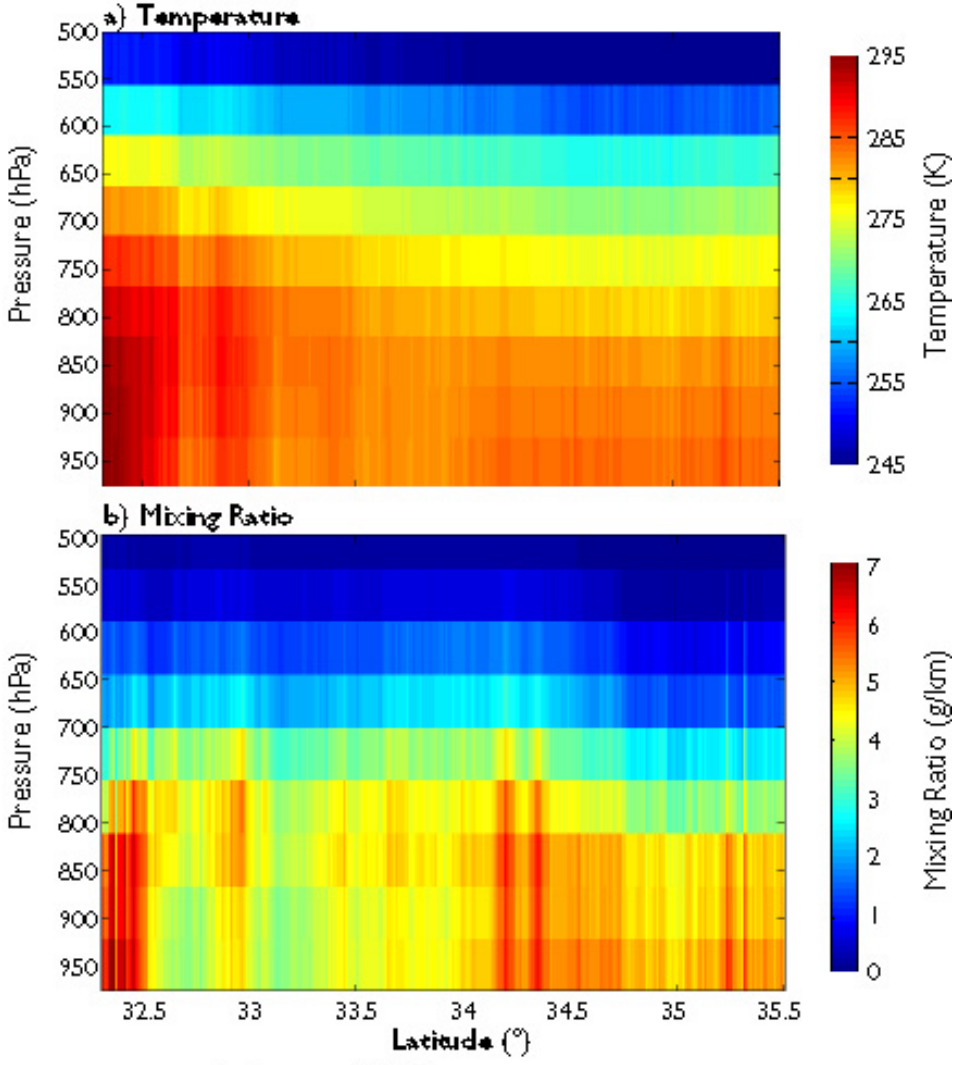

Clear sky layers of temperature and moisture

Application Opportunities with Multispectral Remote Sensing Data

Satellite Remote Sensing
Energy Balance
VIS, IR, and MW Radiative Transfer
EOS Terra & Aqua MODIS
Multispectral Applications
(Ocean Color, Snow/Ice, Vegetation, Aerosols, Fires, Volcanic Ash, Clouds, Moisture)
Detecting Climate Trends

Climate System Energy Balance

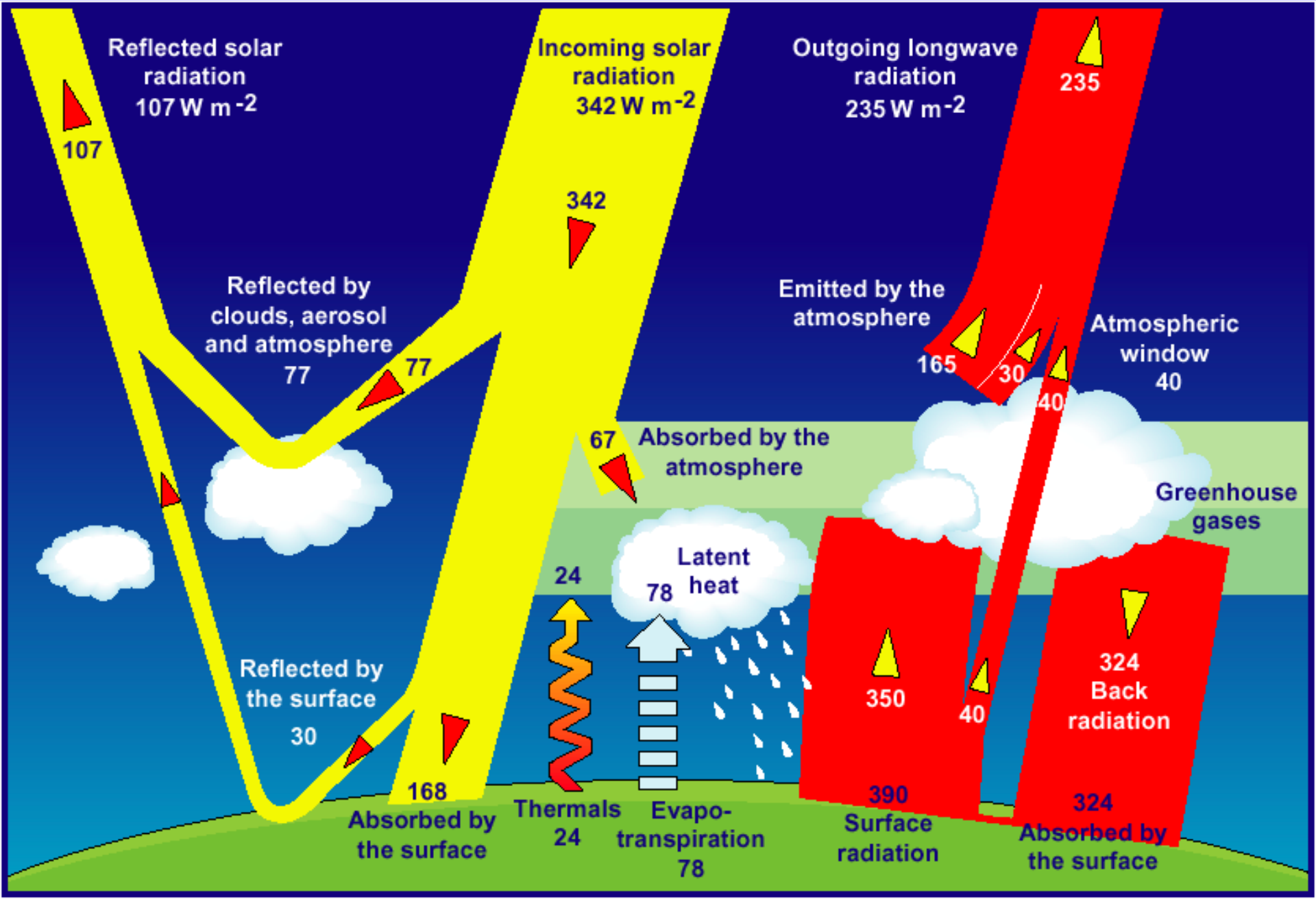

Major Climate System Elements

Carbon Cycle

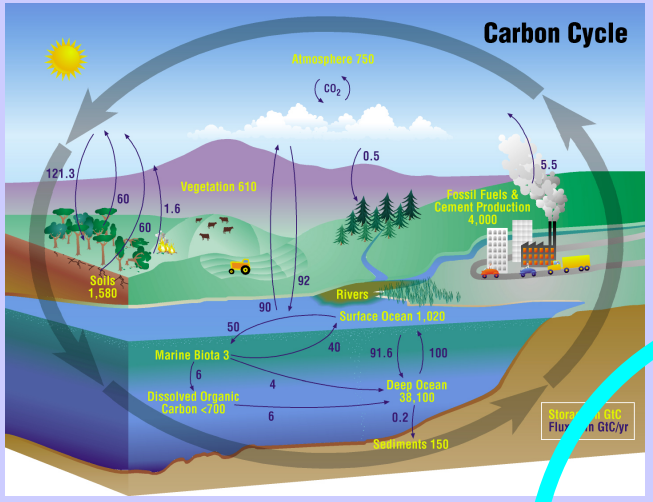

Water & Energy Cycle

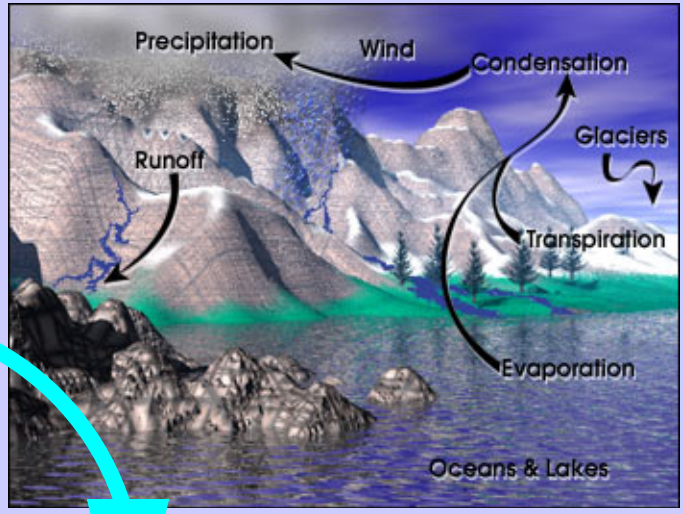

Coupled Chaotic Nonlinear

Atmospheric Chemistry

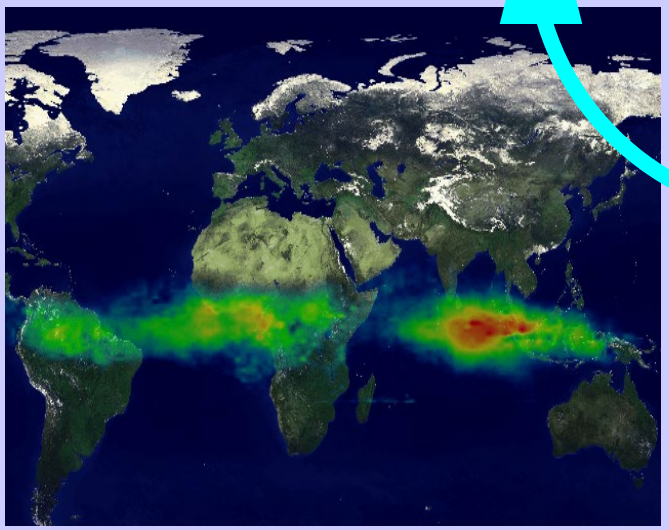

Atmosphere and Ocean Dynamics

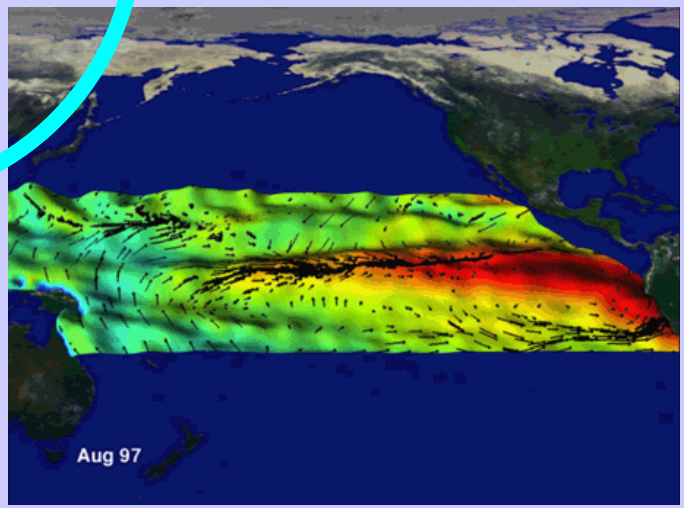

What global surface temperature change has occurred so far?

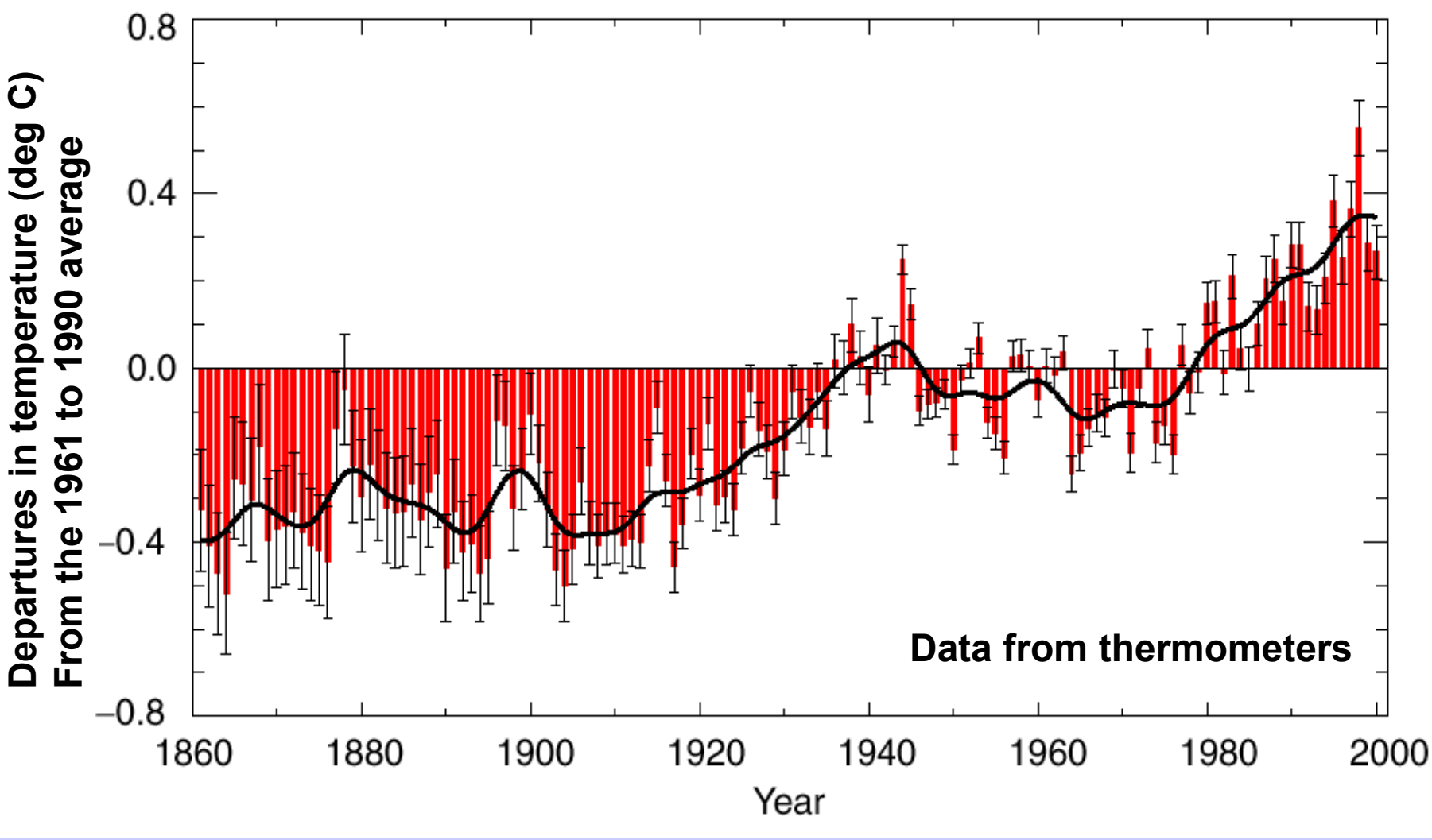

IPCC 2001

Human Influence on Climate

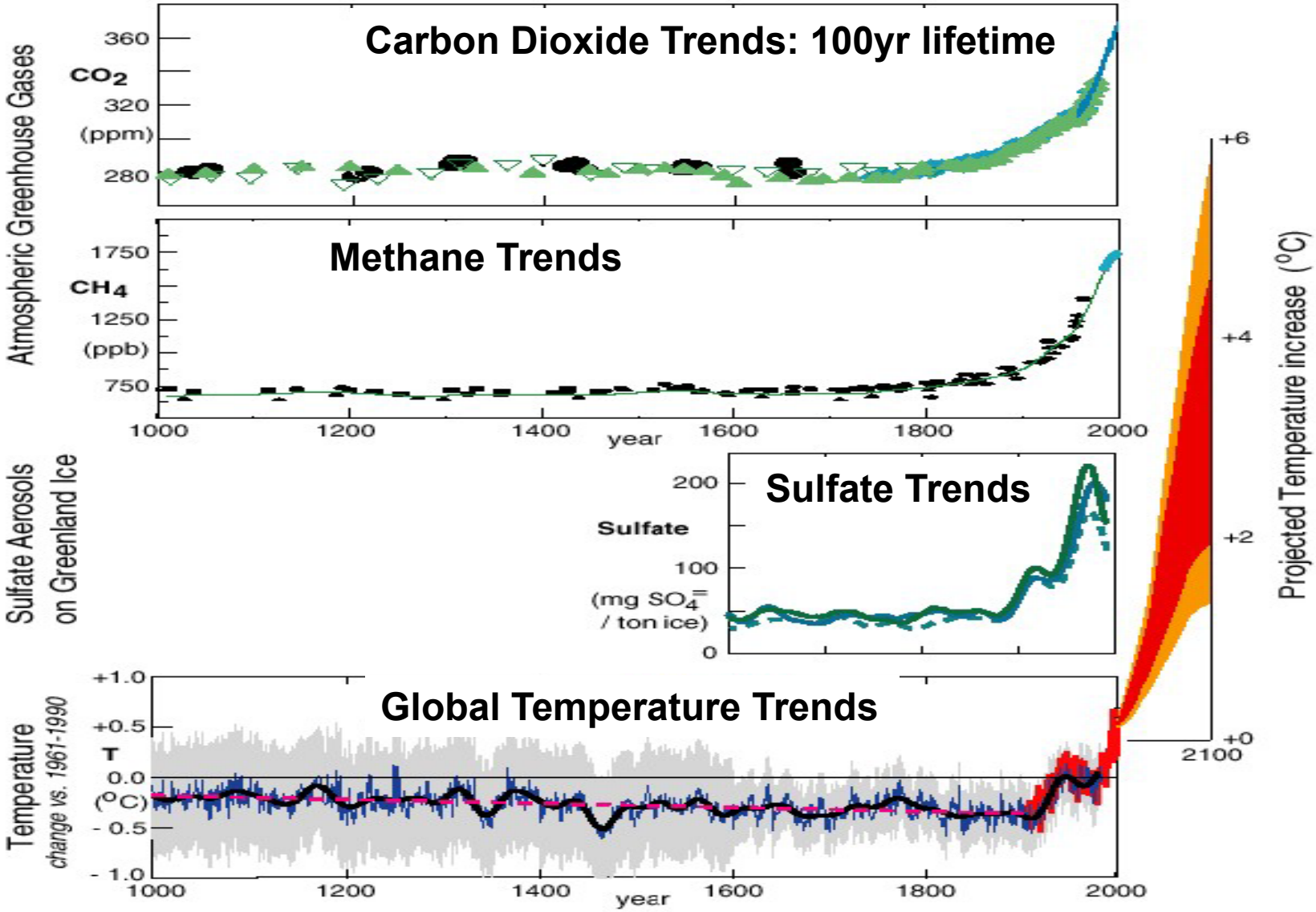

From M. Prather University of California at Irvine

Striving for the Sustainable Society

"A place where humans and their use of the environment are in balance with nature"

"living in harmony with the environment and having resilience to natural hazards"